Functional Organic Monolayers on Semiconductor Surfaces

by

Sofiya Hlynchuk

A dissertation submitted in partial fulfillment
of the requirements for the degree of
Doctor of Philosophy
(Chemistry)
in the University of Michigan
2019

Doctoral Committee:

Professor Stephen Maldonado, Chair
Assistant Professor Neil Dasgupta
Professor Adam Matzger
Assistant Professor Charles McCrory

Sofiya Hlynchuk

hlynsofi@umich.edu

ORCID iD: 0000-0003-1316-1551

DEDICATION

To my family.

ACKNOWLEDGEMENTS

I want to express my gratitude to my family for their constant support and help. I also want to thank my undergraduate advisor Prof. Jeremy Cody and my graduate advisor Prof. Stephen Maldonado. Your advice and encouragement have helped me form my path. Lastly, I want to thank all the amazing people I have met along this journey, you truly made it an experience to remember.

TABLE OF CONTENTS

LIST OF FIGURES

LIST OF TABLES

LIST OF EQUATIONS

.

ABSTRACT

This thesis describes wet chemical surface functionalization strategies that introduce organic groups onto semiconductor surfaces silicon (Si) and gallium phosphide (GaP). The overarching motivation is to develop tailored interfaces for particular electrical and photoelectrochemical applications. This thesis employs concepts developed by previous group members to design semiconductor surfaces with specific wetting properties, with better adhesion to photoresists, and with molecular sensitizers for sensitization. This thesis also demonstrates a new avenue for functionalizing GaP surfaces.

In chapter 2, surface functionalization strategies on Si are developed that yield surficial hydroxyl and amine functional groups. These functionalities alter the wetting properties of Si while also acting as reactive handles for surface reactions. These organic monolayers were characterized by grazing angle attenuated total reflectance infrared (GAATR-IR) and X-ray photoelectron (XP) spectroscopies. The qualities of the interface were assessed by measuring surface recombination velocities of photogenerated charge carriers by microwave photoconductivity. The net results show that it is possible to achieve three distinct surface properties on Si: hydrophilicity, secondary reactivity, and good electronic passivation. In chapter 3, a specific demonstration of Si surface functionalization is presented. The objective is to improve adhesion between a photoresist film and a Si surface under humid (wet) conditions. Si surfaces with a monolayer consisting of terminal alkene groups were prepared and characterized by GAATR-IR and XP spectroscopies. The adhesion between SU8 photoresist and alkene-terminated Si surfaces was probed using the nanoindentation method and the chemical integrity of adhesion was studied determined after exposure to strongly alkaline conditions. The chemical structure of several types of Si/SU8 interfaces were additionally characterized using sum frequency generation (SFG) vibrational spectroscopy. Overall, the experimental data illustrate that a purposely functionalized Si surface can yield Si/SU8 contacts with desirable properties.

The second portion of this thesis focuses on the surface chemistry of GaP. Chapter 4 describes the sensitization of p-GaP photocathodes in the presence of physisorbed dye. Freshly etched p-GaP(100) and p-GaP(111)A electrodes were loaded with several triarylmethane dyes by soaking the electrodes in an aqueous solution of dye. Dye coverages were evaluated using XP and Auger electron spectroscopies. The magnitude of sensitization currents were probed by measuring steady-state photoelectrochemical responses. The cumulative findings showed low dye loading and cathodic degradation were common occurrences when sensitization was attempted with bare GaP. The data suggest that avoiding these issues requires developing p-GaP electrodes where the dye is covalently attached and the underlying GaP surface is otherwise passivated. In chapter 5, the idea of deliberately functionalizing GaP surface with a method that is agnostic to crystallographic surface type is investigated. Functionalization of GaP(100) and GaP(111)A using thermal activation of alkenes is described. Alkene grafting reactioins were evaluated under various temperatures, reactions times, and surface pretreatments. Although functional groups were introduced on various GaP surfaces successfully, low surface coverages were routinely observed. This aspect limited the ability of this methodology to yield surface passivation layers that inhibited chemical oxidation in ambient conditions. However, this reaction did provide a path to higher dye loadings. Quaternary amines were introduced to GaP surfaces to attract anionic dye. High dye loading was detected by XP spectroscopy. Still, the sensitization currents remained low. Some potential reasons are presented in the text. Finally, chapter 6 provides a summary of the major conclusions of the cumulative work, with additional details regarding possible future experiments.

CHAPTER 1

Introduction

1. Motivation

Crystalline inorganic semiconductor materials are omnipresent in society, embedded in modern electronics and impacting sociological and economic aspects of life. Existing and emerging optoelectronic, energy, and micro(nano)electronic devices specifically depend critically on a set of group IV and III-V semiconductors. This thesis focuses on two such materials. Silicon (Si) is 'the' ubiquitous semiconductor used in everything from electronics, biomedical devices, to solar energy conversion.[1-9] Gallium phosphide (GaP) is found in fewer (niche) applications (e.g. LEDs)[10] but has great potential for use in photoelectrochemistry.

In general, the performance of any semiconductor in a given optoelectronic application is a function of its bulk and surface properties. Bulk properties are controlled by material composition, crystal structure, and purity.[11] The band gap ($\mathbf{E}_{gap}$), the energy position of the valence and conduction bands edges ($\mathbf{E}_{vb}$ and $\mathbf{E}_{cb}$, respectively), and doping level are all critical in applications such as solar energy capture and conversion. For example, under illumination semiconductors can absorb photons with energy equal to or greater than $\mathbf{E}_{gap}$. Immediately after light absorption, charge separation within the semiconductor occurs, resulting in electrons and holes promotion to the conduction and valance bands, respectively. Hence, $\mathbf{E}_{gap}$ not only governs semiconductors' light absorption properties but, the maximum free energy available from a thermalized electron-hole pair. If charge transfer with a molecular acceptor/donor is thermodynamically favorable, photogenerated charge carriers can drive oxidation and reduction reactions in solution. Consequently, the energy values of $\mathbf{E}_{vb}$ and $\mathbf{E}_{cb}$ need to be considered relative to the energy necessary to drive a desired redox process. For instance, to produce a desirable chemical fuel such as H_2(g) by splitting water, a semiconductor must have a minimum band gap of at least 1.23 eV at standard pressure and temperature.[12] To overcome kinetic and mass transport losses, a bandgap closer to 1.8 eV is more desirable.[13] For a single semiconductor to effect water

splitting, its conduction band edge must be more negative than the potential for water reduction reaction while its valance band edge must be more positive than the potential for water oxidation reaction.

Surface properties are controlled by the type of uniformity of bonding at the outer most layer of a semiconductor material. As the dimensions of semiconductor devices continue to decrease (as of this writing, the current state of the art for a microprocessor chip involves devices with a length scale of 10 nm),[14] controlling surface properties is even more important. The interface character of a semiconductor should be constant over whatever lifespan is expected of the associated device so as not to alter or impede the desired function. Introduction of a layer that is stable under experimental conditions of interest is useful in this regard. For example, the passivating layer can be introduced through electrochemical methods[15-16] (i.e. deposition), atomic layer deposition[17-18] or organic monolayers[19-21]. The ability to only modify the outer surface atoms without changing the bulk is highly desirable so that materials with suitable bulk properties can be selected and their surfaces tailored for broad applications. Hence, understanding and controlling interfacial surface chemistry under moderate conditions is of utmost importance. The goal of the work presented in this thesis is to develop new surface modification strategies and assess their efficacies in a variety of contexts.

2. Relevant Wet Chemical Surface Modification Strategies

Silicon Surface Reactions

Since the 1960s, the most common routes for exerting Si surface control is by controlled oxidation. While, a surface oxide has several advantages, it is inherently insulating and, in many cases, electrically defective.[22-23] As a result, alternative forms of passivation, have been explored.

Pioneering works have shown an organic monolayer on a Si surface can be thermally grafted by treating a surface in a solution of primary alkenes in a presence of a radical initiator, in order to form Si-C surface bonds[24] and to introduce organic monolayers on Si. Additional reagents such as alkynes[25], aryldiazonium salts[26], silanes[27], dichalcogenides[28], azides[29] and Grignard reagents[21, 30] have also been demonstrated. Figure 1.1. summarizes some of the most popular surface reactions. Despite the rich diversity of reactions for Si surfaces, attaining a surface layer with a high electronic quality is still difficult. To date, a chlorination-Grignard[31] reaction sequence

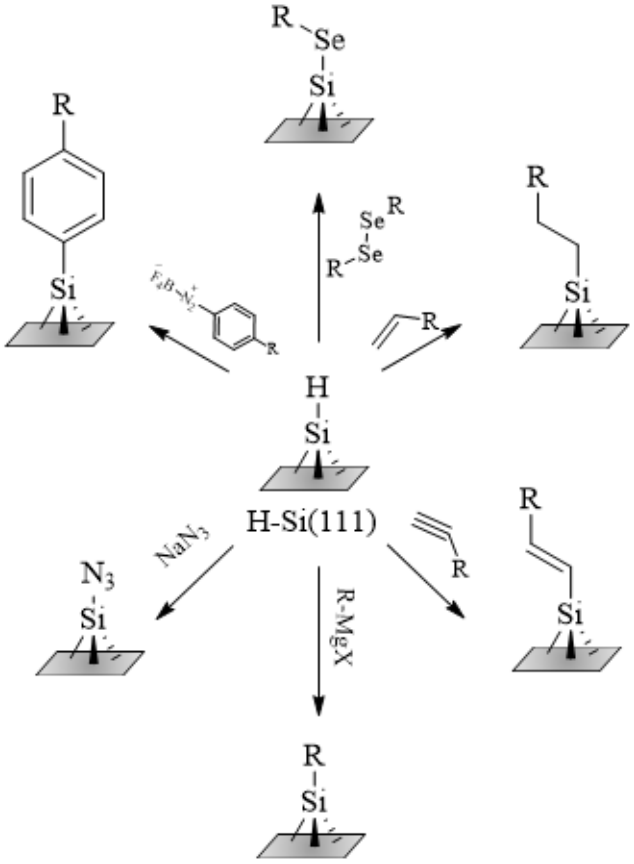

Figure 1.1 Schematic overview of chemical modification pathways on Si.

binding alkyl functional groups on Si(111) is the most reliable method to produce interfaces that have low density of surface defects and high chemical resistance against oxidation. [32-34]Alkyl Grignard reagents allow for attaching organic monolayers on Si through defined surface attachment points resulting in fine tuning of electronic properties of devices.[35-37] An aspect that is lacking with these reagents is the ability to perform secondary surface reactions. In this thesis several demonstrations of expanding the Grignard-based surface passivation route to realize additional surface properties while still, maintaining oxide and defect free surfaces are presented.

Gallium Phosphide Surface Reactions

Gallium phosphide has the necessary bulk material properties to function as a photoelectrode in photoelectrochemical cell. GaP has a mid-size band gap of 2.26 eV, can generate photo voltages of greater than 1 eV and has band edge position that allow for both water and CO_2 reduction.[38-42]

Over the years majority of research focused on developing suitable photoanodes for water splitting.[43-44] Composition, architecture and surface treatments of photoanodes have been studied to realize water splitting. The realization of a photocathode has not been as widely studied. Considering a tandem cell, where both half reactions of water splitting occur simultaneously, the current follows Kirchoff's law[45-47] and the total current is limited by the lowest current at each junction. Therefore, it is imperative that photocathodes are identified and matured so as not to be limiting.

To realize the potential of GaP as a photocathode material, two challenges need to be solved. The first challenge is the weak light absorption by GaP in the visible spectrum at wavelengths longer than 550nm.[48] A large portion of the solar spectrum is therefore not utilized by GaP, which limits its efficiency as a photocathode material. Previous work in the Maldonado group has focused on using the morphology of GaP to trap light. [49-50]The second challenge with utilizing GaP as a photocathode is surface instability in water.[51] The stability of the photocathode-solution interface must be considered in photoelectrochemical cells. The degradation of GaP interface will impact aspects such as charge transfer kinetics and loading of active species.[52-55] The native and thermal oxides of GaP are populated with a high density of defects, which are detrimental to device performance.[56-57] Although effective wet etching techniques have been

identified for GaP surfaces, rapid oxidation is unavoidable on bare surfaces and complicates subsequent reactivity.[58] These two challenges can be addressed by understanding surface chemistry of GaP and applying appropriate surface modification strategies.

To improve light absorption, sensitizers (e.g. molecular dyes, quantum dots) have been investigated that absorb light at wavelengths longer than 550nm.[59-61] The simplest route for sensitization involves submerging a photocathode in dye solution and then measuring the spectral profile of the photocurrent. Despite this process being known for almost six decades, very little information exists on dye sensitized GaP photoelectrodes.

In terms of functionalizing III-V semiconductors, comparatively fewer strategies have been realized. Thiols, sulfides and Grignard reagents are currently the predominant regents.[62-64] Figure 1.2 briefly summaries reactions with these reagents and atop Ga atoms on GaP(111)A. Although the first and most intently studied route, the reaction of thiols/sulfides with GaP results in metastable surface that degrade in air and in water.[62, 65] In contrast, functionalization of III-V semiconductor surfaces with Grignard reagents, has resulted in robust monolayers, capable of passivating the surface in ambient conditions and preventing reductive degradation under illumination.[64, 66-67]

Several pertinent questions remain unanswered. Specifically, what are the key experimental parameters that govern sensitization of GaP by molecular dyes and can we go beyond simple Grignard chemistry and to introduce organic monolayers on GaP for photoelectrochemical applications? The second portion of this thesis addresses these questions.

3. Dissertation Overview

The work presented in this dissertation focuses on investigating surface reactions of silicon and gallium phosphide to design organic monolayers that will allow us to tailor a semiconductor's surface properties.

Chapter 2 describes chemically modified Si(111) surfaces that been prepared through wet chemical surface treatments, adapted from homogenous organic reactions. Prepared surfaces showed resistance towards surface oxidation, selective reactivity towards chemical reagents, and areal defect densities comparable to unannealed thermal oxides. Functional groups such allyl-, 3,4-

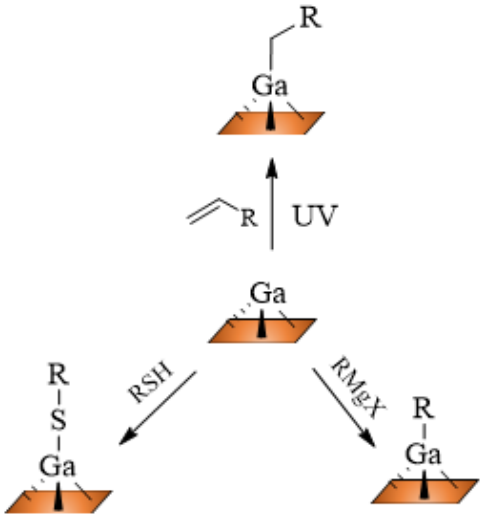

Figure 1.2 Schematic overview of chemical modification strategies on GaP.

methylenedioxybenzene-, or 4-[bis(trimethylsilyl)amino]phenyl-terminated surfaces were introduced on Si(111) via Grignard chemistry. Following, the functional groups were converted to either hydroxylated or amine terminated surfaces. Grazing angle attenuated total reflectance infrared and X-ray photoelectron (XP) spectroscopies were used to characterize surfaces after each surface treatment. Hydroxylated surfaces were further confirmed through reaction with 4-(trifluoromethyl)benzyl bromide and quantified by XP spectroscopy. Surface hydrophilicity was assessed by measuring contact angle between a water droplet and a functionalized surface. All surface exhibited hydrophilic character, consistent with polar surface groups. Surface recombination velocity measurements by way of microwave photoconductivity transients showed the relative defect-character of as-prepared and aged surfaces.

Chapter 3 describes a method to improve adhesion of SU8 films on Si(111) wafers. Common photoresist pretreatment involving hexamethyldisilazane (HMDS) is replaced by utilizing chlorination-Grignard sequence to introduce organic monolayers, bonded to the surface via Si-C bonds. Following, SU8 is developed on functionalized surfaces and adhesion is assessed. In this work monolayers consisting of terminal alkenes were selected. Monolayers were characterized by grazing angle attenuated total reflectance infrared and XP spectroscopies. Si surfaces reacted with allylmagnesium bromide exhibited the largest force necessary for film delamination in comparison to those treated with HMDS or those reacted with 4-pentenylmagensium bromide, as measured by nanoindentation. Interfaces functionalized through Si-C bond formation also showed improved chemical adhesion. Only samples reacted with alkene Grignard reagents maintained the SU8 film without any visible damage after soaking in pH 11.3 buffer for 72 h. This result suggests that by converting the silicon interface from Si-O to Si-C bonds, monolayer hydrolysis is inhibited and SU8 delamination is avoided. To gain insight on interfacial molecular structures in a Si (111)-monolayer-SU8 system infrared-visible SFG vibrational spectroscopy was employed. By SFG alkene functionality was no longer detected after SU8 films were developed. Hence, it is hypothesized that the alkene group undergoes a reaction with the SU8 monomer during film development, forming a covalent attachment at the interface and subsequently aiding in adhesion.

Chapter 4 investigates dye sensitization of bare p-type GaP electrodes in a presence of physisorbed triarylmethane dyes. Freshly etched p-GaP(100) and p-GaP(111)A electrodes were

loaded with physisorbed dye by brief soaking in solutions of Fast Green. X-ray photoelectron spectroscopy, corroborated by Auger electron spectroscopy, indicated that such treatments yield undetectable surface coverages. However, steady-state photoelectrochemical responses consistently showed sub-bandgap photoresponses corresponding to light absorption by the adsorbed dye. The photoresponse characteristics were clearly insensitive to the identity and amount of redox mediators dissolved in solution at low light intensities. Instead, the data suggest electrochemically active surface states related to the cathodic degradation of GaP can accept electrons from photoexcited physisorbed dye. Measurements at high illumination intensities showed sensitivity towards redox mediators in solution, indicating that the conventional mode of dye regeneration by redox species in solution is possible with p-GaP. Separate measurements with covalently modified p-GaP(111)A photoelectrodes further suggested that deliberate modification to minimize/eliminate surface states is also possible. Collectively, this work indicates that although some types of dye readily adsorb onto native GaP interfaces, the low dye loadings and the susceptibility of the interface to chemical attack during the sensitization process argue against using bare p-GaP photocathodes with physisorbed triarylmethane dyes. Instead, these studies suggest that dye-sensitized photocathodes based on p-GaP require deliberate surface chemical modification methods to overcome the low loading and inhibit unwanted charge transfer between the surface and the photoexcited dye.

Chapter 5 investigates an alternative method to introduce organic monolayers on GaP surfaces. Alkene grafting on GaP(111)A and GaP(100) was studied as a function of reaction time, temperature and surface pretreatment. Test reactions were performed using 1-octadecene. Degree of grafting was evaluated as a function of contact angle value between a water droplet and reacted surfaces. Surface reaction independent of reaction time and temperature were observed. Changes in grafting were only observed when surfaces were dry etched with either oxygen or argon plasma. Degree of surface passivation against chemical oxidation in ambient conditions was characterized using XP spectroscopy. Monolayers prepared through a reaction with 1-octadecene were incapable of passivating GaP surfaces against surface oxide growth. This suggests that monolayers grafted through alkenes are less compact and potentially more disordered, in comparison to those introduced via Grignard chemistry. In summary, data presented in this chapter illustrated the ability to thermally graft alkene groups to GaP surface. However, the data suggest surface anomalies act as grafting sites. Lastly, grafting cationic surface group was explored to prepare a surface capable

of adsorbing anionic dye, Fast Green. Although dye loading was improved, low dye sensitization was measured. Possible explanations are presented in the chapter.

Chapter 6 provides a summary of major conclusions of each chapter. Additionally, the chapter provides prospects for future works. Unanswered question from chapters 3 and 5 are reemphasized and potential routes for further exploration are presented.

4. References

1. Banerjee, I.; Pangule, R. C.; Kane, R. S., *Adv. Mater.* **2011,** *23* (6), 690-718.
2. Chen, K.-I.; Li, B.-R.; Chen, Y.-T., *Nano Today* **2011,** *6* (2), 131-154.
3. Desai, N. P.; Hossainy, S. F. A.; Hubbell, J. A., *Biomaterials* **1992,** *13* (7), 417-420.
4. Wang, Q.; Uzunoglu, E.; Wu, Y.; Libera, M., *ACS Appl. Mater. Interfaces* **2012,** *4* (5), 2498-2506.
5. Abdi, F. F.; Han, L.; Smets, A. H. M.; Zeman, M.; Dam, B.; van de Krol, R., *Nat. Commun.* **2013,** *4*, 2195.
6. Ji, L.; McDaniel, M. D.; Wang, S.; Posadas, A. B.; Li, X.; Huang, H.; Lee, J. C.; Demkov, A. A.; Bard, A. J.; Ekerdt, J. G.; Yu, E. T., *Nat. Nanotechnol.* **2014,** *10*, 84.
7. Cui, Y.; Lieber, C. M., *Science* **2001,** *291* (5505), 851-853.
8. Qu, Y.; Li, F.; Zhang, P.; Zhao, L.; Liu, J.; Song, X.; Gao, L., *Appl. Surf. Sci.* **2019,** *471*, 528-536.
9. Ding, Q.; Meng, F.; English, C. R.; Cabán-Acevedo, M.; Shearer, M. J.; Liang, D.; Daniel, A. S.; Hamers, R. J.; Jin, S., *J. Am. Chem. Soc.* **2014,** *136* (24), 8504-8507.
10. Craford, M. G.; Groves, W. O., *Proc. IEEE 61* (7), 862-880.
11. Sze, S. M.; Lee, M. K., *Semiconductor devices, physics and technology*. 3rd ed.; Wiley: Hoboken, N.J., 2012; p ix, 578 p.
12. Fujishima, A.; Honda, K., *Nature* **1972,** *238* (5358), 37-38.
13. Walter, M. G.; Warren, E. L.; McKone, J. R.; Boettcher, S. W.; Mi, Q.; Santori, E. A.; Lewis, N. S., *Chem. Rev.* **2010,** *110* (11), 6446-6473.
14. Shahidi, G. G., *IEEE Acess* **2019,** *7*, 851-856.
15. Klahr, B.; Gimenez, S.; Fabregat-Santiago, F.; Bisquert, J.; Hamann, T. W., *J. Am. Chem. Soc.* **2012,** *134* (40), 16693-16700.
16. Rovelli, L.; Tilley, S. D.; Sivula, K., *ACS Appl. Mater. Interfaces* **2013,** *5* (16), 8018-8024.
17. Chen, Y. W.; Prange, J. D.; Dühnen, S.; Park, Y.; Gunji, M.; Chidsey, C. E. D.; McIntyre, P. C., *Nat. Mater.* **2011,** *10*, 539.
18. Strandwitz, N. C.; Comstock, D. J.; Grimm, R. L.; Nichols-Nielander, A. C.; Elam, J.; Lewis, N. S., *J. Phys. Chem. C* **2013,** *117* (10), 4931-4936.
19. Bansal, A.; Lewis, N. S., *J. Phys. Chem. B* **1998,** *102* (21), 4058-4060.
20. Cicero, R. L.; Linford, M. R.; Chidsey, C. E. D., *Langmuir* **2000,** *16* (13), 5688-5695.
21. Webb, L. J.; Lewis, N. S., *J. Phys. Chem. B* **2003,** *107* (23), 5404-5412.
22. Fonash, S. J.; Fonash, S. J.; Fonash, S. J., *Solar cell device physics*. 2nd ed. ed.; Academic Press/Elsevier: Burlington, MA :, 2010; Vol. Burlington, MA :.
23. Kumar, A.; Rosenblum, M. D.; Gilmore, D. L.; Tufts, B. J.; Rosenbluth, M. L.; Lewis, N. S., *Appl. Phys. Lett.* **1990,** *56* (19), 1919-1921.
24. Linford, M. R.; Fenter, P.; Eisenberger, P. M.; Chidsey, C. E. D., *J. Am. Chem. Soc.* **1995,** *117* (11), 3145-3155.
25. Sieval, A. B.; Opitz, R.; Maas, H. P. A.; Schoeman, M. G.; Meijer, G.; Vergeldt, F. J.; Zuilhof, H.; Sudhölter, E. J. R., *Langmuir* **2000,** *16* (26), 10359-10368.
26. Stewart, M. P.; Maya, F.; Kosynkin, D. V.; Dirk, S. M.; Stapleton, J. J.; McGuiness, C. L.; Allara, D. L.; Tour, J. M., *J. Am. Chem. Soc.* **2004,** *126* (1), 370-378.

27. Herzer, N.; Hoeppener, S.; Schubert, U. S., *Chem. Commun.* **2010,** *46* (31), 5634-5652.
28. Hu, M.; Liu, F.; Buriak, J. M., *ACS Appl. Mater. Interfaces* **2016,** *8* (17), 11091-11099.
29. Cao, P.; Xu, K.; Heath, J. R., *J. Am. Chem. Soc.* **2008,** *130* (45), 14910-14911.
30. O'Leary, L. E.; Strandwitz, N. C.; Roske, C. W.; Pyo, S.; Brunschwig, B. S.; Lewis, N. S., *J Phys Chem Lett* **2015,** *6* (4), 722-6.
31. Bansal, A.; Li, X.; Lauermann, I.; Lewis, N. S.; Yi, S. I.; Weinberg, W. H., *J. Am. Chem. Soc.* **1996,** *118* (30), 7225-7226.
32. Webb, L. J.; Rivillon, S.; Michalak, D. J.; Chabal, Y. J.; Lewis, N. S., *J. Phys. Chem. B* **2006,** *110* (14), 7349-7356.
33. Plass, K. E.; Liu, X.; Brunschwig, B. S.; Lewis, N. S., *Chem. Mater.* **2008,** *20* (6), 2228-2233.
34. Nemanick, E. J.; Hurley, P. T.; Brunschwig, B. S.; Lewis, N. S., *J Phys Chem B* **2006,** *110* (30), 14800-8.
35. Alderman, N.; Danos, L.; Grossel, M. C.; Markvart, T., *RSC Adv.* **2013,** *3* (43), 20125-20131.
36. Vilan, A.; Cahen, D., *Chem. Rev.* **2017,** *117* (5), 4624-4666.
37. Pekarek, R. T.; Celio, H.; Rose, M. J., *Langmuir* **2018,** *34* (22), 6328-6337.
38. Bockris, J. O. M.; Uosaki, K., *J. Electrochem. Soc.* **1977,** *124* (9), 1348-1355.
39. Halmann, M., *Nature* **1978,** *275* (5676), 115-116.
40. Kaname, I.; Shoichiro, I.; Makoto, Y.; Soji, O.; Takaya, I., *Bull. Chem. Soc. Jpn.* **1984,** *57* (2), 583-584.
41. Gronet, C. M.; Lewis, N. S., *Nature* **1982,** *300* (5894), 733-735.
42. Kohl, P. A.; Bard, A. J., *J. Am. Chem. Soc.* **1977,** *99* (23), 7531-7539.
43. Alibabaei, L.; Luo, H.; House, R. L.; Hoertz, P. G.; Lopez, R.; Meyer, T. J., *J. Mater. Chem. A* **2013,** *1* (13), 4133-4145.
44. Odobel, F.; Le Pleux, L.; Pellegrin, Y.; Blart, E., *Acc. Chem. Res.* **2010,** *43* (8), 1063-1071.
45. Werner, J.; Niesen, B.; Ballif, C., *Adv. Mater. Intefaces* **2018,** *5* (1), 1700731.
46. Vos, A. D., *J. Phys. D: Appl. Phys.* **1980,** *13* (5), 839-846.
47. Würfel, P. D.; Würfel, U., Physics of solar cells. Wiley-VCH: Weinheim, 2009.
48. Price, M. J.; Maldonado, S., *J. Phys. Chem. C* **2009,** *113* (28), 11988-11994.
49. Hagedorn, K.; Collins, S.; Maldonado, S., *J. Electrochem. Soc.* **2010,** *157* (11), D588-D592.
50. Lee, S.; Bielinski, A. R.; Fahrenkrug, E.; Dasgupta, N. P.; Maldonado, S., *ACS Appl. Mater. Interfaces* **2016,** *8* (25), 16178-16185.
51. Gerischer, H., *J. Vac. Sci. Technol.* **1978,** *15* (4), 1422-1428.
52. Rosenbluth, M. L.; Lewis, N. S., *J. Am. Chem. Soc.* **1986,** *108* (16), 4689-4695.
53. Maçaira, J.; Andrade, L.; Mendes, A., *Renew. Sust. Energ. Rev.* **2013,** *27*, 334-349.
54. Langmar, O.; Ganivet, C. R.; Schol, P.; Scharl, T.; de la Torre, G.; Torres, T.; Costa, R. D.; Guldi, D. M., *J. Mater. Chem. C* **2018,** *6* (19), 5176-5180.
55. Bonomo, M.; Magistris, C.; Buscaino, R.; Fin, A.; Barolo, C.; Dini, D., *ChemistrySelect* **2018,** *3* (4), 1066-1075.
56. Gershenzon, M.; Mikulyak, R. M., *Appl. Phys. Lett.* **1966,** *8* (10), 245-247.
57. Stringfellow, G. B., *J. Vac. Sci. Technol.* **1976,** *13* (4), 908-913.
58. Mukherjee, J.; Erickson, B.; Maldonado, S., *J. Electrochem. Soc.* **2010,** *157* (4), H487-H495.
59. Memming, R.; Tributsch, H., *J. Phys. Chem.* **1971,** *75* (4), 562-570.
60. Ilic, S.; Brown, E. S.; Xie, Y.; Maldonado, S.; Glusac, K. D., *J. Phys. Chem. C* **2016,** *120* (6), 3145-3155.
61. Wang, Z.; Shakya, A.; Gu, J.; Lian, S.; Maldonado, S., *J. Am. Chem. Soc.* **2013,** *135* (25), 9275-9278.
62. Suzuki, Y.; Sanada, N.; Shimomura, M.; Fukuda, Y., *Appl. Surf. Sci.* **2004,** *235* (3), 260-266.
63. Flores-Perez, R.; Zemlyanov, D. Y.; Ivanisevic, A., *J. Phys. Chem. C* **2008,** *112* (6), 2147-2155.
64. Mukherjee, J.; Peczonczyk, S.; Maldonado, S., *Langmuir* **2010,** *26* (13), 10890-10896.
65. Richards, D.; Zemlyanov, D.; Ivanisevic, A., *Langmuir* **2010,** *26* (11), 8141-8146.

66. Brown, E. S.; Peczonczyk, S. L.; Wang, Z.; Maldonado, S., *J. Phys. Chem. C* **2014,** *118* (22), 11593-11600.
67. Peczonczyk, S. L.; Mukherjee, J.; Carim, A. I.; Maldonado, S., *Langmuir* **2012,** *28* (10), 4672-4682.

CHAPTER 2

Chemically Modified Si(111) Surfaces Simultaneously Demonstrating Hydrophilicity, Resistance Against Oxidation, and Low Trap State Densities

Reprinted from Surface Science, Vol. 645, Chemically Modified Si(111) Surfaces Simultaneously Demonstrating Hydrophilicity, Resistance Against Oxidation, and Low Trap State Densities, Brown, E.S.; Hlynchuk, S.; Maldonado, S., 49-55, Copyright 2019, with permission from Elsevier.

1. Introduction

Three features are highly desirable in semiconductor interfaces when used to construct optoelectronic technologies. First, the chemical integrity of the semiconductor surface must be both compatible with all device fabrication/metallurgical steps. Second, the electrical quality of each semiconductor interface must be sufficiently good so as not to present an operational bottleneck or otherwise adversely affect the device. Third, the semiconductor surface should be (and remain) either highly conducting or insulating (depending on the application) with respect to heterogeneous charge transfer. No native semiconductor surface perfectly and simultaneously demonstrates these aspects, motivating the development of new and improved chemical modification strategies of semiconductor interfaces.

Vapor phase atomic layer deposition (ALD)[1-2] and spin casting of aqueous metal oxo cluster solutions[3-4] are highly advantageous for rapidly and simply constructing high quality semiconductor heterojunctions. However, they are best suited for hydrophilic semiconductor interfaces that can withstand elevated temperatures and have proton donating/accepting character. The majority of technologically relevant Groups IV and III-V have native interfaces that do not possess these attributes in addition to retaining a low defect density. Although native oxides on such semiconductors are generally hydrophilic,[5-6] they possess deleterious levels of trap states. Of the few high quality oxides (e.g. annealed thermal oxide Si(100)[7]), they are naturally insulating.

Chemical methods to eliminate electrically active surface states on Groups IV and III-V surfaces (e.g. etching with NH_4F;[8] lattice matched AlGaAs epilayers[9]) render surfaces that have too few nucleation sites for ALD[10] and/or are neither wettable nor stable towards exposure to aqueous solutions.[11-19]

This report focuses on the potential of wet chemical surface modification to yield semiconductor surfaces that are jointly hydrophilic, resistant against oxidation, and possesses a low level of surface defects. Using single crystalline Si(111) as a model surface, we demonstrate organically modified interfaces prepared through a sequence of reactions involving Grignard reagents[20-21] and subsequent activation steps. Specifically, we show the preparation of Si(111) surfaces decorated with either a terminal primary alcohol, a terminal diol, or a terminal amine group (Figure 2.1). Distinctions between the surfaces prepared here and the prior art in organically-modified Si surfaces[22-33] are drawn through measurements of oxide growth via X-ray photoelectron spectroscopy, contact angle wetting measurements, reactivity towards model test reagents, and surface recombination velocities, *S*, of photogenerated carriers. The purpose of the work is to not only identify the attainable physicochemical properties of these modified Si interfaces but more generally to show that semiconductor surfaces that are reactive towards modification by Grignard reagents can be deterministically tailored as needed.

2. Experimental

Materials and Chemicals

All chemicals were purchased from Sigma-Aldrich and used as received unless noted. Methanol (anhydrous >99.8%,), chlorobenzene (Acros, 99.8%), tetrahydrofuran (THF) (anhydrous ≥ 99.9%, inhibitor free), acetone (Fisher, HPLC grade), hexanes (Macron Chemicals, ACS grade), dichloromethane (anhydrous > 99.8%), phosphorus (V) oxychloride, borane-tetrahydrofuran (1 M), diethyl ether (anhydrous), potassium bis(trimethylsilyl)amide (KHMDS), 40% ammonium fluoride (Transene Electronic Chemicals, semiconductor grade), sodium hydroxide (Fisher, 95.0 to 100.5% FCC grade), 30wt% in H_2O hydrogen peroxide (ACS grade), trifluoroacetic acid (TFA) (99%), 2,2,3,3,4,4,5,5-octafluoro-1-pentanol (98%), and 37% hydrochloric acid (ACS grade) were used as received. Methylmagnesium chloride (3.0 M), allyl magnesium chloride (2.0 M), and 4-[bis(trimethylsilyl)amino]phenyl magnesium bromide (0.5 M) were used as received. 3,4-(methylenedioxy)phenylmagnesium bromide (1.0 M) was diluted to 0.5

M with THF to help prevent polymerization during reaction. 4-(trifluoromethyl)benzyl bromide (Sigma-Aldrich, 98%) was outgassed by three freeze-pump-thaw cycles before use. Benzoyl peroxide (Fluka, ≥ 97%) was dried under a vacuum of < 200 mTorr for at least 24 h and placed in the nitrogen-atmosphere glovebox. Water with a resistivity of 18.2MΩ cm^{-1} (Barnsted Nanopure system) was used throughout. For surface characterization studies, one-side polished, n-type Si (111) wafers doped with As were purchased from Wafer Works Corp. and had thickness of 525 ± 15 μm. For SRV measurements, float-zone (FZ), intrinsically-doped Si(111) (El-Cat) wafers with a resistivity equal to 16500 ± 3500 Ω·cm, a thickness of 460 ± 15 μm, and both sides polished were used.

Sample Preparation

Samples were diced into 0.5 cm by 0.5 cm squares for surface characterization and into 1 cm by 1.5 cm rectangles for SRV measurements. Si(111) samples were etched prior to use in 40% NH_4F solution for 5 minutes while continuously purging with nitrogen gas, rinsed with water, and dried in a stream of nitrogen gas. Immediately after etching, wafers were transferred to a nitrogen-purged glove box. Freshly etched wafers were chlorinated at 90 °C for 50 minutes using a saturated solution of phosphorous (V) pentachloride in chlorobenzene, to which a few grains of benzoyl peroxide were added.[34] Following the chlorination step, samples were washed with THF, dried in the glovebox, and transferred to reaction vessels to which designated Grignard reagents were added (Figure 2.1).

Preparation of 1 and 1a

Chlorinated wafers were transferred to closed reaction vessels to which a solution of allylmagnesium chloride was added. Reaction solution was heated for 13 h at 110 ± 5 °C. Samples were rinsed with THF and methanol (**1**). To prepare ***1a*** surfaces, ***1*** surfaces were hydroborated and hydroxylated with a procedure modified from Toledano, *et al.*[30] In a nitrogen-purged glove box, ***1*** wafers were immersed in a solution of BH_3 •THF complex at room temperature for 5 h , rinsed with THF and allowed to dry, and transferred to a round bottom flasks, sealed with a rubber stopper and taken out of the glove box. To the flask, 1 mL 3 M NaOH and 1 mL 30% H_2O_2 injected through a rubber septum via syringe were added stepwise. After 20 min at room temperature, the wafers were removed from the flask, washed with water and methanol, and dried under a stream N_2(g).

Preparation of 2, 2a, 2b and 2c

Chlorinated wafers were transferred to closed reaction vessels to which a solution of 3,4-(methylenedioxy)phenylmagnesium bromide was added and diluted to 0.5 M. Reaction temperature was reduced to 90 ± 5 °C to prevent polymerization of the reagent. Upon completion, samples were rinsed with THF and methanol (***2***). Samples were either backfilled with methylmagnesium chloride in a new reaction vessel for additional 13 h at 110 ± 5 °C, rinsed with THF and methanol, and dried in the glovebox (***2b***) or deprotected with a solution of TFA:THF:H_2O (1:20:5) for 4 h at room temperature outside of the glovebox (***2a*** and ***2c***).[35]

Preparation of 3, 3a, 3b and 3c

Chlorinated wafers were transferred to closed reaction vessels to which a solution of 4-[bis(trimethylsilyl)amino]phenyl magnesium bromide was added. Reaction vessel was heated to 110 ± 5 °C for 12-16 h, samples were rinsed with THF and methanol, and allowed to dry in the glovebox (**3**). Samples were either backfilled with methylmagnesium chloride in a new reaction vessel for additional 3 h at 90 ± 5 °C, rinsed with THF and methanol, and dried in the glovebox (***3b***) or deprotected with a 20% v/v HCl solution for 1 h at room temperature outside of the glovebox **(*3a*** and ***3c***).

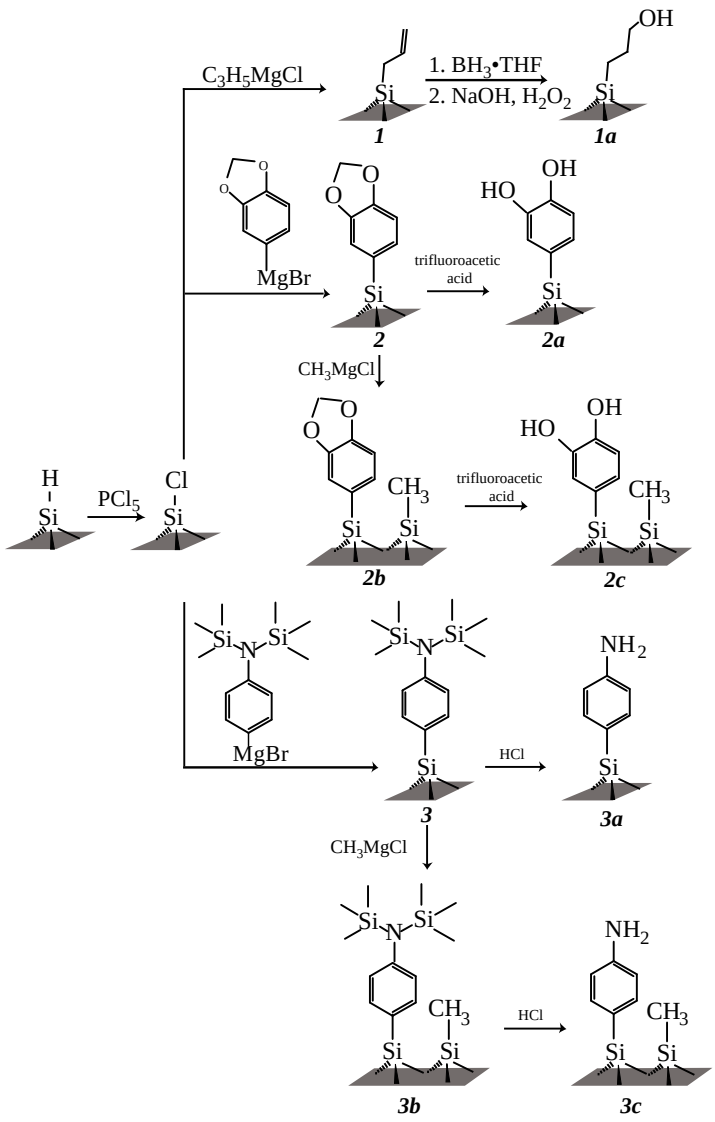

Figure 2.1 Chemical modification routes for Si surfaces outlined in this work.

Nucleophilic Reaction with 4-(trifluoromethyl)benzyl bromide

In the glovebox, samples were reacted with 0.02 M TFB with <1 mg KHMDS in hexanes at 60 °C for 1 h. Samples were rinsed with hexanes, diethyl ether, and methanol, sonicated in methanol for 2 min, and dried with a stream of nitrogen gas.

X-ray Photoelectron Spectroscopy

Elemental composition of functionalized Si(111) surfaces was collected using a PHI 5400 analyzer equipped with Al K α(1486.6 eV) source, without a monochromator. Acquisition took place at a pressure of < 2.5×10^{-9} torr, without the need for charge neutralization due to the natural conductivity of the samples. A 6 mA current emission and a 12 kV anode high tension were used. For each sample survey scans were recorded between 0 and 1350 eV at pass energy of 117.40 eV. While high resolution spectra were collected at pass energy of 23.5 eV. All binding energies were referenced to the expected binding energy for adventitious carbon (284.6 eV).[36] Spectrum analysis was performed with CASA XPS 2.3.13 software. Further characterization of the surfaces were performed by calculating oxide thickness using a simplified substrate/overlayer model[37] and calculating fractional monolayer coverage of the surface using three-layer model.[38]

For surface oxides, the thickness of oxide at the surface was calculated using the simplified substrate overlayer model,[37]

$$d = \lambda_{ov} \sin\varphi \left(\ln\left(1 + \frac{I_{overlayer}}{I_{substrate}} \frac{I^{0}{}_{substrate}}{I^{0}{}_{overlayer}} \right) \right)$$

Equation 2.1 Simplified Substrate Overlayer Equation.

where d is the thickness of the oxide overlayer in nanometer, λ_{ov} is escape depth of emitted electrons through the oxide layer, φ is the takeoff angle (54.6°) between the sample surface and the detector, I is the integrated area as follows: $I_{substrate}$ for bulk signal, $I_{overlayer}$ of oxide signals, $I^{0}{}_{substrate}$ for Si freshly etched in NH_4F for 1 min, $I^{0}{}_{overlayer}$ for a thick (>500 nm) thermal oxide layer on Si. The escape depth for electrons was estimated:

$$\lambda = 0.41 A^{3/2} E^{1/2}$$

Equation 2.2 Electron Escape Depth Calculation.

where *A* is the mean diameter of one unit in the overlayer (nm) and *E* is the kinetic energy of the ejected core electron (eV). The mean diameter of one unit, *A*, is

$$A = \sqrt[3]{\frac{MW}{\rho N_A}}$$

Equation 2.3 Mean Diameter Calculation.

where *MW* is mean atomic weight (g mol^{-1}), ρ is the density (g cm^{-3}), and N_A is Avogadro's number.

Due to the larger size of all molecules tested here, a simple model of three-layer structure was used for monolayer coverage calculations.[38] For calculations of coverage of ***3a***, the high resolution N 1s XP spectrum was used. Aniline was used as a model molecule and parameters of interest are listed in Table 2.1. The topmost layer included the $–NH_2$ (t_1), the Si substrate served as the bottom layer (*sub*) and the linker in between t_1 and the substrate served as t_2 (Figure 2.2).

To calculate overlayer coverage using the simple three-layer model, Equation 2.4 was adopted from Asami, *et al*.[4]

$$\frac{I_{ov}}{I_{sub}} = \left(\frac{SF_{ov}}{SF_{sub}}\right)\left(\frac{\rho_{ov}}{\rho_{sub}}\right)\left(\frac{1 - e^{\left[\frac{-t_1}{\lambda_{ov}\cos\varphi}\right]}}{e^{\left[\frac{-(t_1+t_2)}{\lambda_{sub}\cos\varphi}\right]}}\right)$$

Equation 2.4 Three-Layer Model for Monolayer Calculation.

where SF_{sub} is the sensitivity factor for the element of interest in the substrate, SF_{ov} is the instrument sensitivity factor for the element of interest in the substrate, ρ_{ov} is the density of the element of interest in the overlayer. For Si, ρ_{sub} is 2.32 g cm^{-3} and SF_{sub} is 0.339.[39] Parameters referring to *ov* are referencing the topmost layer containing an *N* atom in this situation. The variable t_1 is the thickness of the second layer and t_2 is the thickness of the intermediate layer. Values of t_1 and t_2 were approximated using known data from model molecules, which are listed in Table 2.2, and using previously reported data on bond lengths and molecule size.[40-42] The sum of the thicknesses is *d*, the total thickness of the organic overlayer.

Table 2.1 Monolayer Coverage Calculation Parameters for Various Reactants.

Surface Type (Element Measured)	ρ (g cm^{-3})	n	a_m (nm)	λ_x	λ_{Si}	**SF**[a]	**Length** (nm)[b]	**No. Density** (atoms cm^{-2})
3a (N 1s)[c]	1.20	0.40	0.502	5.26	5.94	0.477	0.70	4.22 x 10^{14}
***1a*+TFB** (F 1s)[d]	1.30	0.18	0.641	5.95	7.83	1.0	1.08	2.44 x 10^{14}
***2a*+TFB** (F 1s)[e]	1.30	0.14	0.815	8.53	11.23	1.0	1.51	1.52 x 10^{14}
***3a*+TFB** (F 1s)[f]	1.32	0.14	0.672	6.38	8.41	1.0	1.38	2.22 x 10^{14}

[a]*SF* values from Asami, *et al*.[38] [b]Molecule lengths were estimated from tabulated bond length values.[40, 42] [c]Parameters for aniline were used. [d]Parameters for methyl 4-(trifluoromethyl)benzyl ether were used. [e]MW and density were obtained from Chemdraw approximation since data could not be found for analogous structures. Values were also used for ***2c***+TFB. [f]Parameters for N-phenyl-3-(trifluoromethy)aniline were used. Values were also used for ***3c***+TFB.

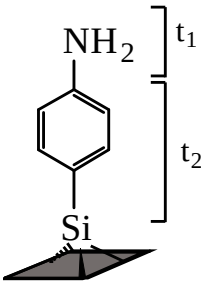

Figure 2.2 Surface Labeled with t_1 and t_2.

The following relationship also holds true:

$$t_1 = nt_2$$

Equation 2.5 Relationship Between Two Sub-Layers in Three-Layer Model.

where *n* is the ratio of thicknesses of the two layers. The relationship was entered into the equation in place of t_2 and subsequently t_1 was solved for. Total thickness of the organic layer was calculated:

$$d = t_1 + t_2$$

Equation 2.6 Relationship Between Total Overlayer Thickness and Two Sub-Layers.

Monolayer coverage was calculated:

$$ML = \frac{d}{d_{lit}}$$

Equation 2.7 Monolayer Coverage Relationship.

where d_{lit} is the sum of expected lengths t_1 and t_2 published in the literature.[41, 43] Fractional monolayer coverage, θ, was calculated to determine the number of aniline molecules per atop Si atom. Converting the density of aniline to number density (atoms cm^{-2}) and multiplying by the monolayer coverage, we divide by the number of unreconstructed atop atoms on Si(111) (7.83 x 10^{-14} atoms cm^{-2}) to get θ.[44]

For calculations of surface coverage after etherification, the topmost layer included the $-CF_3$ (t_1), the Si substrate served as the bottom layer (*sub*), and the linker in between t_1 and the substrate served as t_2 (Figure 2.3). Here, *ov* is referencing the topmost layer containing F atoms and the value of I_{ov} was divided by 3 to account for three F atoms per molecule. The F 1s intensities of ***2a*** and ***2c*** surfaces reacted with TFB were divided by 6 to account for attachment of more than one TFB molecule. Parameters of interest are tabulated in Table 2.1.

Tabulated ML coverage and θ values for surface reactions on Si(111) quantified by XP spectra are shown in Table 2.2.

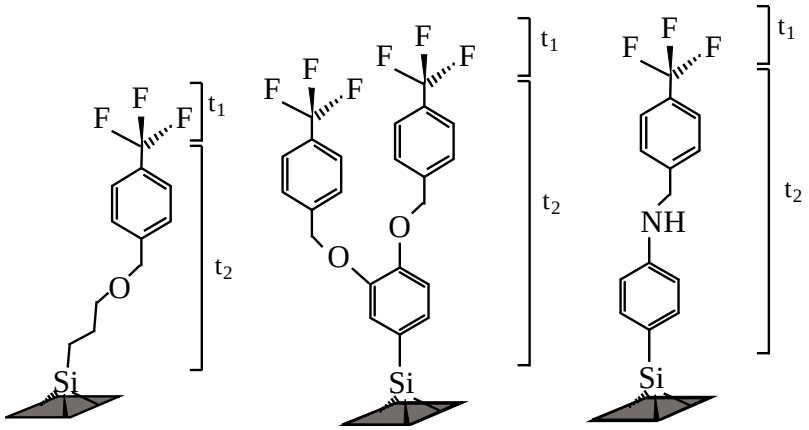

Figure 2.3 Modified Si(111) surfaces after reaction with 4-(trifluoromethyl)benzyl bromide.

Table 2.2 Monolayer Coverage and Fractional Coverage (θ) of Modified Si(111) Surfaces.

Surface	ML Coverage	θ
***1a*+TFB**	0.60	0.19
***2a*+TFB**	1.13	0.22
***2c*+TFB**	1.03	0.21
3a[a]	0.91	0.49
***3a*+TFB**	0.78	0.22
3c[a]	0.93	0.50
***3c*+TFB**	0.63	0.18

[a]Calculated with N 1s XP spectra. All other ML values calculated with F 1s spectra.

Infrared Spectroscopy

Infrared spectra were acquired using a Thermo- Fisher 6700 FT-IR spectrometer equipped with a deuterated triglycerine sulfate (DTGS) detector and a Ge hemisphere grazing angle attenuated total reflectance (GATR) accessory. P-polarized light at an incident angle of 65^{o} was applied and spectra were recorded with 4 cm^{-1} resolution and referenced to spectrum of clean Ge hemisphere.

Static Sessile Drop Contact Angle Measurements

Surface wettability was determined by recording the contact angles of water droplets formed on functionalized surfaces. CAM 100 optical contact angle meter (KSV instrument, Helsinki, Finland) and KSV software analysis package were utilized during data collection and analysis.

Surface Recombination Velocity Measurement

A custom-built microwave photoconductivity system[38, 45] was used to measure the minority carrier lifetime in Si wafer sections after various surface treatments. Float-grown Si with low resistivity (R > 13000 ohm cm) and a thickness of 0.046 cm was used exclusively for these measurements. A Continuum Minilite Nd:YAG laser operating at λ = 1064 nm was used to produce excitation pulses with a full-width at half-maximum of < 10 ns. Photoexcitation was performed on the sample side opposite of where microwave radiation was incident. The microwave source was a HP 8350B Sweep Oscillator with a 83570A module operating at a frequency of 18.670 GHz and a nominal output power of 3.16 mW. The reflected signal was measured with an Advanced Control Devices diode (ACSP2644NZ, rise time < 1 ns) connected to a Tektronix TDS 1002B digital oscilloscope. The transient responses were normalized by the reflected signal at t = 0 and plotted as '$\Delta P/P_0$'. The apparent photoconductivity lifetime, τ, was then determined from plots of $\Delta P/P_0$ vs t through a fit with a single exponential function. The explicit relation between τ and the surface recombination velocity, S, is given in Equation 2.8,[46]

$$\frac{1}{\tau} = \frac{1}{\tau_b} + \left(\frac{2S\pi^2 D}{W\pi^2 D + 2SW^2} \right)$$

Equation 2.8 Relationship Between Lifetime and Surface Recombination Velocity.

where τ_b is the bulk lifetime of the Si wafer section, D is the ambipolar diffusion constant in crystalline Si (10 cm^2 s^{-1} at T = 300 K)[47], and W is the wafer thickness. Equation 2.8 defines several important bounds. The shortest time constant (= $W^2\pi^{-2}D^{-1}$) occurs when S is infinitely large. For the materials used here, the shortest measurable value of τ is 2 x 10^{-5} s. The largest possible value of τ occurs when S = 0 cm s^{-1} and corresponds exactly to τ_b. According to the manufacturer, τ_b > 2 x 10^{-3} s for the wafers used here. All values of τ measured between these two bounds thus report on S. Since $\pi^2 D >> 2SW$ for S <10^3 cm s^{-1} for all measured samples, the following approximation was used to estimate S:

$$\frac{1}{\tau} = \frac{1}{\tau_b} + \frac{2S}{W}$$

Equation 2.9 Relationship Between Lifetime and Surface Recombination Velocity when Wafer Thickness Is Small.

3. Results

Three different surface terminations were evaluated for achieving a hydrophilic, stable, and electronically passivated surface (Figure 2.1). After etching with NH_4F(aq) and then chlorination with PCl_5 in chlorobenzene, samples were reacted with one of three Grignard reagents to achieve surfaces decorated by either an allyl group, a cyclic diether, or a bis(trimethylsilyl)amino group. We henceforth refer to these surfaces as types ***1***, ***2***, and ***3*** (Figure 2.1). These surfaces were subsequently modified by introducing Bronsted-Lowry functionality without affecting the underlying putative Si-C bond. The resultant surfaces were selectively decorated with primary alcohols, diols, and amine groups. These surfaces are henceforth denoted as types ***1a***, ***2a***, and ***3a***. The characterization and properties of each surface are described individually below.

Passivated Surface Featuring Chemisorbed Primary Alcohols (1a)

The preparation of Si surfaces decorated with allyl groups was first described by Lewis and co-workers.[48] In this work, we specifically set out to selectively oxidize the terminal olefin to a primary alcohol, i.e. the anti-Markovnikov addition of an alcohol across the '-C=C-' group. A hydroboration/hydroxylation method was employed, similar to an approach used to oxidize surface-grafted 1-decene reported previously by Cahen and co-workers.[30] That procedure was

modified for surface ***1*** by extending both hydroboration times (>5 h) and subsequent hydroxylation (20 min) as long as possible without inducing surface oxidation, as monitored by high resolution Si 2p XP spectra. These surfaces are denoted as type ***1a***. The oxide thickness inferred from the integrated intensity of the shoulder centered at 103 eV was below <0.09 nm (Figure 2.4a). Before reaction, a peak for the C=C-H stretch at 3051 cm^{-1} was observable in the infrared spectrum but was absent after reaction (Figure 2.4b). Further, analysis of GATR-IR spectra of ***1a*** resulted in a peak at 1265 cm^{-1} ascribed to COH bend of primary alcohols (Figure 2.5) and no signatures at 2500-3000 cm^{-1} that indicated oxidation to a terminal carboxylic acid group (Figure 2.6). The wetting properties of type ***1*** and ***1a*** surfaces were decidedly different, with the sessile contact angles with water of 75 ± 5° to 42 ± 3°, respectively (Table 2.3). This contact angle value for type ***1a*** surfaces is broadly in agreement with the value of 50° demonstrated by Zhong and Bernasek for Si surfaces decorated with long primary alcohols.[49] The reactivity of type ***1a*** surfaces was probed with test reagents so as to identify the predominant surface group (e.g. alcohol, carboxylic acid). Specifically, we attempted to perform both an etherification reaction with an organic halide and an esterification reaction with a primary alcohol. The hypothesis was that a surface decorated with primary alcohols is only reactive (under the employed reactions) towards organic halides for ether bond formation and wholly unreactive towards molecular alcohols. Upon reaction of ***1a*** with 4-(trifluoromethyl)benzyl bromide (TFB) as shown in Figure 2.7, a new signal was observed in the F 1s XP spectrum Figure 2.4c. Fractional coverage was calculated to be 0.19 molecules per Si atom (Table 2.2). Conversely, exposure to 2,2,3,3,4,4,5,5-octafluoro-1-pentanol (OFP) yielded no change in the recorded F 1s XP spectra (Figure 2.8). These cumulative observations strongly suggest that type ***1a*** surfaces were populated by terminal alcohol groups.

The presence of surface-based electrical traps on these two surfaces was assessed through contactless microwave photoconductivity transients (Figure 2.4 d and e). The measured value of *S* for type ***1*** surfaces was 40 ± 30 cm s^{-1}, consistent with prior estimates of *S* for allyl-terminated Si.[48, 50] The values of *S* for ***1*** slightly increased over the course of 4 days (Table 2.4). After conversion to ***1a***, the value of *S* increased significantly to 220 ± 150 cm s^{-1}, well above any *S* value measured for ***1***. However, for type ***1a*** surfaces, the values of *S* slightly *decreased* to 90 ± 50 cm s^{-1} after 4 days. Concurrently, the measured oxide thickness over the same time frame increased substantially to 0.55 nm (Table 2.5).

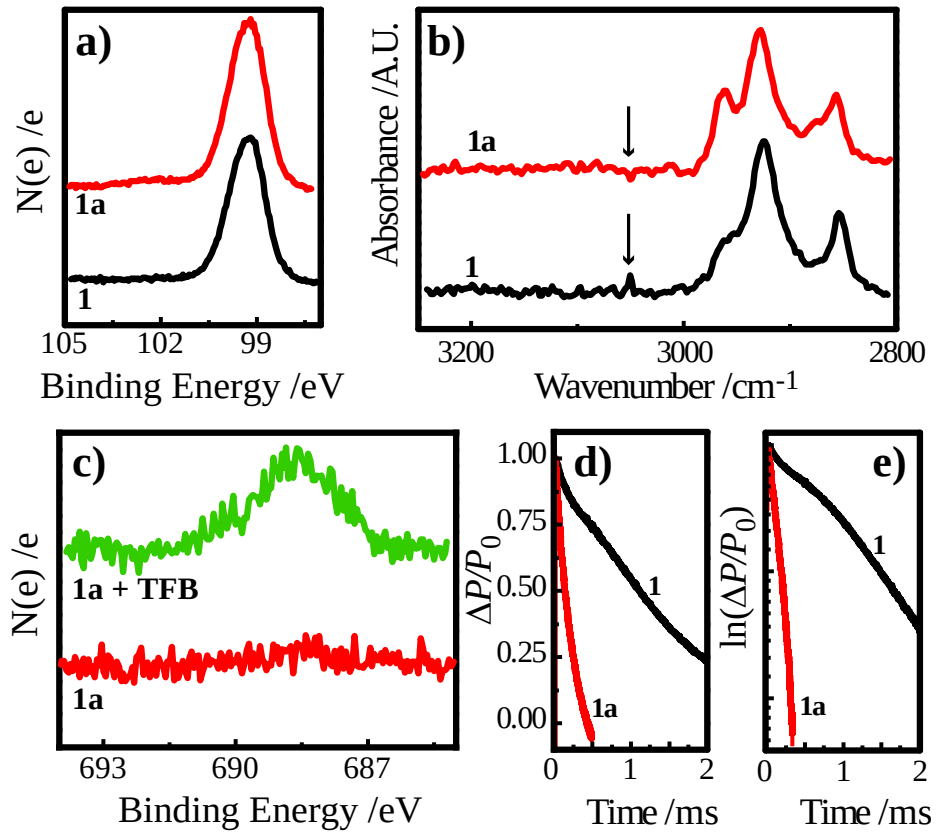

Figure 2.4 Comparison of (a) Si 2p XP and (b) infrared spectra for freshly prepared type ***1*** and ***1a*** surfaces. (c) Comparison of F 1s XP spectra before and after reaction of a type ***1a*** surface with 4-(trifluoromethyl)benzyl bromide. All spectra offset vertically for clarity. Representative microwave photoconductivity transients presented as (d) normalized and (e) natural log signal vs time.

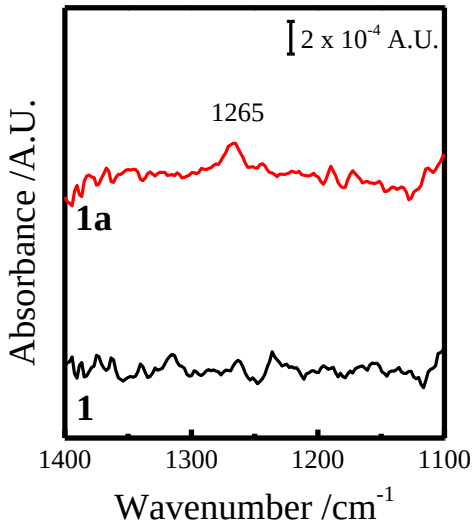

Figure 2.5 GATR-FTIR of ***1*** and ***1a*** surfaces in the COH bend region. Scale bar indicates 2 x 10^{-4} A.U. Spectra were baseline corrected and offset for clarity.

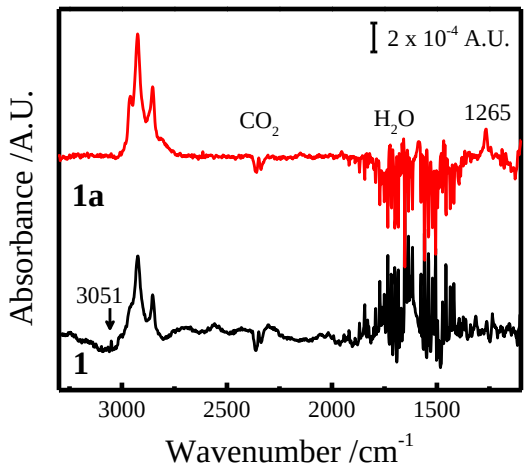

Figure 2.6 GATR-FTIR of ***1*** and ***1a*** surfaces. Scale bar indicates 2 x 10^{-4} A.U. Spectra were baseline corrected and offset for clarity.

Table 2.3 Contact Angle Data for Modified Si(111) Surfaces.

Surface Type	Number of Samples Measured	Contact Angle /°
1	10	75±5
1a	16	42±3
2	10	64±2
2a	7	57±3
2b	10	57±3
2c	4	53±4
3	11	70±6
3a	7	57±4
3b	3	76±1
3c	3	64±2

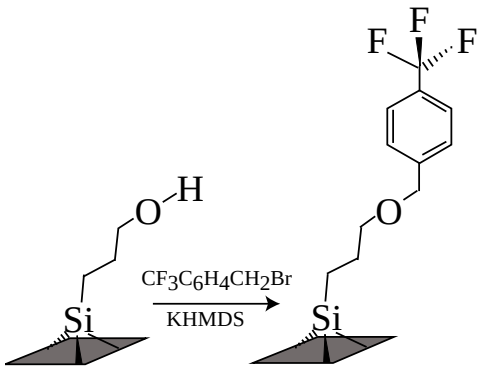

Figure 2.7 Representative etherification reaction, showing reaction ***1a*** with TFB with base promotor (KHMDS).

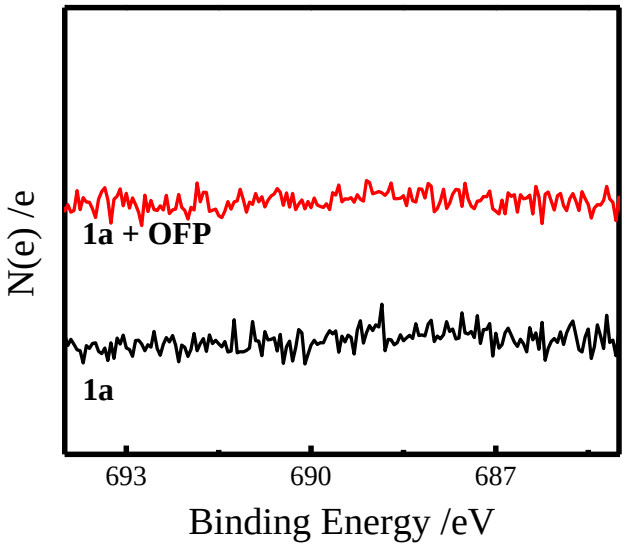

Figure 2.8 High resolution F 1s XP spectra of pristine ***1a*** (bottom) and after reaction with OFP (top). Spectra offset for clarity.

Table 2.4 Calculated SRV Values in cm s^{-1} Over Time in Ambient Conditions for N=3.

Time/hr	1	1a	2	2a	2b	2c	3	3a	3b	3c
0	40 ± 30	200 ± 150	150 ± 120	170 ± 40	75 ± 2	110 ± 40	140 ± 90	190 ± 50	190 ± 80	180 ± 90
1	40 ± 30	210 ± 170	110 ± 70	190 ± 60	82 ± 3	90 ± 20	170 ± 60	170 ± 40	140 ± 20	180 ± 100
4	40 ± 10	220 ± 150	110 ± 90	170 ± 50	130 ± 40	130 ± 60	400 ± 200	170 ± 50	210 ± 70	200 ± 120
24	70 ± 60	160 ± 120	170 ± 120	120 ± 50	120 ± 10	110 ± 50	210± 120	170 ± 70	200 ± 110	220 ±110
48	40 ± 40	150 ± 90	220 ± 170	140 ± 50	90 ± 20	100 ± 40	--	300 ± 140	160 ± 40	180 ± 80
96	70 ± 70	90 ± 50	180 ± 110	110 ± 30	100 ± 2	80 ± 40	--	350 ± 100	170 ± 80	173 ± 130

Table 2.5 Average Oxide Thickness of Modified Si(111) Surfaces in nm.

Surface	Initial	Aged 48 h
1	0.025	0.361
1a	0.050	0.550
2	0.171	0.454
2a	0.135	0.382
2b	0.051	0.045
2c	0.011	0.020
3	0.016	0.210
3a	0.018	0.033
3b	0.038	0.181
3c	0.031	0.011

Passivated Surface Featuring Chemisorbed Diols

H-terminated Si(111) was converted to a surface decorated with 3,4-(methylenedioxy)phenyl groups (type ***2*** surfaces). These surfaces could be reacted with trifluoroacetic acid without substantially increasing the surface oxide content (Figure 2.9a).

However, the wetting character became slightly more hydrophilic, decreasing from 64 ± 2° to 57 ± 3° (Table 2.3). Further, after reaction with trifluoroacetic acid, new modes corresponding to a CO stretch at 1288 cm^{-1}, an OH bend at 1198 cm^{-1}, and a CH bend at 1076 cm^{-1} in the GATR-IR spectra were observed (Figure 2.9b), consistent with deprotection of the 3,4-(methylenedioxy)phenyl groups to a 3,4-benzenediol. These type **2a** surfaces were then reactive towards 4-(trifluoromethyl)benzyl bromide. F1s XP spectra of these surfaces showed a clear signature indicative of grafted trifluoromethyl groups (Figure 2.9c). The integrated intensity of these spectra corresponded to a total fractional surface coverage of 0.22 per atop Si atom (assuming no surface roughness and each 3,4-benzenediol was functionalized with two 4-(trifluoromethyl)benzyl groups).

Because these surface groups have a large areal footprint (0.8 nm^2, assuming phenyl ring plane is perpendicular to the surface plane and freely rotates about the putative Si-C bond), a significant fraction of the available atop Si atoms remain unreacted. A mixed monolayer approach based on the premise of using CH_3- groups to occupy unreacted sites was established previously.[50-53] We sought to apply this premise on type ***2*** surfaces. Reaction of ***2*** with CH_3MgCl yielded surface ***2b*.** The measured water contact angles for ***2b*** were only slightly changed relative to ***2*** (Table 2.3). Reaction of type ***2b*** surfaces with trifluoroacetic acid (yielding type ***2c*** surfaces) and then 4-(trifluoromethyl)benzyl bromide yielded signal in the F1s the XP spectrum (Figure 2.10a) comparable to that for type ***2a***, corresponding to a fractional coverage of 0.21 surface groups per atop Si atom.

The photoconductivity transients for type ***2, 2a, 2b,*** and ***2c*** surfaces exposed to the laboratory ambient are shown in Figure 2.9 e and f. Type ***2*** surfaces showed slightly larger initial *S* values than type ***1*** surfaces (Table 2.4) but still demonstrated reasonable levels of passivation on the order of 10^2 cm s^{-1}. Over 4 days, the surface recombination velocities fluctuated with time and increased slightly for type ***2*** surfaces. Type ***2a*** surfaces exhibited *S* values measurably larger than

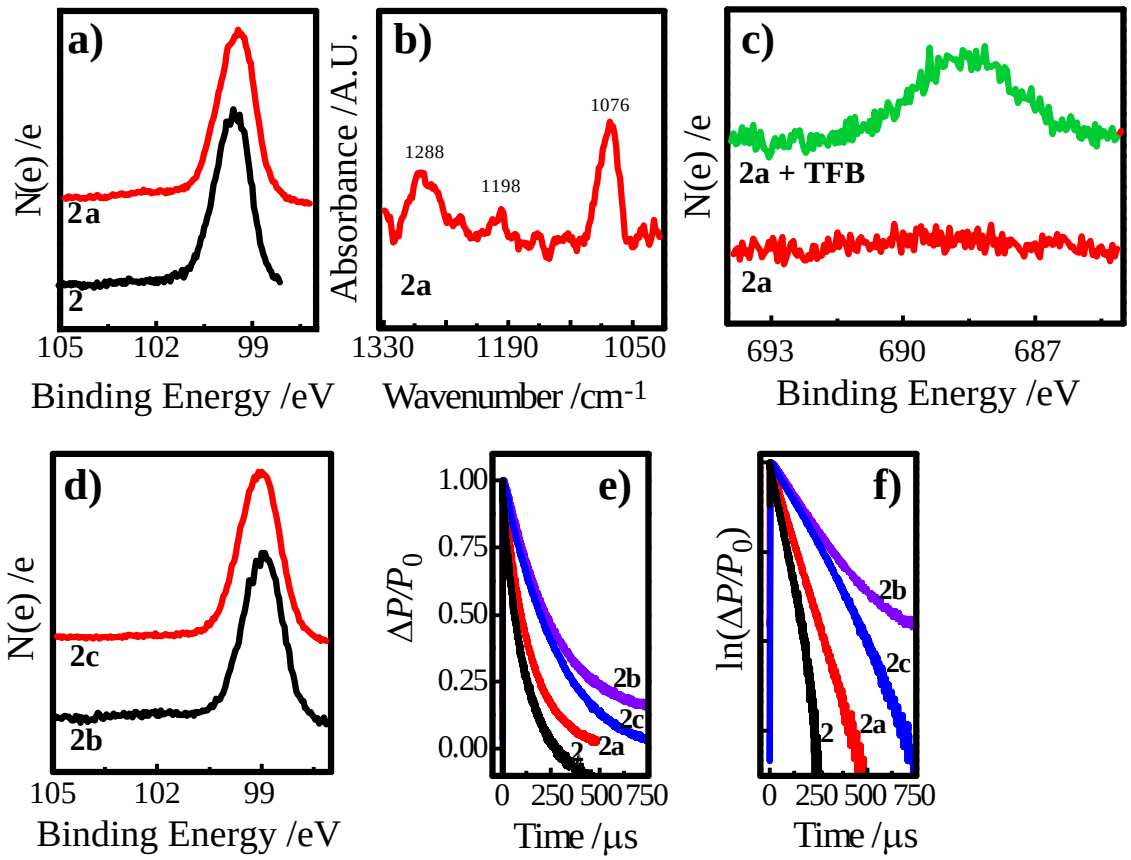

Figure 2.9 (a) Comparison of Si 2p XP spectra for freshly prepared type ***2*** and ***2a*** surfaces. (b) Infrared spectra showing the CO stretches, -OH bend, and CH bend for type ***2a*** surfaces. (c) Comparison of F 1s XP spectra before and after reaction of a type ***2a*** surface with 4-(trifluoromethyl)benzyl bromide. (d) Comparison of Si 2p XP spectra for freshly prepared type ***2b*** and ***2c*** surfaces. All spectra offset vertically for clarity. Representative microwave photoconductivity transients presented as (e) normalized and (f) natural log signal vs time.

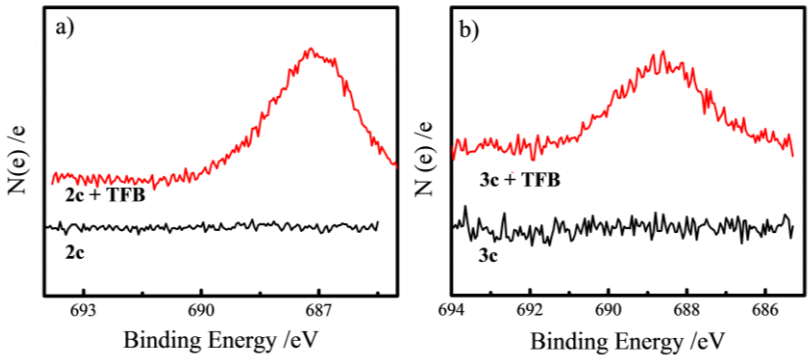

Figure 2.10 High resolution F 1s XP spectra after etherification reaction of TFB with (a) ***2c*** and (b) ***3c***.

for type ***2*** but these values *decreased* over the course of 4 days. In comparison, the methylation 'back-fill' step yielded noticeably lower *S* values for types ***2b*** and ***2c*** surfaces relative to types ***2*** and ***2a*** surfaces. Type ***2b*** surfaces (i.e. functionalized with 3,4-(methylenedioxy)phenyl and methyl groups) showed a general trend of slightly increasing surface recombination velocities over time. Conversely, type ***2c*** surfaces (i.e. functionalized with 3,4-benzenediol and methyl groups) like type ***2a*** surfaces showed *S* values that slightly *decreased* over time.

Passivated Surfaces Featuring Chemisorbed Phenylamine

Type ***3*** surfaces were prepared after reaction with 4-[bis(trimethylsilyl)amino]phenyl magnesium bromide. As-prepared **3** surfaces showed a detectable but low N 1s signal intensity. A peak at 925 cm^{-1} was observed in the IR spectrum which agreed with the Si-N stretch in trimethylsilyl groups (Figure 2.11).[54-55] Deprotection of the surface groups by reaction with acid (i.e. H- replaced the trimethylsilyl groups) resulted in type ***3a*** surfaces. These surfaces did not initially possess substantial oxide (Figure 2.12a) and the N 1s signal in the XP spectrum became more pronounced (Figure 2.12b). The integrated intensity of this signal corresponded to a fractional coverage of 0.49 phenylamine groups per atop Si atom. Further, the wettability towards water increased, with a change in the water contact angle from 70 ± 6° to 57 ± 4° (Table 2.3). In addition, a peak at 3330 cm^{-1} consistent with NH_2 symmetric stretches was now evident in the IR spectra (Figure 2.12c). After aging in ambient conditions for 48 h, types ***3*** and ***3a*** surfaces had oxide layer thicknesses of 0.21 and 0.033 nm, respectively. Type ***3a*** surfaces were selectively reactive towards 4-(trifluoromethyl)benzyl bromide, yielding a surface coverage of 0.22 grafted groups per atop Si atom (Figure 2.12d), indicating not all underlying phenylamine groups were alkylated. Reaction of ***3*** with CH_3MgCl prior to deprotection of the phenylamine groups yielded type ***3b*** surfaces. After deprotection to give type ***3c*** surfaces, the integrated intensity in the N 1s spectra corresponded to a fractional coverage of phenylamine groups of 0.5 per atop Si atom, similar to type ***3a*** surfaces. Type ***3c*** surfaces were similarly reactive towards alkylation via reaction with 4-(trifluoromethyl)benzyl bromide (Figure 2.10b), yielding a surface coverage of 0.18 grafted groups per atop Si atom. Type ***3*** surfaces exhibited an initial surface recombination velocity (100 ± 40 cm s^{-1}), which steadily increased over time. The deprotection step that converted type ***3*** to type ***3a*** surfaces increased the measured value of *S* even though the measured oxide content had not substantially increased (*vide supra*). In addition, these surfaces deteriorated significantly over

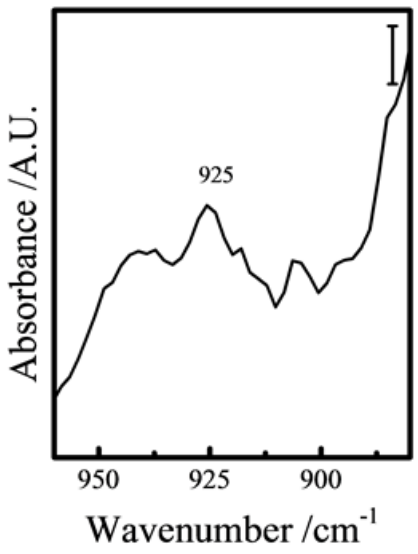

Figure 2.11 GATR-FTIR of surface ***3***. Scale bar is 1 x 10^{-4} A.U.

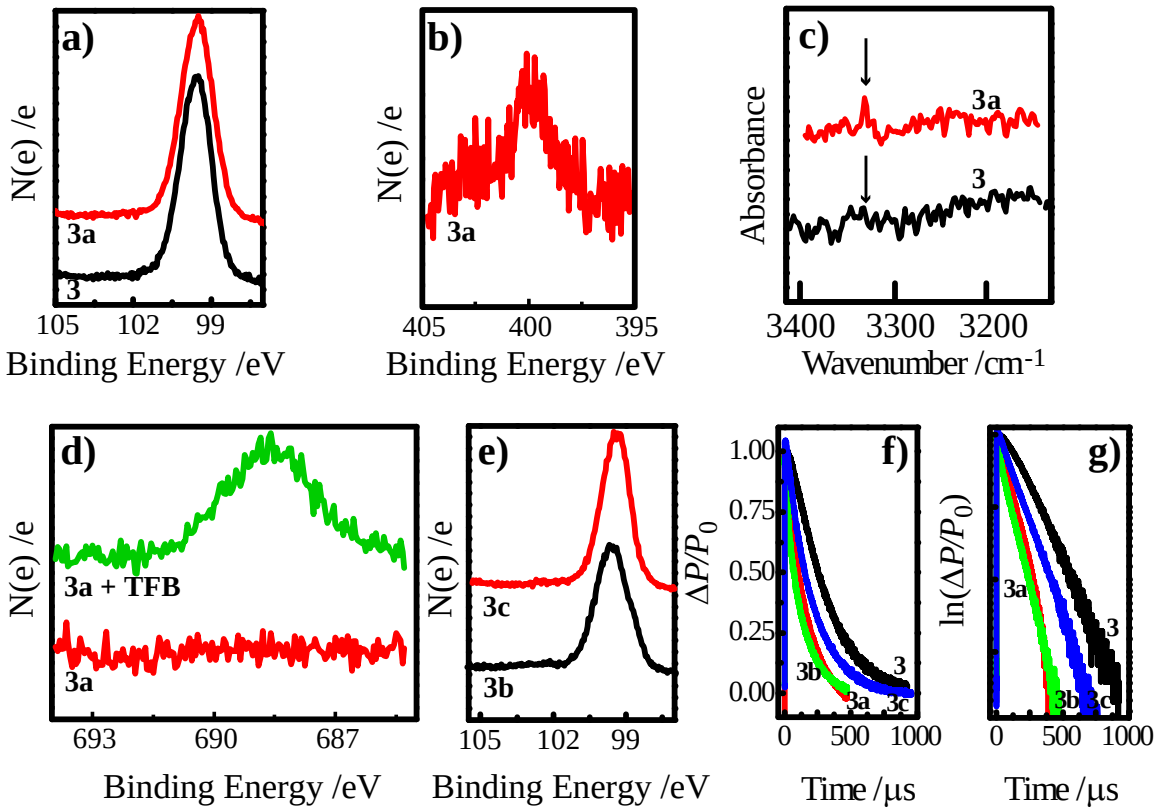

Figure 2.12 (a) Comparison of Si 2p XP spectra for freshly prepared type ***3*** and ***3a*** surfaces. (b) High resolution N1s XP spectrum of a freshly prepared type ***3a*** surface. (c) Comparison of infrared spectra for freshly prepared type ***3*** and ***3a*** surfaces. (d) Comparison of F 1s XP spectra before and after reaction of a type ***3a*** surface with 4-(trifluoromethyl)benzyl bromide. (e) Comparison of Si 2p XP spectra for freshly prepared type ***3b*** and ***3c*** surfaces. All spectra offset vertically for clarity. Representative microwave photoconductivity transients presented as (f) normalized and (g) natural log signal vs time.

4 days, yielding the largest value of *S* among all the surface types that were analyzed (345 ± 100 cm s^{-1}). Unexpectedly, type ***3b*** surfaces (i.e. functionalized with [bis(trimethylsilyl)amino]phenyl and methyl groups) did not possess lower *S* values as compared to type ***3*** surfaces either initially and after 4 days in air (Table 2.4). Steric blocking by the bis(trimethylsilyl)amino]phenyl groups may have prevented sufficient access to populate unreacted sites with -CH_3 groups. Still, type ***3c*** surfaces (i.e. functionalized with phenylamine and methyl groups) demonstrated more stable and lower values of *S* relative to type ***3a*** surfaces, implying a sufficient amount of -CH_3 groups to render some improved passivating effect.

4. Discussion

The presented data cumulatively show three separate surface types that achieve some level of chemical stability, possess proton donating/accepting character, and have low defect density. Here we discuss their respective virtues, the observed correlations between surface stability and electronic passivation, and the prospects for employing such surface chemistry to interfaces beyond Si.

Lewis and co-workers previously showed allyl-terminated Si(111) prepared by a Grignard reaction possesses surface recombination velocities ranging from 50 to 90 cm s^{-1},[48, 50] in line with what was observed here. They later proved that mixed monolayers with allyl-groups demonstrate *S* values as small as 30 cm s^{-1} if 10% of the surface is decorated with allyl groups and the remaining 90% is covered by CH_3- groups.[50] A more recent advancement by this same group was the oxidation of the fraction of allyl groups to primary aldehydes, resulting in a low defect surface amenable for ALD coating.[51] However, the wetting properties were not detailed. The type ***1a*** surfaces reported here are designed to achieve a similar goal but are simpler to prepare (i.e. fewer reaction steps) and have a defined hydrophilicity. However, the initial surface recombination velocity is decidedly higher for these type ***1a*** surfaces, which may or may not be tolerable depending on the specific application. For reference, the initial *S* value for type ***1a*** surfaces is still reasonably good compared to the native oxide of Si and is in fact on par with unannealed thermal oxides.[56] For further comparison, a recent report demonstrating Si(111) surfaces terminated with 4-trifluoromethylsulfonylbenzene exhibited surface recombination velocities of 1372 ± 30 cm s^{-1}.[57] Still, if a lower initial surface recombination velocity is necessary, surface types ***2a***, ***2c***, ***3a***, and ***3c*** are all viable options. Again, surface types ***2a*** and ***3a*** retain the practical advantage of a

minimal number of preparative steps. Further, type ***2a*** surfaces exhibit the greatest wettability towards water in comparison to surface ***3a***, a feature which may aid in coatings cast from aqueous solutions. In comparison to alkyl-terminated Si surfaces rendered hydrophilic by oxidation with oxygen-containing plasmas,[58-59] the wet chemical approach shown here is both controllable and more amenable to 'short' surface layers suited for heterogeneous charge transfer.

The surface stability and surface recombination velocities of some of the surfaces studied here tracked with time in unexpected ways. Surfaces that did not intentionally have any proton donating/accepting character (i.e. type ***1***, ***2, 2b, 3,*** and ***3b***) all exhibited surface recombination velocities that either remained statistically unchanged or slightly increased over time. This observation itself is unsurprising given these surfaces are not indefinitely stable against oxidation and the act of oxidation should introduce strained bonding that act as electronic traps. However, the majority of surfaces that did have explicit proton donating/accepting character (i.e. type ***1a***, ***2a,*** and ***2c***) had surface recombination velocities that *decreased* over time even though the underlying surface oxide layer *increased*. That is, even though these surfaces were somewhat susceptible to oxidation of the underlying substrate, the resultant oxide growth did not add significant numbers of new electrical traps. Surface type ***1a*** is a noteworthy example, as the surface oxide that grew after 24 h (0.55 nm) in air was greater than the thickness of a complete oxide monolayer on Si(111) (0.4 nm),[60] yet the measured surface recombination velocity was actually lower than the initial value. Although the present dataset does not provide any direct microscopic insight on the cause of this observation, we comment on two possibilities. First, the presence of the grafted surface groups imparted some directing effect on the growth of any new oxide. Similar arguments have been made previously for modified surfaces whose surface recombination velocities decrease over time[61-62] and there is no data to conclusively rule out this scenario. Still, since the physicochemical nature of the modifying groups in these three sets of surfaces differ significantly, an equivalent 'oxide templating' effect seems unlikely. Second, the acid/base functionality of the modified surfaces influences/introduces charge within the growing oxide. Such oxides could artificially lower the observable surface recombination velocity through charge screening.[8] A hallmark of such an effect is a strong dependence of the surface recombination velocity with illumination intensity.[8] The accessible illumination intensities were limited by the linearity of the microwave reflection method only at low charge carrier concentrations.[63] Nevertheless, we did not observe any significant dependence of the measured lifetimes with

changes in laser intensity, arguing against this possibility. Hence, additional studies are necessary to explain this curious phenomenon.

The wet chemical strategies applied here are not limited to just Si interfaces. The approaches demonstrated in this work to convert the grafted moieties into alcohols and amines should generally apply to these same groups when bonded to other semiconductors. We have shown previously that III-V semiconductor surfaces (e.g. GaAs(111)A, GaP(111)A, GaN(0001))[64-66] are reactive towards Grignard reagents and therefore these interface could be initially functionalized in a similar manner as explored here. Since the intrinsic instability of the native surfaces of these III-V semiconductors substantially complicates coating these semiconductors with either solid dielectrics[67-68] or molecular films,[69] such wet chemical methods should prove useful. Work in our group to attain similar levels of control over wetting, stability, and interfacial defect densities on III-V semiconductor surfaces is ongoing.

5. Summary

Three separate wet chemical reaction sequences were performed on Si(111) to achieve hydrophilic, chemically stable, and electronically passivated surfaces. These general features were attained although an unexpected improvement in the apparent surface recombination velocities was observed for many of the surfaces with acid/base character. These modified Si surfaces should be amenable for contacting methods such as ALD or spin-casting of solutions of oxo-clusters. With regards to ALD, these interfaces ought to provide a high number of nucleating sites during the initial deposition cycles, potentially leading to more uniform films. In the context of solution-cast oxides, the low level of initial defects and good chemical stability should improve the quality of the resultant junction. Separate studies are needed to rigorously test these hypotheses. This study adds three sets of Si surfaces to the number of interfaces that are quantitatively categorized in terms of their stability, wettability, and electrical quality. This work thus defines protocols and benchmarks so as to evaluate these surfaces in heterojunctions as well as to apply to other semiconductor interfaces.

6. References

1. Leskela, M.; Ritala, M., *Thin Solid Films* **2002,** *409* (1), 138-146.
2. Kim, H. J.; Kearney, K. L.; Le, L. H.; Pekarek, R. T.; Roses, M. J., *ACS Appl. Mater. Interfaces* **2015,** *7* (16), 8572-8584.

3. Oleksak, R. P.; Ruther, R. E.; Luo, F.; Fairley, K. C.; Decker, S. R.; Stickle, W. F.; Johnson, D. W.; Garfunkel, E. L.; Herman, G. S.; Keszler, D. A., *ACS Appl. Mater. Interfaces* **2014,** *6* (4), 2917-2921.
4. Wager, J. F.; Yeh, B.; Hoffman, R. L.; Keszler, D. A., *Curr. Opin. Solid State Mater. Sci.* **2014,** *18* (2), 53-61.
5. Masteika, V.; Kowal, J.; Braithwaite, N. S. J.; Rogers, T., *ECS J. Solid State Sci. Technol.* **2014,** *3* (4), Q42-Q54.
6. Royea, W. J.; Juang, A.; Lewis, N. S., *Appl. Phys. Lett.* **2000,** *77* (13), 1988-1990.
7. Eades, W. D.; Swanson, R. M., *J. Appl. Phys.* **1985,** *58* (11), 4267-4276.
8. Yablonovitch, E.; Allara, D. L.; Chang, C. C.; Gmitter, T.; Bright, T. B., *Phys. Rev. Lett.* **1986,** *57* (2), 249-252.
9. Titova, L. V.; Hoang, T. B.; Jackson, H. E.; Smith, L. M.; Yarrison-Rice, J. M.; Kim, Y.; Joyce, H. J.; Tan, H. H.; Jagadish, C., *Appl. Phys. Lett.* **2006,** *89* (17).
10. George, S. M., *Chem. Rev.* **2010,** *110* (1), 111-131.
11. Khaselev, O.; Turner, J. A., *J. Electrochem. Soc.* **1998,** *145* (10), 3335-3339.
12. Gerischer, H., *J. Vac. Sci. Technol.* **1978,** *15* (4), 1422-1428.
13. Price, M. J.; Maldonado, S., *J. Phys. Chem. C* **2009,** *113* (28), 11988-11994.
14. Mukherjee, J.; Erickson, B.; Maldonado, S., *J. Electrochem. Soc.* **2010,** *157* (4), H487-H495.
15. Gershenzon, M.; Mikulyak, R. M., *Appl. Phys. Lett.* **1966,** *8* (10), 245-247.
16. Stringfellow, G. B., *J. Vac. Sci. Technol.* **1976,** *13* (4), 908-913.
17. Bansal, A.; Lewis, N. S., *J. Phys. Chem. B* **1998,** *102* (7), 1067-1070.
18. Bocarsly, A. B.; Walton, E. G.; Bradley, M. G.; Wrighton, M. S., *J. Electroanal. Chem.* **1979,** *100* (1-2), 283-306.
19. Bocarsly, A. B.; Walton, E. G.; Wrighton, M. S., *J. Am. Chem. Soc.* **1980,** *102* (10), 3390-3398.
20. Bansal, A.; Li, X. L.; Lauermann, I.; Lewis, N. S.; Yi, S. I.; Weinberg, W. H., *J. Am. Chem. Soc.* **1996,** *118* (30), 7225-7226.
21. Bansal, A.; Lewis, N. S., *J. Phys. Chem. B* **1998,** *102* (21), 4058-4060.
22. Aberle, A. G., *Prog. Photovoltaics* **2000,** *8* (5), 473-487.
23. Buriak, J. M., *Chem. Rev.* **2002,** *102* (5), 1271-1308.
24. Waltenburg, H. N.; Yates, J. T., *Chem. Rev.* **1995,** *95* (5), 1589-1673.
25. Filler, M. A.; Bent, S. F., *Prog. Surf. Sci.* **2003,** *73* (1-3), 1-56.
26. Cicero, R. L.; Linford, M. R.; Chidsey, C. E. D., *Langmuir* **2000,** *16* (13), 5688-5695.
27. Sun, Q. Y.; de Smet, L.; van Lagen, B.; Giesbers, M.; Thune, P. C.; van Engelenburg, J.; de Wolf, F. A.; Zuilhof, H.; Sudholter, E. J. R., *J. Am. Chem. Soc.* **2005,** *127* (8), 2514-2523.
28. Linford, M. R.; Fenter, P.; Eisenberger, P. M.; Chidsey, C. E. D., *J. Am. Chem. Soc.* **1995,** *117* (11), 3145-3155.
29. Wasserman, S. R.; Tao, Y. T.; Whitesides, G. M., *Langmuir* **1989,** *5* (4), 1074-1087.
30. Toledano, T.; Biller, A.; Bendikov, T.; Cohen, H.; Vilan, A.; Cahen, D., *J. Phys. Chem. C* **2012,** *116* (21), 11434-11443.
31. Chhabra, B.; Bowden, S.; Opila, R. L.; Honsberg, C. B., *Appl. Phys. Lett.* **2010,** *96* (6).
32. Takato, H.; Sakata, I.; Shimokawa, R., *JJAP Part 2* **2002,** *41* (8A), L870-L872.
33. Takato, H.; Sakata, I.; Shimokawa, R., *JJAP Part 2* **2001,** *40* (10A), L1003-L1004.
34. Bansal, A.; Li, X. L.; Yi, S. I.; Weinberg, W. H.; Lewis, N. S., *J. Phys. Chem. B* **2001,** *105* (42), 10266-10277.
35. Leblanc, Y.; Fitzsimmons, B. J.; Adams, J.; Perez, F.; Rokach, J., *J. Org. Chem.* **1986,** *51* (6), 789-793.
36. Barr, T. L.; Seal, S., *J. Vac. Sci. Technol. A* **1995,** *13* (3), 1239-1246.
37. Briggs, D.; Seah, M. P., *Practical Surface Analysis*. John Wiley & Sons: Chichester, 1983.
38. Asami, K.; Hashimoto, K.; Shimodaira, S., *Corros. Sci.* **1977,** *17* (9), 713-723.
39. Wagner, C. D.; Davis, L. E.; Zeller, M. V.; Taylor, J. A.; Raymond, R. H.; Gale, L. H., *Surf. Interface Anal.* **1981,** *3* (5), 211-225.
40. Laibinis, P. E.; Bain, C. D.; Whitesides, G. M., *J. Phys. Chem.* **1991,** *95* (18), 7017-7021.

41. Sturzenegger, M.; Prokopuk, N.; Kenyon, C. N.; Royea, W. J.; Lewis, N. S., *J. Phys. Chem. B* **1999,** *103* (49), 10838-10849.
42. Pies, W., Weiss, A., *Crystal Structure Data of Inorganic Compounds*. Springer-Verlag: Berlin, 1979.
43. Allen, F. H.; Kennard, O.; Watson, D. G.; Brammer, L.; Orpen, A. G.; Taylor, R., *J. Chem. Soc., Perkin Trans. 2* **1987,** (12), S1-S19.
44. O'Leary, L. E.; Rose, M. J.; Ding, T. X.; Johansson, E.; Brunschwig, B. S.; Lewis, N. S., *J. Am. Chem. Soc.* **2013,** *135* (27), 10081-10090.
45. Eady, S. C.; Peczonczyk, S. L.; Maldonado, S.; Lehnert, N., *Chem. Commun.* **2014,** *50* (59), 8065-8068.
46. Horanyi, T. S.; Pavelka, T.; Tutto, P., *Appl. Surf. Sci.* **1993,** *63* (1-4), 306-311.
47. Rosling, M.; Bleichner, H.; Jonsson, P.; Nordlander, E., *J. Appl. Phys.* **1994,** *76* (5), 2855-2859.
48. Plass, K. E.; Liu, X. L.; Brunschwig, B. S.; Lewis, N. S., *Chem. Mater.* **2008,** *20* (6), 2228-2233.
49. Zhong, Y. L.; Bernasek, S. L., *Langmuir* **2011,** *27* (5), 1796-1802.
50. O'Leary, L. E.; Johansson, E.; Brunschwig, B. S.; Lewis, N. S., *J. Phys. Chem. B* **2010,** *114* (45), 14298-14302.
51. O'Leary, L. E.; Strandwitz, N. C.; Roske, C. W.; Pyo, S.; Brunschwig, B. S.; Lewis, N. S., *J. Phys. Chem. Lett* **2015,** *6* (4), 722-726.
52. Lattimer, J. R. C.; Brunschwig, B. S.; Lewis, N. S.; Gray, H. B., *J. Phys. Chem. C* **2013,** *117* (51), 27012-27022.
53. Li, F.; Basile, V. M.; Pekarek, R. T.; Rose, M. J., *ACS Appl. Mater. Interfaces* **2014,** *6* (22), 20557-20568.
54. Smith, A. L., *Spectrochim. Acta* **1960,** *16* (1-2), 87-105.
55. Badawi, H. M.; Forner, W.; Ali, S. A., *Spectrochim. Acta A Mol. Biomol. Spectrosc.* **2013,** *112*, 388-396.
56. Opsal, J.; Taylor, M. W.; Smith, W. L.; Rosencwaig, A., *J. Appl. Phys.* **1987,** *61* (1), 240-248.
57. Seo, J.; Kim, H. J.; Pekarek, R. T.; Rose, M. J., *J. Am. Chem. Soc.* **2015,** *137* (9), 3173-3176.
58. Rosso, M.; Giesbers, M.; Schroen, K.; Zuilhof, H., *Langmuir* **2010,** *26* (2), 866-872.
59. Aureau, D.; Morscheidt, W.; Etcheberry, A.; Vigneron, J.; Ozanam, F.; Allongue, P.; Chazalvielt, J. N., *J. Phys. Chem. C* **2009,** *113* (32), 14418-14428.
60. Kobayashi, Y.; Sugii, K., *J. Vac. Sci. Technol.* **1992,** *10* (4), 2308-2313.
61. Webb, L. J.; Lewis, N. S., *J. Phys. Chem. B* **2003,** *107* (23), 5404-5412.
62. Nemanick, E. J.; Hurley, P. T.; Brunschwig, B. S.; Lewis, N. S., *J Phys Chem B* **2006,** *110* (30), 14800-8.
63. Kunst, M.; Beck, G., *J. Appl. Phys.* **1986,** *60* (10), 3558-3566.
64. Mukherjee, J.; Peczonczyk, S.; Maldonado, S., *Langmuir* **2010,** *26* (13), 10890-10896.
65. Peczonczyk, S. L.; Mukherjee, J.; Carim, A. I.; Maldonado, S., *Langmuir* **2012,** *28* (10), 4672-4682.
66. Peczonczyk, S. L.; Brown, E. S.; Maldonado, S., *Langmuir* **2014,** *30* (1), 156-164.
67. Granados-Alpizar, B.; Muscat, A. J., *Surf Sci.* **2011,** *605* (13-14), 1243-1248.
68. Delabie, A.; Brunco, D. P.; Conard, T.; Favia, P.; Bender, H.; Franquet, A.; Sioncke, S.; Vandervorst, W.; Van Elshocht, S.; Heyns, M.; Meuris, M.; Kim, E.; McIntyre, P. C.; Saraswat, K. C.; LeBeau, J. M.; Cagnon, J.; Stemmer, S.; Tsai, W., *J. Electrochem. Soc.* **2008,** *155* (12), H937-H944.
69. Chitambar, M.; Wang, Z. J.; Liu, Y. M.; Rockett, A.; Maldonado, S., *J. Am. Chem. Soc.* **2012,** *134* (25), 10670-10681.

CHAPTER 3

Improvement in Adhesion Properties of SU8 Photoresist Layers on Functionalized Si(111) Surfaces

This chapter represents work from a collaboration between the Maldonado and Chen groups. Dr. Eli Fahrenkrug (Maldonado Group) performed adhesion measurements and Dr. John Myers (Chen Group) collected SFG spectra.

1. Introduction

Photolithography is a fundamental processing step for microfabrication of many optical, mechanical, and electronic devices.[1] It is used to develop features on metal and semiconductor substrates using a light sensitive polymer film, photoresist. In most cases a photoresist template is first patterned onto a substrate for material deposition or etching, and later removed. Whereas in other applications, the photoresist comprises a permanent structure of the device.[2-4] Photoresists consisting of epoxy monomers are commonly used. During the development step, cross-linking via the epoxy groups results in a three-dimensional covalent network that gives the material its structural stability.

Bisphenol A novolac epoxy in gamma-butyrolactone (SU8) is an example of a popular photoresist where each monomer unit is made of eight epoxy groups. SU8 is routinely used as structural component in microelectromechanical systems (MEMS) due to its low cost, the possibility of forming high aspect ratios once cured, ease of processing, good chemical stability, and biocompatibility.[1, 5-9]

Although cross-linked SU8 polymers themselves are both chemically and mechanically robust, the substrate-SU8 interface is sensitive to environmental conditions, i.e. humidity and temperature.[10-11] When the substrate is a silicon (Si) wafer, the adhesion of SU8 is particularly

poor when wet.[9, 12-13] Film delamination takes places, resulting in buckling and/or blister formation.[14]

The adhesion between a photoresist and a substrate can be broadly characterized by two forms of interactions. Induced interactions due to Van der Waals forces' and/or coulombic forces due to permanent differences in polarity or surface charge.[15] Various treatments have been developed to augment photoresist adhesion. For example, oxygen plasma etching is often used to remove adventitious residues to ensure an intimate contact.[16] Additionally, photoresist primers can change surface hydrophilicity to favor uniform film formation. Finally, reactive ion etching has been used to form pits for mechanical interlocking of the photoresist and the substrate.[17-18]

For a silicon-SU8 device interface, a common pretreatment involves spin casting a hexamethyldisilazane (HMDS) primer. During HMDS pretreatment, Si substrates are cleaned and chemically etched to generate hydroxyl surface moieties. When freshly etched wafers are exposed to HMDS, -Si(CH_3)$_3$ are grafted through surficial hydroxyl groups.[19] The terminal trimethylsilyl groups of the resultant HMDS layer accomplish two objectives. First, a hydrophobic layer is generated allowing for wetting of SU8 and subsequent development. Second, the bulky methylsilane groups serve to block solvent species like water molecules from penetrating the substrate-photoresist interface.[20] Unfortunately, this is not a permanent solution as HMDS delaminates eventually.[21] The failure mechanism is at the underlying surface attachment, where cleavage of Si-O-Si bonds at the interfaces occurs through hydrolysis.[22-23]

In this work we propose an alternative method for Si surface modification to improve the adhesion of SU8 films on Si(111) wafers. Our work focuses on replacing the HMDS treatment by introducing an organic monolayer bonded at the surface through silicon-carbon (Si-C) framework, hence alleviating the issues associated with hydrolyzation. Monolayers tethered through Si-C bonds are robust, capable of withstanding both acidic/alkaline treatments[24] and high temperatures.[25] Additionally, control of terminal functional groups can be achieved. This aspect allows for tailoring the degree of interaction between the silicon substrate and a photoresist layer, further facilitating strong adhesion. To introduce Si-C bonding at the surface, this work describes using a well established chlorination-Grignard reaction sequence for alkylation of Si(111) surfaces.[26-28] A H-terminated Si surface exposed to a chlorinating reagent (PCl_5) in the presence of a radical initiator leads to a formation of surface Si-Cl bonds. Treatment of the chlorinated Si

surface in a Grignard (*R*MgX) reagent solution produces *R*-terminated surface with surface Si-C bonds. Herein, the *R* groups of interest are terminal alkenes. Reacted surfaces were characterized with X-ray photoelectron spectroscopy and infrared spectroscopy. Buried interfaces were characterized by sum frequency generation (SFG) vibrational spectroscopy. The adhesion strength was probed with nanoindentation and the chemical stability was tested by aging samples in alkaline solutions.

2. Experimental

Materials and chemicals

All chemicals were purchased from Sigma-Aldrich and used as received unless noted otherwise. Methanol (anhydrous >99.8%), dichloromethane (anhydrous > 99.8%), chlorobenzene (Across, 99.8%), tetrahydrofuran (THF) (anhydrous ≥ 99.9%, inhibitor free), acetone (Fisher, HPLC grade), hexanes (Macro Chemicals, ACS grade), phosphorous (V) chloride and 40% ammonium fluoride (Transene Electronic Chemicals, semiconductors grade). Methylmagnesium chloride (3.0 M in THF), allylmagnesium bromide (2.0 M in THF) and 4-pentenylmagenesium bromide (0.5M in THF) were used as received. Benzoyl peroxide (Fluke, ≥ 97%) was dried under a vacuum of < 200mTorr for 24h and placed in the nitrogen-atmosphere glovebox. Water with a resistivity of 18.2 $M\Omega cm^{-1}$ (Barnsted Nanopure system) was used during all sample preparation. Silicon (111) substrate, n-doped, was purchased from Wafer Works Corp with a thickness of 525 ± 15μm.

Chemical Functionalization

Samples were cut into 0.5 cm by 0.5 cm squares. Si wafers were degreased via sonication for 5 min each in hexanes, acetone, methanol, and water. Prior to functionalization, surfaces were etched in 40% NH_4F solution (5 min), rinsed with water, and dried using N_2 gas. Following etching, wafers were promptly transferred to a nitrogen-purge glove box, where the surfaces were chlorinated at 90 °C for 50 min using a saturated solution of phosphorous (V) pentachloride in chlorobenzene and a few grains of benzoyl peroxide. Upon completion, samples were washed with THF and transferred to reaction vessels to which appropriate Grignard reagents were added. All Grignard reactions were carried out at 100 °C for 12 hours. In ambient conditions selected samples were reacted with HBr in dichloromethane (1:1 v/v) solution in the presence of benzoyl peroxide

at room temperature for 1 h. Samples were rinsed and sonicated with dichloromethane to remove any residual bromine.

Photolithography

SU8 2007 (Microchem Corp.) was spin-coated over functionalized Si wafer samples and soft-baked at 95 C for 3 min on a hot plate. Nanoindentation and SFG samples were exposed to the UV source (OAI) for 13 s at 26 Wcm^{-2} without a photomask to create a 10 μm thick continuous SU8 film. Samples for chemical adhesion testing were patterned with a 10 x 10 um hole array photomask to allow electrolyte to reach the SU8/Si interface. All substrates were then subject to a post-exposure bake at 95 C for 5 min on a hot plate. Development for 5 min under agitation with SU8 developer (Microchem Corp) removed unexposed regions of the photoresist. Samples were then rinsed in isopropanol and dried under N_2 (g).

X-ray Photoelectron Spectroscopy

Prepared surfaces before and after bromination where characterized by X-ray photoelectron (XP) spectroscopy. Elemental composition was collected using a PHI 5400 analyzer equipped with Al K α (1486.6 eV) source, without a monochromator. Data collection took place at a pressure of < 2.5 x 10^{-9} Torr, without the need for charge neutralization due to the natural conductivity of the samples. A 6 mA current emission and a 12 kV anode high tension were used. High resolution spectra were collected at pass energy of 23.5 eV. All binding energies were referenced to the expected binding energy for adventitious carbon (284.6 eV). Spectrum analysis was performed with CASA XPS 2.3.13 software. Surface coverage after each bromination reaction was calculated using a simplified substrate/overlayer model.

Infrared Spectroscopy

Infrared spectra were acquire using a Thermo-Fisher 6700 FT-IR spectrometer equipped with a deuterated triglycerine sulfate (DTGS) detector. Spectra were acquired in a N_2-purge sample compartment. All spectra were recorded between 400-4000 cm^{-1} (4 cm^{-1} spectral resolution) with an incident IR beam angle of 75º off normal. The H-terminated silicon surfaces, as well surfaces containing native oxide, were used as a reference.

Nanoindentation

A Hysitron TI950 Triboindenter equipped with a diamond Berkovich tip was used to measure force-displacement curves during delamination of SU8 films from Si surfaces. Nanoindendation was conducted in load-controlled feedback mode for the lowest loads where an abrupt change in displacement was observed. The inflection was taken as the onset of film delamination as described for similar systems elsewhere.[14] Ten separate indents were collected at various points over each sample surface.

Chemical Stability

Chemical stability of prepared samples was assessed by aging samples in alkaline solutions (pH 11.3). Optical images were taken at t = 0h and t = 72 h.

Sum Frequency Generation Vibrational Spectroscopy

All SFG spectra were acquired using a commercial infrared frequency scanning SFG spectrometer purchased from EKSPLA. Details about the SFG spectrometer can be found elsewhere. A picosecond Nd:YAG laser (λ = 1064 nm, 50 Hz repetition rate, ~30 ps pulse duration) was used to pump an optical parametric generation/optical parametric amplification/difference frequency generation (OPG/OPA/DFG) system. Homodyne-detected SFG spectra were acquired from buried Si(111)/SU-8 interfaces using a 'sandwich' geometry where a ~500 nm thick SU-8 film was cured between a Si(111) surface and a fused silica or calcium fluoride window. The vertical plane of the collinear input visible and infrared beams was placed along the Si(111) $1\bar{1}0$ direction. The input angles of the overlapped visible and infrared beam were 60° and 51° versus the Si(111) surface normal, respectively. The input visible and infrared beam pulse energies were ~10 and ~90 μJ, respectively. All SFG spectra were acquired using the SSP polarization combination (s-polarized SFG beam, s-polarized visible beam, p-polarized infrared beam).

The beam intensity measured in homodyne-detected SFG spectra was proportional to the square of the effective second order nonlinear optical susceptibility ($\chi_{eff}^{(2)}$) and to the intensities of the input laser beams:

$$I_{SFG} \propto \left|\chi_{eff}^{(2)}\right| I_{IR} I_{vis}$$

Equation 3.1 Beam Intensity Relationship.

where I_{SFG}, I_{IR}, and I_{vis} are the intensities of the generated SFG beam, the input infrared beam, and the input visible beam, respectively. The resonant and non-resonant components of the measured effective second order nonlinear optical susceptibility were determined by fitting all spectra using a sum of Lorentzian functions:

$$\chi_{eff}^{(2)} = \chi_{NR}^{(2)} + \chi_{R}^{(2)} = \sum_{q} \frac{A_q}{\omega - \omega_q + i\Gamma_q}$$

Equation 3.2 Effective Second Order Nonlinear Optical Susceptibility.

where $\chi_{NR}^{(2)}$ and $\chi_{R}^{(2)}$ are the non-resonant and resonant contributions to $\chi_{eff}^{(2)}$, respectively, and A_q, ω_q, and Γ_q are the amplitude of the resonant term, frequency of the q_{th} vibrational mode, and damping factor, respectively. The non-resonant contribution to the detected SFG signal will be dominated by a non-resonant background arising from the silicon (111) substrate and can be modeled as having a fixed amplitude and phase at all input infrared frequencies.

3. Results

Surface Functionalization

A chlorination, Grignard reaction sequence was used to introduce surface functionalities on Si(111).[26] Three unique monolayers were examined, consisting of the following units; allyl, 1-pentene and methyl (Figure 3.1). The double bond functionality was verified by treating the surfaces with hydrobromic acid in the presence of benzoyl peroxide. XP spectroscopy was used to characterize the surfaces after the bromination reaction (Figure 3.2). High resolution Br 3d spectrum showed a signal at 70eV corresponding to Br 3d. Using a simplified over-layer model and Br 3d XP signal, surface fractional coverage for alkene terminated monolayers was approximated to be 10-15%. Br signal was not detected on methyl terminated surfaces.

Infrared spectroscopy

Infrared spectroscopy was also used to confirm the presence of surface functionalities after a chlorination-Grignard reaction. Figure 3.3a depicts infrared spectra for Si(111) reacted with

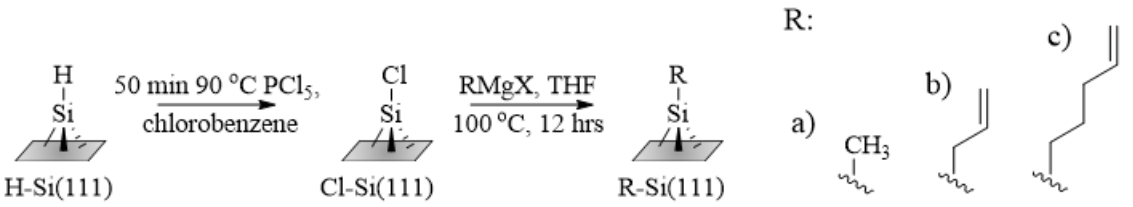

Figure 3.1 Reaction scheme for the formation of organic monolayers on silicon; R: a) methyl, b) allyl, and c) pentenyl.

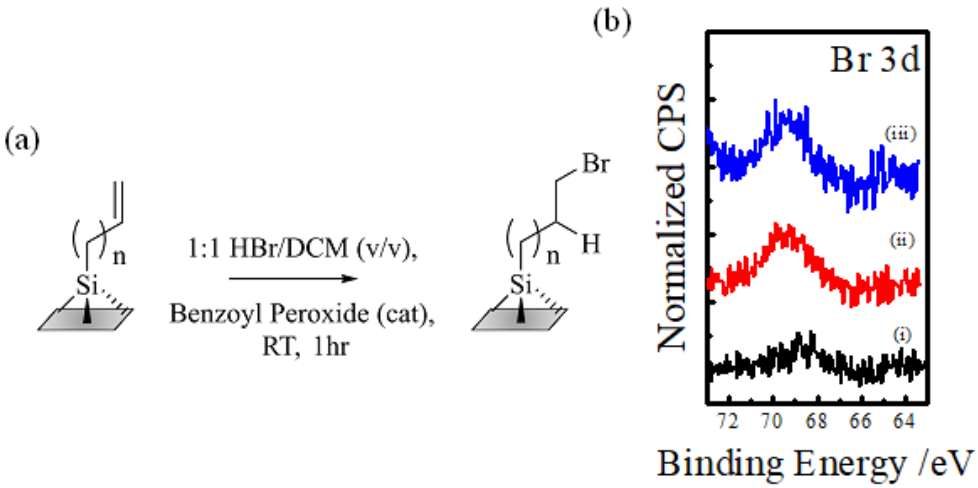

Figure 3.2 (a) Bromination of silicon surface. (b) High resolution Br 3d XP spectra of silicon surfaces reacted with HBr in dichloromethane for 1hr.;(i) methyl terminated, (ii) allyl terminated and (iii) pentenyl terminated surfaces.

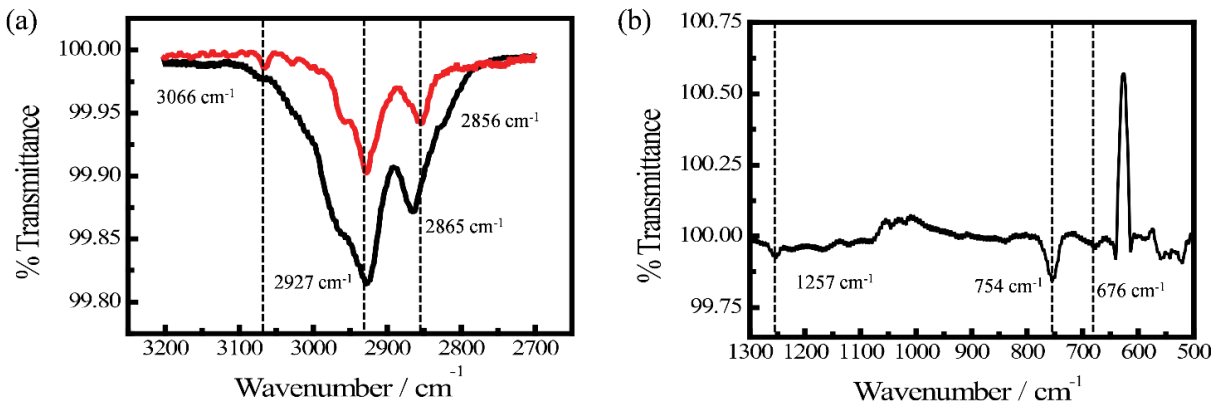

Figure 3.3 Transmission infrared spectra for functionalized Si(111) surfaces. (a) Allyl terminated Si(111) surface (red) and pentenyl terminated Si(111) surface (black). Spectra referenced to a native oxide silicon surface. (b) CH_3 terminated Si(111) surface. Spectrum referenced to freshly etched Si-H terminated surface.

allylmagnesium bromide (red) and 4-pentenylmagnesium bromide (black). After functionalization a peak at 3066 cm^{-1} was detected corresponding to C=C-H stretch. Additionally, peaks at 2927 cm^{-1} and 2856 cm^{-1} all correspond to asymmetric and symmetric CH_2 stretching vibration, respectively.[29-30] Figure 3.3b depicts infrared spectrum for Si(111) reacted with methylmagnesium chloride. The peak centered at 1257 cm^{-1} was assigned the Si-CH_3 umbrella mode, while peaks at 754 cm^{-1} and 676 cm^{-1} corresponded to Si-CH_3 rocking mode and Si-C stretch mode, respectively.[31] The inverse peak at 626 cm^{-1} corresponded to a Si-H bend mode. After functionalization, this peak was no longer present.

Nanoindentation

To measure the force necessary for film delamination, nanoindentation was performed on functionalized and bare Si surfaces. Figure 3.4 depicts the force-displacement responses for SU8 films observed prior to delamination that was induced by a nanoindentation probe. Film delamination is taken as the abrupt change in force-displacement curve, where the local maximum denotes buckling of the film (i.e. blister formation).[14] The average force needed to induce delamination for HMDS-treated Si was 715 ± 1.1 mN, for allyl-terminated Si was 834 ± 4.7 mN, and for pentenyl-terminated Si was 504 ± 10.3 mN (Table 3.1).

Chemical Stability.

The chemical stability of functionalized Si-SU8 interfaces was tested by immersing samples in alkaline (pH 11.3) solutions. Figure 3.5 shows optical images of samples before and after immersion. After 72 h, SU8 films on a bare Si and HMDS samples were almost completely detached, with the patterned SU8 film floating in solution. Large portions of the film flaked off during the rinse step. In strong contrast, Si functionalized with terminal alkenes remained optically unchanged.

Characterization of the buried Si (111)-SU8 Interface.

Infrared-visible SFG vibrational spectroscopy was used to characterize the molecular structure at buried Si(111)-SU8 interfaces to correlate interfacial molecular structures to interfacial adhesion properties (Figure 3.6).

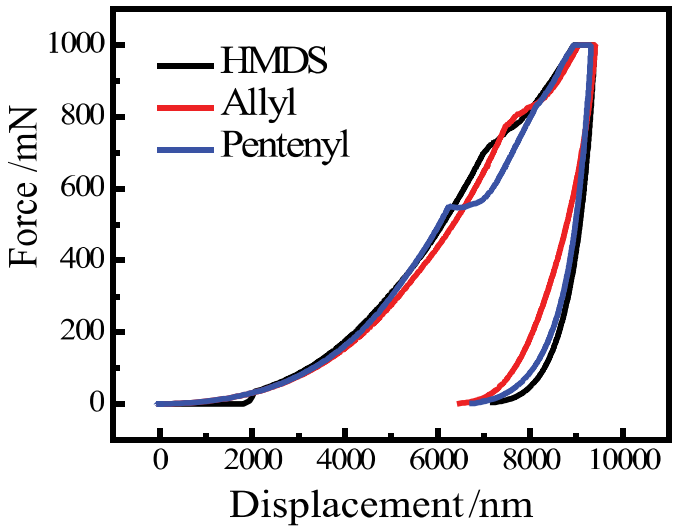

Figure 3.4 Load-displacement profiles of functionalized Si/SU8 interfaces.

Table 3.1 Summary of measured force necessary for film delamination.

Interface	Force/ mN
HMDS	715 ±1.1 %
Allyl	834 ± 4.7 %
Pentenyl	504 ± 10.3 %

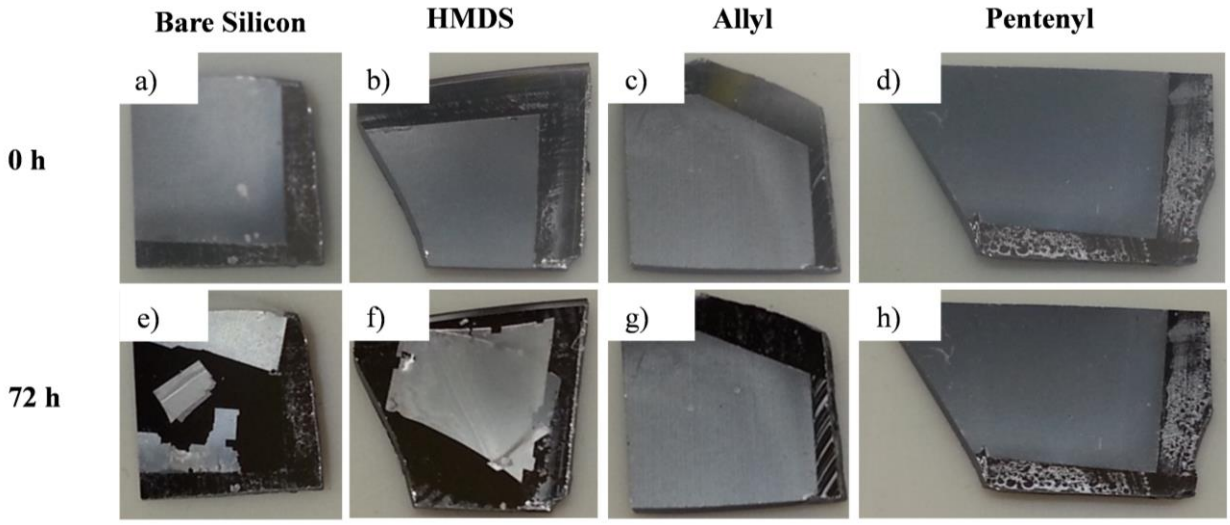

Figure 3.5 Chemical Stability of functionalized Si/SU8 interfaces after soaking in pH 11.3 buffer for 72h.

SFG spectra were acquired from the pristine Si(111)-SU8 interface (Figure 3.6b). Three peaks near 2880, 2915, and 2965 cm^{-1} were detected which can be assigned to the methyl C-H symmetric, methylene C-H asymmetric, and methyl C-H asymmetric stretching vibrational modes, respectively. The detection of peaks in the SFG spectrum acquired from the pristine Si(111)-SU8 buried interface indicates that methyl and methylene groups on the SU8 cross-linked structure were ordered at the Si (111) interface. No strong features were detected near 2990 cm^{-1} which suggests that little to no epoxide groups were present at the interface. Therefore, all or most of the epoxide groups had undergone ring-opening reactions or the epoxide groups were randomly oriented at the buried interface. In addition, the signal contributed by the methyl C-H asymmetric stretching vibrational mode was stronger than the symmetric stretching vibrational mode which indicates that the methyl groups were oriented with the primary axis lying partially parallel to the Si(111) surface.

To confirm that the measured SFG intensity was dominated by contributions from the buried Si (111)-SU8 rather than the silica/SU8 interface, SFG spectra were acquired from a silica-Si(111)-SU8 system where the SU8 thickness was ~10 μm. Using a thick film would result in substantial attenuation of the infrared beam power and would thus limit SFG signal generation from the buried Si(111)-SU8 interface. No SFG signal was detected in the 2700-3100 cm^{-1} input infrared frequency when a thick SU8 film was used, indicating that silica/SU8 did not contribute to SFG spectra acquired using the 'sandwich' geometry.

SFG spectra were then acquired from a Si(111)/SU8 buried interface where the Si(111) surface was treated with HMDS (Figure 3.6c). Four peaks were detected in the SFG spectra near 2880, 2915, 2950, and 2965 cm^{-1} which can be assigned to the methyl C-H symmetric, methylene C-H asymmetric, methyl Fermi resonance, and methyl C-H asymmetric stretching vibrational modes, respectively. Unlike at the pristine Si(111)SU8 interface, SFG spectra acquired from Si(111)HMDS-SU8 interfaces where the silicon was functionalized can contain contributions from the HMDS layer and the SU8. However, the SFG signal intensity contributed by the functionalized interface was substantially stronger than the corresponding intensity from the pristine interface which indicates that the HMDS strongly contributed to the signal or induced ordering of the SU8 structure in contact with the HMDS. No discernable peak near 2990 cm^{-1} was detected which again indicates that the epoxide cross-linking reactions were nearly complete.

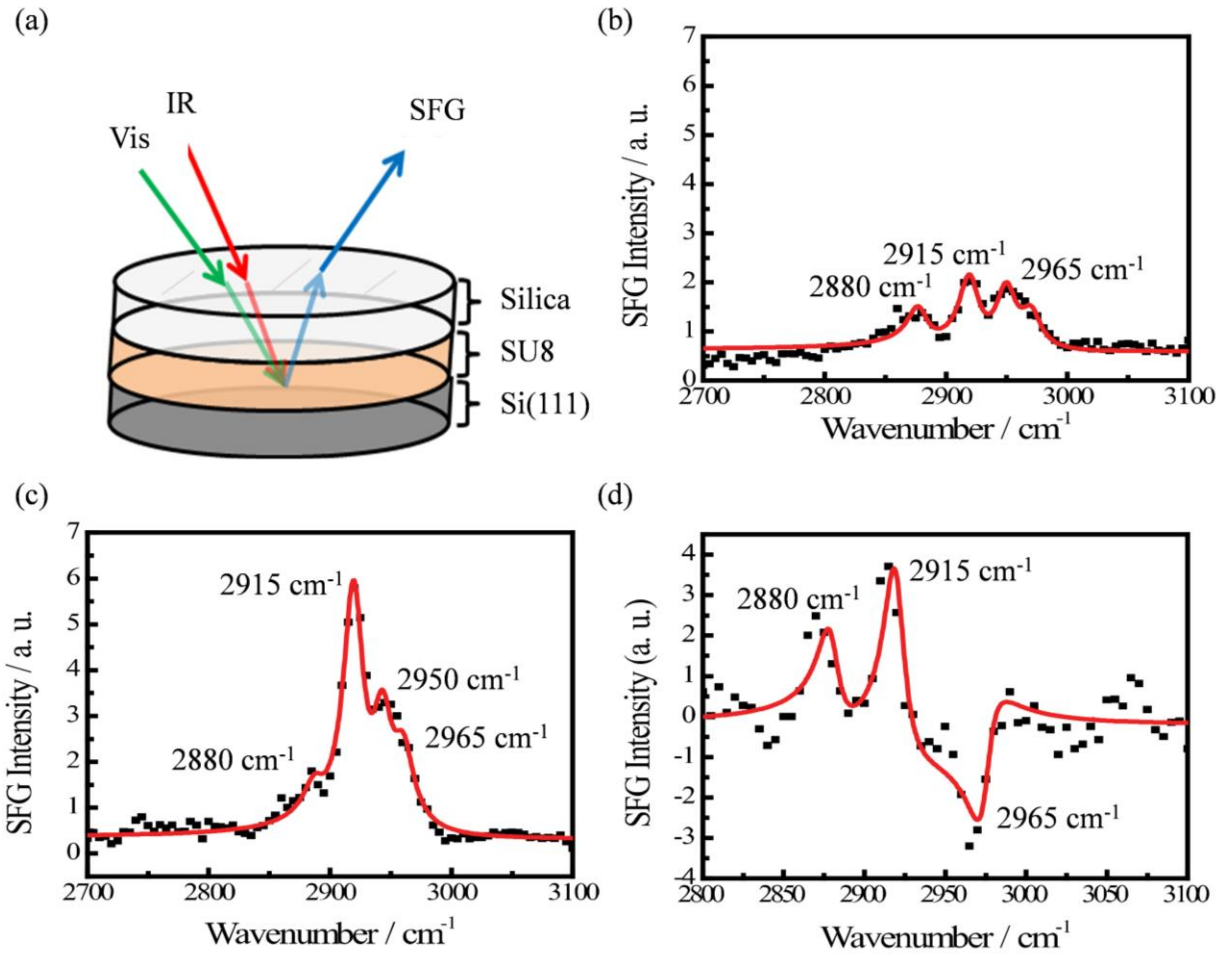

Figure 3.6 (a) Experimental geometry used to acquire SFG spectra from buried Si-SU8 interfaces. SFG spectra for the (b) Si(111)-SU8, (c) Si(111)-HMDS-SU8, (d) Si(111)-pentenyl-SU8 interfaces.

The buried interfaces between alkene functionalized silicon surfaces and SU8 were then characterized (Figure 3.6d). Three peaks near 2880, 2915, and 2965 cm^{-1} were detected in the SFG spectrum acquired from the pentenyl functionalized interface which can be assigned to the methyl C-H symmetric, methylene C-H asymmetric, and methyl C-H asymmetric stretching vibrational modes, respectively. The pentenyl group does not contain methyl groups which indicates that methyl groups on the SU8 backbone were ordered at the buried interface. The methyl asymmetric feature appeared as a dip in the spectrum rather than as a peak. The shape of peaks in homodyne-detected SFG spectra where a non-resonant background is present has been studied and details can be found elsewhere. Briefly, interference between the non-resonant background and resonant components of the effective nonlinear susceptibility can result in features appearing as peaks or dips in SFG spectra. The peak centers found by fitting the experimental data are the frequencies of specific vibrational modes which enables selective detection of functional groups at interfaces.

No SFG peak near 3000 cm^{-1} was observed suggesting that no alkene functional groups were present at the buried interface or that the groups were randomly distributed. Considering that the alkene groups were the terminal groups of the organic monolayer after the Grignard reaction, they should be ordered and oriented nearly perpendicular to the silicon surface. Therefore, the SFG results indicate that alkene groups had undergone a chemical reaction during the SU8 curing process. To further monitor the alkene group, SFG spectra were acquired in the 1300-1800 cm^{-1} range which eliminates possible spectral interferences from methyl and methylene functional groups. Therefore, the lack of detected SFG signal at ~1400 cm^{-1} supports the conclusion that alkene groups had undergone a chemical reaction at the buried interface.

Similar to the pentenyl functionalized interface, three peaks near 2880, 2915, and 2965 cm^{-1} were detected in the SFG spectrum acquired from the allyl functionalized interface which can be assigned to the methyl C-H symmetric, methylene C-H asymmetric, and methyl C-H asymmetric stretching vibrational modes, respectively. In addition, no alkene groups were detected at the allyl functionalized buried interface which again suggests that the alkene groups underwent a chemical reaction during the SU8 curing.

4. Discussion

Manipulation of inorganic semiconductor surface properties is critical in photolithographic applications, specifically during photoresist development step. Surface pretreatment either through cleaning, etching or priming will govern properties such as film homogeneity and adhesion.[32-34] In this work the nature of the priming layer, the method of surface attachment, and the consequent adhesion were explored. The data presented here speaks to the following points and how they impact film adhesion. First, chemical structure of the monolayer can be tailored to improve adhesion. Second, organic monolayers formed through surface Si-C bonds are robust in aqueous conditions, hence assisting in prolonged adhesion.

The chemical structure of the monolayer is tailorable, and it will impact overall photoresist adhesion. Both allyl (Si-CH_2CHCH_2) and pentenyl (Si-$CH_2CH_2CH_2CHCH_2$) monolayers consist of terminal alkene groups but, the carbon chain length is different. The methyl monolayer in contrast, consists of single CH_3 groups (Si-CH_3). By selecting these three monolayers comparisons are possible regarding the overall photoresist adhesion based on; (1) the importance of surface coverage or packing density and (2) the influence of surface functionality.

According to the nanoindentation experiments, allyl-terminated Si surfaces required the greatest amount of force necessary for film delamination, even in comparison to HMDS treated surfaces. A possible trend is observed for allyl and pentenyl surfaces regarding measured force. This trend can be attributed to surface coverage. The relative size of allyl groups is smaller in comparison to pentenyl functionalities which leads to higher surface coverage. It is possible that having a greater number of functional surface groups could favor interaction between the SU8 film and Si. Si surfaces with $–CH_3$ groups did not permit SU8 adhesion. Even though near full surface coverage is reported for CH_3-terminated Si surfaces, complete delamination occurred during the SU8 development step, preventing subsequent characterization[31] and implying that just hydrophobicity is not a sufficient criterion for good adhesion.

An interesting observation in this work is that after the photoresist was applied and cured on olefin-terminated Si surfaces, neither alkene and epoxide functionalities were detected at the Si/SU8 interface. The lack of epoxide groups is not by itself unusual since UV exposure is what triggers SU8 polymerization. Still, the lack of alkenes indicates those groups did undergo reaction

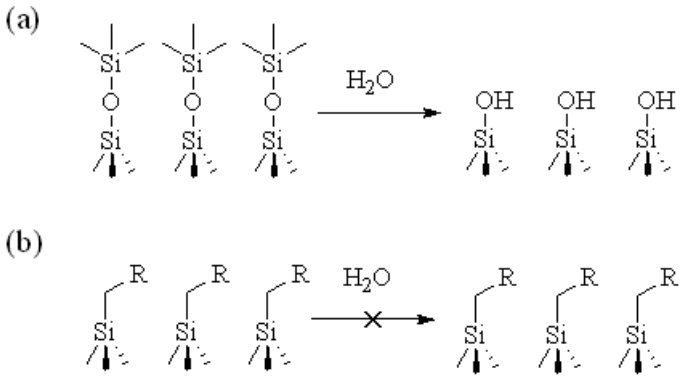

Figure 3.7 (a) Hydrolysis of interfacial of Si-O-Si bonds. (b) Interface resistance against hydrolysis due to presence of Si-C bonds.

Step 1 Decomposition of photoacid generator

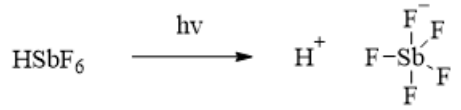

Step 2 Protonation of the double bond

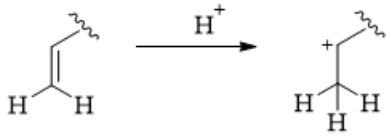

Step 3 Nucleophilic addition/ epoxide opening cascade

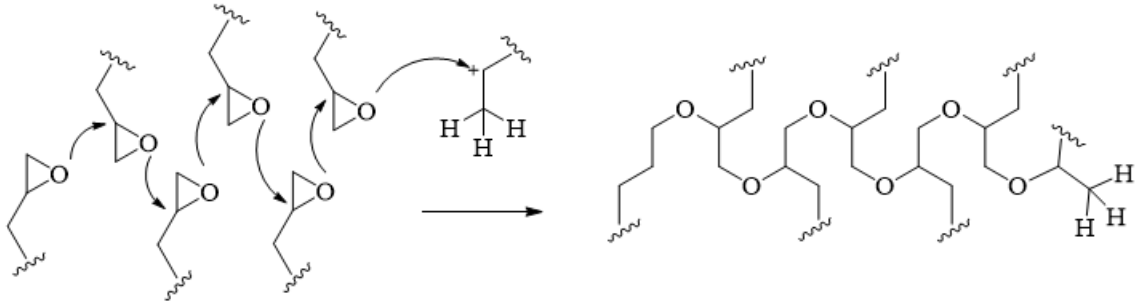

Figure 3.8 Proposed mechanism for covalent linkage between a terminal alkene group and SU8 film.

which could have promoted direct reaction with SU8. We propose a covalent linkage between the alkene groups and the SU8 film could occur which is consistent with the measured adhesion enhancement and the lack of detectable alkene functionality by SFG. Strong acids can catalyze alkylation reactions by ionizing alkenes to alkylcarbenium ions.[35] If terminal olefin groups undergo reaction with SU8 monomers in a presence of a photoacid (a key component in the formulation of SU8 resists, (Figure 3.7), the SU8 is effectively grafted on to the surface monolayer. This scenario is consistent with another observation in the SFG data. The notable disorganization of the SU8 chains at olefin-terminated Si surfaces was different than the SU8 ordering at the Si/SU8 interface for HMDS treated samples. This difference could arise because bonding between the SU8 and the Si monolayer disrupted the possibility of chain reorganization. Supplementary experiments are necessary to further test this hypothesis.

Irrespective, allyl and pentenyl monolayers did lead to stable adhesion even in wet environments. The data with these surfaces, after spin coating on SU8 films and subjecting to soaking in pH = 11.3 buffer for 72 h, were clear on this point. The lack of delamination after this time (in strong contrast to HMDS treated surfaces) is strong evidence supporting the durability of the Si-C linkage. Therefore, the data suggests that by converting the silicon interface from Si-O to Si-C, a reaction between the alkaline solution and the interface is significantly (kinetically) inhibited (Figure 3.8).

5. Conclusion

The cumulative experimental data shown here illustrate the ability to improve adhesion of SU8 photoresist films introduced on Si(111) surfaces. Although functional groups were introduced via Grignard chemistry to form the Si-C interface, surface reactions on silicon are highly explored thus one is not limited to Grignard reagents. UV and thermal grafting are some additional pathways. In overall, it is imperative that the nature of the monolayer and interfacial bonding is considered to best suit the chemical characteristics and application of a photoresist film. This report argues that conversion of interfacial Si-O bonds to Si-C bonds is one way to improve overall adhesion between the substrate and a photoresist film in aqueous conditions.

6. References

1. Franssila, S.; Tuomikoski, S., Lindroos, V.; Tilli, M.; Lehto, A.; Motooka, T., Eds. William Andrew Publishing: Boston, 2010; pp 333-348.
2. Jung-Hwan, P.; Davis, S.; Yong-Kyu, Y.; Prausnitz, M. R.; Allen, M. G. In *Micromachined biodegradable microstructures*, The Sixteenth Annual International Conference on Micro Electro Mechanical Systems, 2003. MEMS-03 Kyoto. IEEE, 23-23 Jan. 2003; 2003; pp 371-374.
3. Park, J.-H.; Allen, M. G.; Prausnitz, M. R., *J. Controlled Release* **2005,** *104* (1), 51-66.
4. Richa, M.; Tapas Kumar, M.; Tarun Kanti, B., *J Micromech. Microeng.* **2018,** *28* (10), 105017.
5. Lorenz, H.; Despont, M.; Fahrni, N.; LaBianca, N.; Renaud, P.; Vettiger, P., *J Micromech. Microeng.* **1997,** *7* (3), 121-124.
6. Lorenz, H.; Laudon, M.; Renaud, P., *Microelectron. Eng.* **1998,** *42*, 371-374.
7. Blagoi, G.; Keller, S.; Johansson, A.; Boisen, A.; Dufva, M., *Appl. Surf. Sci.* **2008,** *255* (5), 2896-2902.
8. Marie, R.; Schmid, S.; Johansson, A.; Ejsing, L. E.; Nordstrom, M.; Hafliger, D.; Christensen, C. B. V.; Boisen, A.; Dufva, M., *Biosens. Bioelectron.* **2006,** *21* (7), 1327-1332.
9. Voskerician, G.; Shive, M. S.; Shawgo, R. S.; von Recum, H.; Anderson, J. M.; Cima, M. J.; Langer, R., *Biomaterials* **2003,** *24* (11), 1959-1967.
10. Feng, R.; Farris, R. J., *J. Mater. Sci.* **2002,** *37* (22), 4793-4799.
11. Zhang, J.; Tan, K. L.; Gong, H. Q., *Polym. Test.* **2001,** *20* (6), 693-701.
12. Tam, L. H.; Lau, D., *Polymer* **2015,** *57*, 132-142.
13. V.M. Blanco Carballo, J. M., C. Salm, J. Schmitz, *Microelectron. Eng.* **2000,** *86* (4-6), 765-768.
14. Marshall, D. B.; Evans, A. G., *J. Appl. Phys.* **1984,** *56* (10), 2632-2638.
15. Nagata, H.; Kawai, A., *Jpn. J. Appl. Phys.* **1989,** *28* (Part 1, No. 10), 2137-2141.
16. Liston, E. M., *J. Adhes.* **1989,** *30* (1-4), 199-218.
17. Larsson, M. P.; Syms, R. R. A.; Wojcik, A. G., *J. Micromech. Microeng.* **2005,** *15* (11), 2074-2082.
18. Morikaku, T.; Kaibara, Y.; Inoue, M.; Miura, T.; Suzuki, T.; Oohira, F.; Inoue, S.; Namazu, T., *J Micromech. Microeng.* **2013,** *23* (10).
19. Ivanisevic, A.; Mirkin, C. A., *J. Am. Chem. Soc.* **2001,** *123* (32), 7887-7889.
20. Yanazawa, H., *Colloids Surf.* **1984,** *9* (2), 133-145.
21. Lassnig, A.; Nakamura, N.; Jörg, T.; Reeja-Jayan, B.; Cordill, M. J., *Surf. Coat. Technol.* **2018,** *349*, 963-968.
22. J. Ponjee, J.; B. Marriott, V.; C. B. A. Michielsen, M.; J. Touwslager, F.; N. T. van Velzen, P.; van der Wel, H., *J Vac. Sci. Technol. B Microelectron. Nanometer. Struct. Process. Meas. Phenom.* **1990,** *8*, 463-466.
23. Bhairamadgi, N. S.; Pujari, S. P.; Trovela, F. G.; Debrassi, A.; Khamis, A. A.; Alonso, J. M.; Al Zahrani, A. A.; Wennekes, T.; Al-Turaif, H. A.; van Rijn, C.; Alhamed, Y. A.; Zuilhof, H., *Langmuir* **2014,** *30* (20), 5829-5839.
24. Niederhauser, T. L.; Lua, Y.-Y.; Jiang, G.; Davis, S. D.; Matheson, R.; Hess, D. A.; Mowat, I. A.; Linford, M. R., *Angew. Chem. Int. Ed.* **2002,** *41* (13), 2353-2356.
25. Sung, M. M.; Kluth, G. J.; Yauw, O. W.; Maboudian, R., *Langmuir* **1997,** *13* (23), 6164-6168.
26. Linford, M. R.; Chidsey, C. E. D., *J. Am. Chem. Soc.* **1993,** *115* (26), 12631-12632.
27. Bansal, A.; Li, X.; Lauermann, I.; Lewis, N. S.; Yi, S. I.; Weinberg, W. H., *J. Am. Chem. Soc.* **1996,** *118* (30), 7225-7226.
28. Terry, J.; Linford, M. R.; Wigren, C.; Cao, R.; Pianetta, P.; Chidsey, C. E. D., *J. Appl. Phys.* **1998,** *85* (1), 213-221.
29. Li, Y. J.; Tero, R.; Nagasawa, T.; Nagata, T.; Urisu, T., *Appl. Surf. Sci.* **2004,** *238* (1), 238-241.
30. Yamada, T.; Shirasaka, K.; Noto, M.; Kato, H. S.; Kawai, M., *J. Phys. Chem. B* **2006,** *110* (14), 7357-7366.
31. Rivillon Amy, S.; Michalak, D. J.; Chabal, Y. J.; Wielunski, L.; Hurley, P. T.; Lewis, N. S., *J. Phys. Chem. C* **2007,** *111* (35), 13053-13061.

32. Zhao, L. L.; Lim, C. Y.; Jiang, C.; Liao, H., *ECS J. Solid State Sci. Technol.* **2016,** *5* (9), P464-P467.
33. Gogolides, E.; Ellinas, K.; Tserepi, A., *Microelectron. Eng.* **2015,** *132*, 135-155.
34. Ge, J.; Kivilahti, J. K., *J. Appl. Phys.* **2002,** *92* (6), 3007-3015.
35. Olah, G. A.; Schilling, P.; Staral, J. S.; Halpern, Y.; Olah, J. A., *J. Am. Chem. Soc.* **1975,** *97* (23), 6807-6810.

CHAPTER 4

Sensitization of p-GaP by Physisorbed Triarylmethane Dyes

Reprinted with permission from Hlynchuk, S., MacInnes, M. M.; Maldonado, S., Sensitization of p-GaP by Physisorbed Triarylmethane Dyes. *The Journal of Physical Chemistry C* **2018**, *122* (35), 20073-20082.

1. Introduction

Dye-sensitized photocathodes are attractive platforms for solar energy capture, conversion, and storage[1-6] but have been the subject of much less scrutiny than dye-sensitized photoanodes for regenerative photovoltaic applications.[7-8] In lieu of using p-type metal oxides, which are both uncommon and difficult to prepare with high charge-carrier mobilities,[9] multiple groups have explored alternative p-type semiconductors.[10-12]

In this context, gallium phosphide (GaP) has several potential merits. First, this III-V semiconductor can sustain photovoltages in excess of 1 V at 1 sun illumination.[13-14] In principle, an optimal GaP photocathode could supply a large electromotive force for desirable fuel forming reactions. Second, GaP natively demonstrates surface energetics amenable to both proton and CO_2 reduction,[15-17] indicating that dye-sensitized schemes could be used to drive these specific half reactions. Third, GaP is a technologically mature material (e.g. used extensively in commercial light emitting diodes), so methods for its metallurgy (i.e. doping, contacting) are well known.[18] Nevertheless, the use of GaP as a dye-sensitized photocathode platform in water is challenging for several reasons. First, surface of GaP is not indefinitely stable in water. Second, the indirect bandgap of GaP results in long minority charge-carrier diffusion length. As a result, nanostructured GaP tends to outperform planar GaP photoelectrodes but the difference strongly depends on the morphological and electronic properties of the specific GaP material. Finally, although sensitization of p-GaP by organic chromophores was first reported at the onset of the concept of dye sensitization in photoelectrochemistry,[19] the design principles required for high-efficiency and

long-lived dye sensitized p-GaP photocathodes are as yet unclear. That is, how to properly couple dyes to GaP surfaces is unknown.

To date, several organic and inorganic chromophores demonstrate the capacity for light-stimulated hole injection into p-GaP photoelectrodes.[20-23] However, the majority of studies have employed conditions where p-GaP is immersed in an electrolyte containing the dissolved dye, i.e. the chromophore is not permanently adsorbed onto the electrode and is instead involved in some dynamic adsorption/desorption equilibrium. Although this tactic simplifies measurement, it does not address how the sensitizer-electrode combination would operate when the dye is adhered permanently to the semiconductor surface. Two basic questions yet to be addressed are: (*1*) are there any facile methods to adsorb a chromophore on GaP? and (*2*) what aspects are germane to realization of high charge-collection efficiency and stability?

In our ongoing work, we have noted that some common triarylmethane dyes can adsorb to some crystalline faces of GaP. As yet, no report has described the operational characteristics of physisorbed triarylmethane dyes on p-GaP electrodes immersed in otherwise blank electrolytes (i.e. electrolyte solutions that do not contain any dissolved redox mediator or dye). Accordingly, this work focuses on identifying such systems to evaluate their efficacy for constructing regenerative or photosynthetic photoelectrochemical cells featuring dye-sensitized p-GaP photocathodes. Herein, we detail how readily such dyes adhere on native p-GaP interfaces, using Fast Green FCF as a representative triarylmethane dye. This work demonstrates the first proof of sensitization by a physisorbed molecular chromophore on native GaP immersed in a blank, aqueous electrolyte. We further show how Fast Green FCF is regenerated to yield a steady-state photocurrent at sub-bandgap wavelengths and discuss the implications on further electrode design. Finally, we highlight several important criteria that should be considered to improve the prospects for sensitized electrochemistry with p-GaP.

2. Experimental

Chemicals and Materials

Methanol (anhydrous, 99.8%, Aldrich), acetone (HPLC-grade, Fisher), tetrahydrofuran (anhydrous, ≥ 99.9%, Aldrich), methylmagnesium chloride (3M CH_3MgCl solution in THF, Aldrich), phosphorous pentachloride (95%, Aldrich), chlorobenzene (anhydrous, 99.8%, Aldrich),

benzoyl peroxide (≥ 97%, Aldrich), double distilled sulfuric acid (95-98%, Aldrich), hydrofluoric acid (48%, Fisher), potassium chloride (ACS grade, Mallinckrodt), Fast Green FCF dye content (≥85 %, Sigma Aldrich), Crystal Violet (≥90%, Aldrich), Ethyl Violet (<90%, Aldrich), Rose Bengal (≥95 %, Aldrich), tris(ethylenediamine)cobalt(III) chloride dihydrate (<90%, Sigma Aldrich), europium(III) chloride hexahydrate (99.9%, Stream Chemicals), methyl viologen dichloride hydrate(98%, Aldrich), cobalt(III) sepulchrate trichloride (95%, Aldrich), forming gas (5% hydrogen/ 95% nitrogen, Metro Welding), argon gas (Metro Welding), indium (99.99%, gallium Source), and zinc powder (≥99.8%, Baker Analyzed) were used as received. Water with a resistivity of > 18 MΩ cm (Barnsted Nanopure system) was used throughout. Single-side polished (etch pit density = $0.5x10^5$ cm^{-2}) p-type GaP(100) with Zn dopant concentration of 1.8-2.3 $x10^{18}$ cm^{-3} and a thickness of 350 ±25 μm and double-side polished (etch pit density = 1.5 x 10^5 cm^{-2}) p-type GaP(111)A with Zn dopant concentration of $1.4x10^{18}cm^{-3}$ and a thickness of 400 ±20 μm were obtained from University Wafers.

Electrode Fabrication

P-type GaP(100) and p-type GaP(111)A wafers were first cut into roughly 0.5 cm x 0.5 cm sections, degreased by sequential sonication in hexanes, acetone, methanol and water, and then dried under a stream of N_2(g) before further use. Ohmic contacts were then prepared by soldering an In-Zn mixture onto the backs of each GaP wafer section, followed by annealing in forming gas for 10 minutes at 400°C. These GaP sections were then mounted on to tinned copper wire using silver print (GC Electronics), which was then threaded through a glass rod. An inert epoxy (Hysol C) was then used to insulate the back and sides, exposing only the front face of the wafer section for use as an electrode.

Surface Modification

Dye adsorption was performed by immersion of electrodes or wafer sections in aqueous solutions of dissolved dye. Specifically, cleaned and freshly etched (30 sec in hydrofluoric acid) GaP samples were immersed in a 6 mM solution of dye in water for 90 seconds with gentle stirring. After rinsing with water 3 times and then drying with a dry nitrogen stream, the sections were subsequently immediately used for electrochemical or spectroscopic analysis. Following all such studies, surfaces were cleaned and restored to their native state by sonicating in neat methanol and

then etching in 49% HF(aq) for 30 s. This procedure was sufficient to eliminate all sub-bandgap photocurrents, implying complete dye removal.

To prepare CH_3-terminated p-GaP(111)A electrodes, a slight modification was employed. The ohmic back-contacts on p-GaP(111)A wafer sections were prepared as described above. However, prior to functionalization, excess In-Zn present on the backside was etched off with a drop of concentrated H_2SO_4 for 30 seconds. These sections were then moved into N_2-purged glovebox, where they were immersed for 50 min at T = 90 ^oC in a saturated solution of PCl_5 in chlorobenzene with a few grains of dissolved benzoyl peroxide. Following, the front face of the GaP wafer sections were rinsed with neat THF and inserted into a reaction vessel containing 1 mL of 3M CH_3MgCl in THF. The wafer sections were left to react for 3 h at T =100-110 ^oC. After completion, the surfaces were again washed with copious amounts of THF followed by neat methanol. Upon removal from the glovebox, additional In-Zn was soldered onto the back but no further annealing was performed. These wafer sections were then affixed onto tinned copper wire and embedded in insulating epoxy as described above.

(Photo)Electrochemical Measurements

All electrochemical measurements were performed in a three-electrode cell under potentiostatic control (PAR 273) in an airtight Pyrex cell with an optically flat and transparent quartz bottom. All solutions were sparged with N_2(g) and the headspace was kept under a constant flow of N_2(g). A Pt mesh counter electrode and a Ag/AgCl(sat. KCl) reference electrode were used throughout. All potentials are reported with respect to E(Ag/AgCl(sat. KCl)). Care was taken to ensure the position of the electrode was constant, with a distance between the GaP electrode and electrochemical cell window ~2 mm for all measurements to minimize optical losses. Wavelength-dependent external quantum yield measurements were collected with an Oriel 150 W Xe arc lamp (Newport) and a quarter-turn single grating monochromator (Model 74125, Newport). Additionally, all external quantum yield measurements were conducted under chopped illumination at 15Hz and -0.6V vs E(Ag/AgCl). All data was corrected for fluctuations in light intensity, via a quartz beam splitter which directed a portion of the light to a Si photodiode (Model 70316NS, Newport). The output signal from the cell and the reference Si photodiode was passed through a Stanford Instruments SR830 lock-in amplifier and relayed to a computer controlled by custom-written LabVIEW software. Wavelengths were scanned at increments of 5 nm in each

presented plot. Each individual quantum yield value on every plot represents values from at least 200 repetitive measurements. That is, 100 sequential measurements were obtained and averaged. This value was then compared to the average of the previous 100 sequential measurements. If the difference between the two averages was less than 2%, then the latter average was logged as the tabulated value. If the differences was equal to or larger, then another 100 measurements were collected and compared. This cycle was repeated until the 2% criterion was satisfied. The propagated error from the uncertainties in the measurement of current, illumination power, and the width of the emission line from the monochromator (Δ 2 nm), translated into relative errors in each quantum yield measurement of 5.6 - 5.7% in the range from 525-700 nm.

Separate measurements were performed with a light emitting diode (Mightex Systems) whose emission centered at λ= 656 nm with a bandwidth of 20 nm (full width at half maximum of emission spectrum, emission intensity < 1% at λ < 610 nm). The output illumination power from this source was adjusted over several orders of magnitude through a combination of a variable output power supply and a combination of aluminum neutral density filters. An optical beamsplitter was used to direct a portion of the light to a mounted reference Si photodiode. All reported illuminated power densities were corrected for electrode placement.

X-ray Photoelectron (XP) Spectroscopy

X-ray photoelectron spectra were collected using a PHI 5400 analyzer equipped with Al K α (1486.6 eV, 6 mA current emission and a 12 kV anode high tension) source, without a monochromator. Data collection took place at a pressure of < 2.5 x 10^{-9} Torr, without charge neutralization. Sample survey scans were recorded between 0 and 1350 eV at pass energy of 117.40 eV, while high resolution spectra were collected at pass energy of 23.5 eV. All binding energies were referenced to the expected binding energy for adventitious carbon (284.6 eV). Spectrum analysis was performed with CASA XPS 2.3.13 software.

3. Results

Spontaneous Physisorption of Dye on Freshly Etched GaP(100)

Figure 4.1a shows the recorded steady-state voltammogram in deaerated 1M KCl electrolyte containing 5 mM methyl viologen both in the dark and under monochromatic illumination at λ = 650 nm and 0.5 mW cm^{-2}. Without exposure to Fast Green FCF

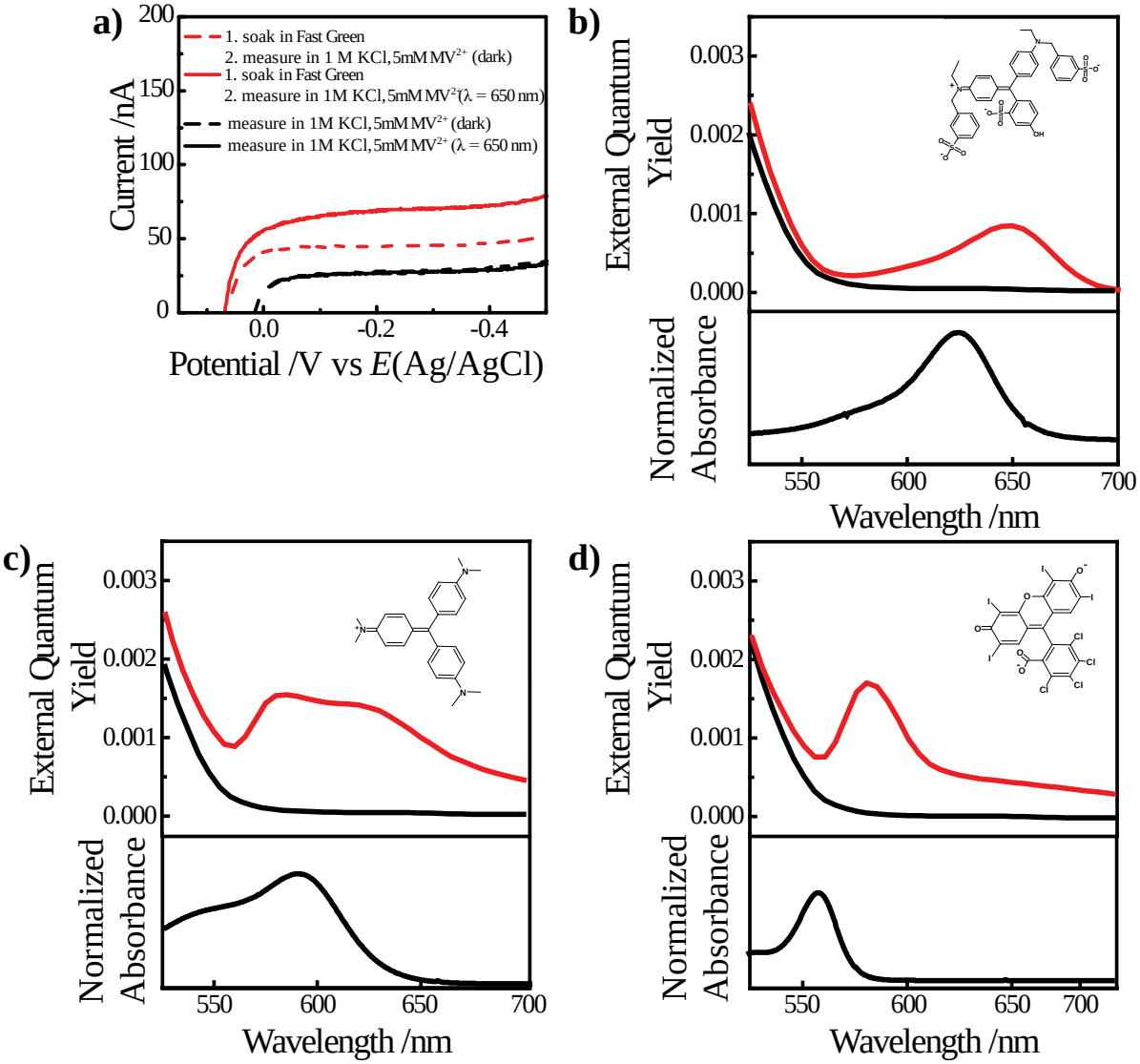

Figure 4.1 a) Steady state voltammograms of freshly etched p-GaP(100) electrodes in deaerated 1M KCl, 5 mM methylviologen (MV^{2+}) electrolyte (dashed lines) in the dark and (solid lines) under illumination at λ = 650 nm and 0.5 mW cm^{-2}. Responses were recorded (black) before and (red) after first soaking the electrode in Fast Green FCF solution for 90 s. b-d) Wavelength-dependence of the external quantum yields measured with a p-GaP(100) electrode poised at E = -0.6 V vs E(AgAg/Cl) in deaerated electrolyte both (black) without and (red) with first soaking in 6 mM b) Fast Green, c) Crystal Violet, or d) Rose Bengal solution for 90 s. The dye structures are shown in the upper left portion of each plot. The bottom portion of each plot shows the normalized absorbance spectrum of corresponding dye dissolved in water at a concentration $\leq 10^{-6}$ M.

(i.e. no prior immersion in dye solution), the photoelectrode responses in the dark and under illumination were nominally identical, in accord with the premise that sub-bandgap illumination does not illicit any substantive photoresponse. In comparison, when the electrode was first immersed in a 6 mM Fast Green FCF solution and then rinsed and immersed in blank electrolyte, the photocurrent-potential response was augmented and showed typical behavior of potential-independent photocurrent at more negative potentials. The low absolute photocurrents corresponded to a small overall external quantum yield for photon-to-electron conversion, as expected for dye distributed across a flat surface plane. The explicit dependence of the photocurrent external quantum yield with wavelength at E = -0.6 V (i.e. in the plateau region of the photoresponse) is shown in Figure 4.1b. The spectral profile of the external quantum yield mirrored the solution absorbance of Fast Green FCF (Figure 4.1b inset), apart from a red shift of 30 nm relative to the peak absorbance wavelength. Such shifts are commonly observed in dye sensitization and typically arise from a different local environment of a chromophore on a charged surface as opposed to dissolved in solution.[24-26] The large difference in high frequency dielectric constants (9.11 for GaP, 80 for H_2O)[27-28] is consistent with this notion. Comparable photoresponses were collected for p-GaP(100) electrodes coated in a similar fashion by first soaking freshly etched p-GaP(100) electrodes in solutions of other triarylmethane dyes including, Crystal Violet and Rose Bengal (Figure 4.1c,d). The wavelength dependence of the external quantum yields measured for adsorbed Crystal Violet suggested the possibility of some H-aggregation, implying at least for this dye adsorbed chromophores were not totally isolated.

To determine the amount of dye spontaneously and persistently (i.e. does not instantaneously desorb upon re-immersion in fresh solution) adsorbed onto GaP(100) surfaces upon soaking in a dye solution, X-ray photoelectron (XP) spectroscopy was employed (Figure 4.2). GaP(100) wafer sections were soaked in a Fast Green FCF solution for either 90 s, 300 s or 600 s and then rinsed with water. Based on the composition of Fast Green FCF ($C_{37}H_{34}N_2O_{10}S_3Na_2$), high resolution of sulfur 2p spectra were acquired before and after treatment. Figure 4.2a shows the respective S 2p spectra for a GaP(100) prior to treatment. A flat base line is seen from 174 eV to160 eV, indicating no detectable signal for sulfonates (> 167 eV)[29] on the native surfaces, as expected. Figure 4.2b shows analogous spectra for a representative sample following immersion for 90 and 600s. There was still no detectable signatures of sulfonates visible above the baseline. Auger spectra were separately collected and again no detectable quantities of

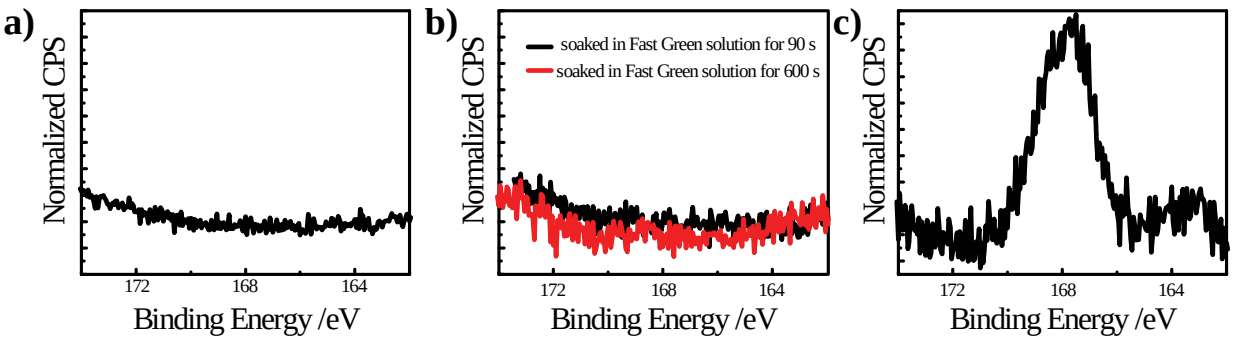

Figure 4.2 High resolution S 2p XP spectra of a) a freshly etched GaP(100) surface, b) GaP(100) soaked in 6 mM Fast Green solution for either (black) 90 s and (red) 600 s, and c) a GaP(100) surface where a 0.05 mL of 6mM Fast Green in methanol was allowed to dry without additional rinsing.

Fast Green FCF were observed. Based on a surface detection limit of 0.1 at %,[30] the XP and Auger data necessarily constrained the maximum surface coverage of physisorbed Fast Green FCF to less than 6.6 $x10^{11}$ molecules cm^{-2}. Additionally, separate measurements of the Ga 2p signal did not change between pre- and post- dye loading, further implying ultra-low levels of physisorbed dye. Similar observations and conclusions were drawn for Rose Bengal, Ethyl Violet, Crystal Violet, and Rhodamine G. For reference, Figure 4.2c also shows an analogous spectrum for a sample where a drop of a Fast Green FCF solution was allowed to evaporate and the surface was then analyzed without rinsing. For these samples, detectable levels of sulfonates were routinely seen.

Factors that Affect Sensitized Photoresponse

Figure 4.3 shows the influence of the redox mediator used for sensitization experiments with putatively physisorbed Fast Green FCF. On average, the photocurrents for freshly dye-loaded electrodes measured at $\lambda = 650$ nm varied by approximately 30%. The use of cobalt(III) sepulchrate (Co(sep)), cobalt(III) tris(ethylenediamine) ($Co(en)_3$), europium(III), and ruthenium(III) hexammine were initially explored to gauge the extent that the standard potential and self-exchange rate constants (Table 4.1)[31-35] of the redox mediator were expected to have on the sensitized signal. However, aside from the significantly larger dark current elicited in electrolytes containing ruthenium(III) hexammine chloride, the steady-state photoelectrode responses were nominally the same in terms of photocurrent magnitude and current-potential profile. This observation is contrary to the well-established precedent for the electrochemical properties of a redox mediator influencing the level and shape of sensitized photoresponses.[36-40] The large dark current for ruthenium(III) hexammine chloride was unexpected and could not be ascribed to the fact it is a 'fast' redox couple. Methyl viologen has an even higher self-exchange rate by several orders of magnitude (Table 4.1) and still did not induce a similarly large increase of the dark current response (Figure 4.1a). Instead, the issue with ruthenium(III) hexammine chloride could be related to some disassociative adsorption by the metal complex. Exposure of III-V photocathodes to solutions containing Ru-complexes is well known to catalyze their activity for H^+ reduction[41-46] presumably through decomposition and formation of Ru^0 clusters. The possibility and extent of Ru^0 formation and adsorption was not analyzed further since the larger dark current implies that overall ruthenium(III) hexammine chloride is not well-suited as a redox mediator with p-GaP.

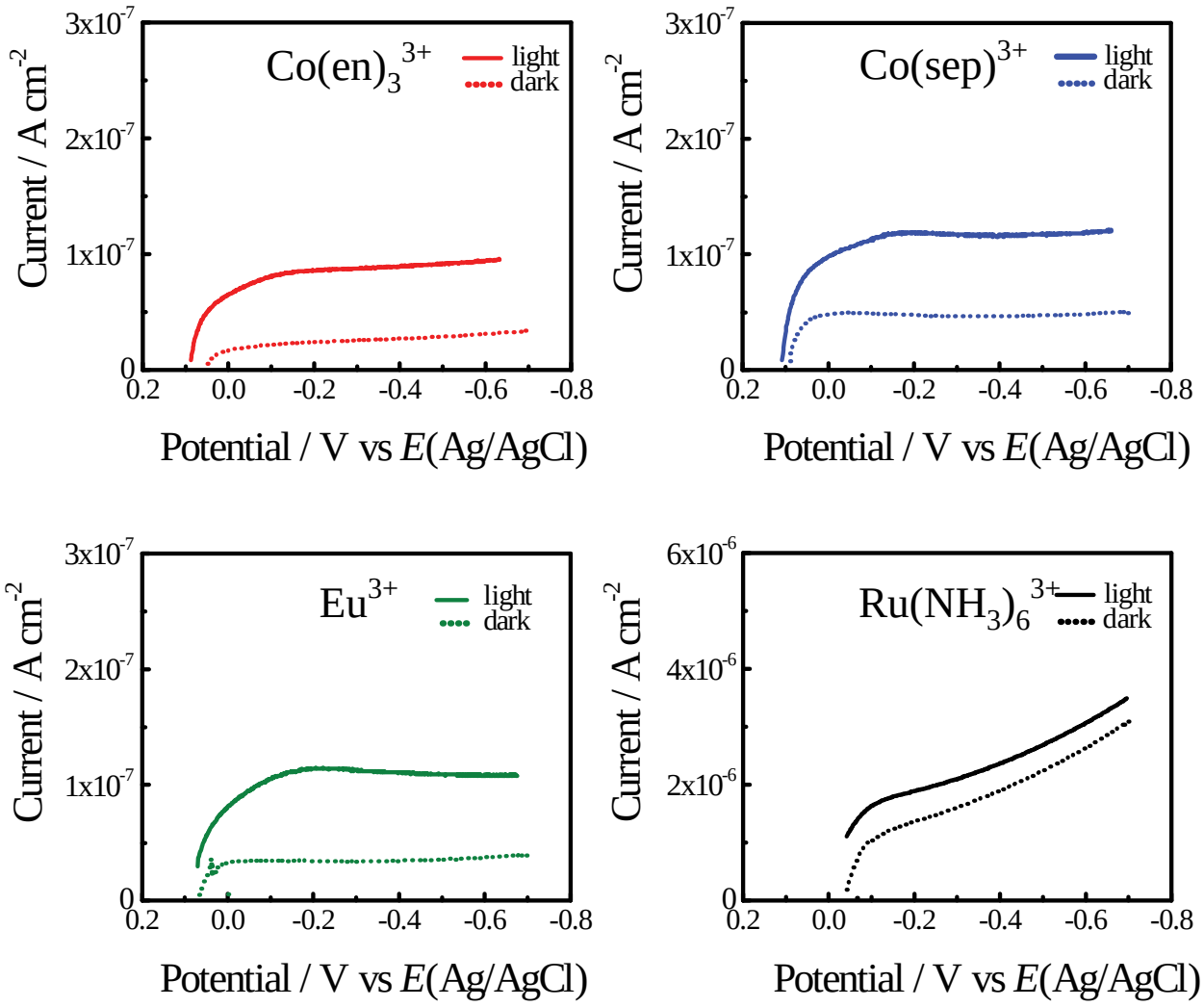

Figure 4.3 Current vs potential responses of p-GaP(100) electrodes that were first soaked in 6 mM Fast Green solution for 90s and then rinsed, dried, and immersed in deaerated 1 M KCl(aq) containing 5 mM of each redox mediator. Responses were recorded both in the dark and under monochromatic illumination at λ = 650 nm and 0.5 mW cm^{-2}.

Table 4.1 Standard Potentials and Self-Exchange Rates of Selected Candidate Redox Mediators.

Redox Mediator	**Abbreviation**	$E^{0'}$ **/V vs.** E **(Ag/Agcl)**		**Self-Exchange Rate /M^{-1} s^{-1}**	
Europium(III)	Eu^{3+}	-0.550	*Ref 31*	$\leq 1 \times 10^{-4}$	*Ref 35*
Cobalt(III) tris(ethylenediamine)	$Co(en)_3^{3+}$	-0.440	*Ref 34*	3×10^{-5}	*Ref 34*
Cobalt(III) sepulchrate	$Co(sep)^{3+}$	-0.540	*Ref 32*	5×10^{0}	*Ref 34*
Ruthenium(III) hexammine	$Ru(NH_3)_6^{3+}$	-0.100	*Ref 31*	4×10^{3}	*Ref 34*
Methyl Viologen	MV^{2+}	-0.650	*Ref 33*	1×10^{7}	*Ref 34*

To probe further, sensitized photocurrent measurements at the sensitization peak wavelength (650 nm) were recorded as a function of mediator concentration. Figure 4.4 shows such data for two redox couples with similar standard potentials but different self-exchange rates, methyl viologen and cobalt(III) sepulchrate. The photocurrents are presented as external quantum yields and are clearly insensitive toward the redox mediator concentration as it was titrated into solution. In fact and unexpectedly, the sensitized signal was comparable (or even higher) in blank electrolyte, i.e. with no redox mediator in solution. To ascertain that some residual amount of dissolved oxygen was not acting as a mediator for sensitization through the generation of singlet oxygent, sodium azide was introduced into the cell. External quantum yield values measured before and after the addition of sodium azide remained constant, eliminating any trace of dissolved oxygen as a potential redox mediator.

The total insensitivity of the sensitized photocurrent towards concentrations of species in solution suggested an unexpected mechanism of dye regeneration. To probe further, separate experiments were performed over a greater range of illumination intensities. Using a light emitting diode centered at λ = 656 nm, photocurrent measurements were taken at a range of illumination intensities both with and without dissolved methyl viologen in solution (Figure 4.5). At light intensities below 0.6 mW cm^{-2}, the photocurrent dependence on the illumination light intensity was nominally linear and equivalent for both solutions. However, above this light intensity, photocurrent measurements in the blank electrolyte saturated. In contrast, the photocurrent measurements continued to monotonically increase at higher light intensities when methyl viologen was in solution, indicating that the photoexcited dye could be regenerated by dissolved methyl viologen.

In lieu of regeneration by dissolved redox mediators at low light intensities, further experiments were performed to explore the regeneration pathway of Fast Green FCF after hole injection into GaP under these conditions. Figure 4.6 shows a series of linear sweep voltammograms obtained in the absence of illumination where the p-GaP(100) electrode was swept from the rest potential out to +0.3 V after first being held at E = -0.6 V. When the electrode was swept in the dark, no appreciable anodic current passed until 0.0 V. At more positive potentials, increased current corresponded to the electrochemical oxidation of GaP.[47] This observation was independent of the total hold time at E = -0.6 V. When the electrode was first

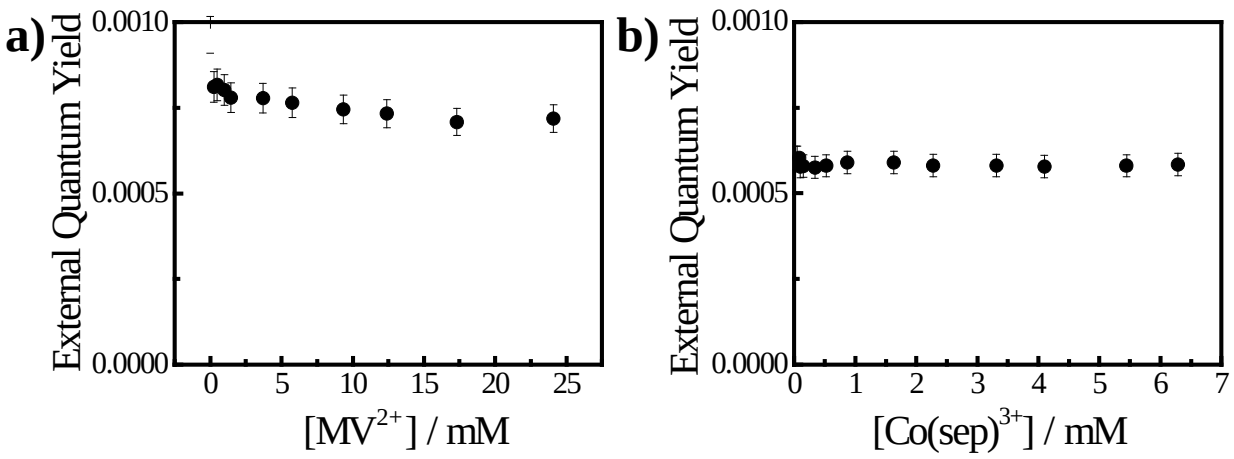

Figure 4.4 Measured quantum yields for net photocurrent generation at λ = 650 nm, 0.507 mW cm^{-2} and E = -0.6 V vs E(Ag/AgCl) as a function of the concentration of either (a) methyl viologen dichloride or (b) cobalt(III) sepulchrate trichloride dissolved in deaerated 1 M KCl(aq).

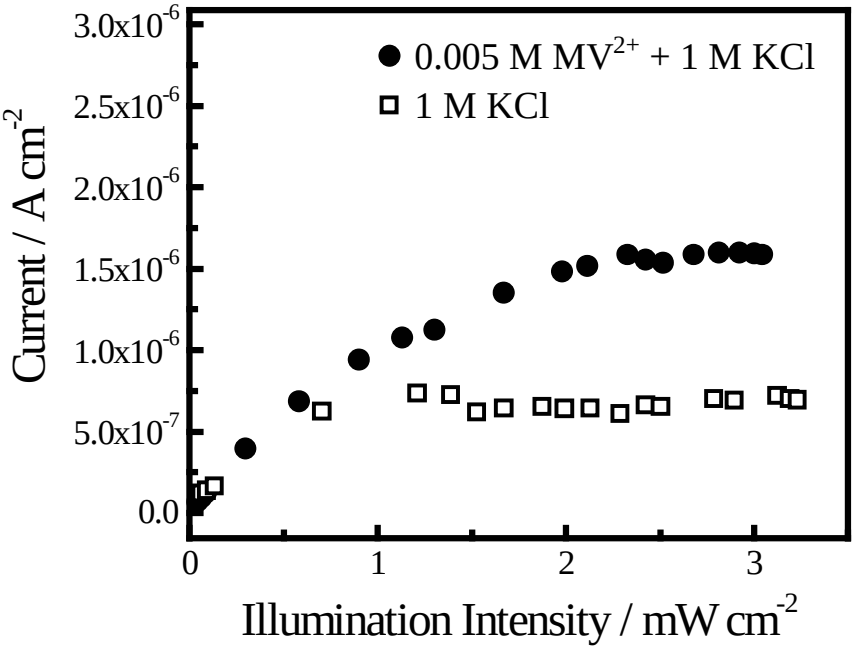

Figure 4.5 Dependence of photocurrent with illumination intensity centered at λ = 656 nm for a p-GaP(100) photoelectrode with adsorbed Fast Green immersed in N_2-purged 1 M KCl(aq) both (●) with and (□) without 0.005 M $MVCl_2$ at E = -0.6 V vs E(Ag/AgCl).

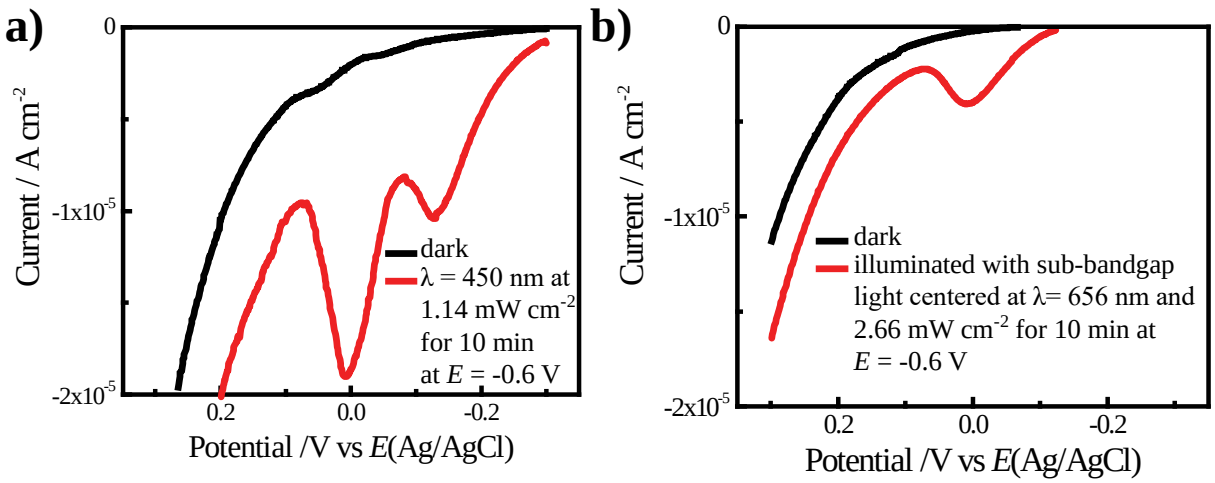

Figure 4.6 Linear sweep voltammograms for freshly etched p-GaP(100) electrodes immersed in deaerated 1 M KCl(aq). a) (black line) The potential of the electrode was swept from open circuit to E = +0.3 V at a scan rate of 20 mV s^{-1}. (red line) The electrode was first held at E = -0.6 V while illuminated with supra-bandgap light at λ = 450 nm and at 1.14 mW cm^{-2} for 10 min before scanning to +0.3 V at 20 mV s^{-1}. b) (black line) The electrode was first soaked in 6 mM Fast Green for 90 s, rinsed, and then immersed in deaerated 1 M KCl(aq). The potential of the electrode was then swept from open circuit to E = +0.3 V at a scan rate of 20 mV s^{-1}. (red line) The electrode was first held at E = -0.6 V while illuminated with sub-bandgap light at λ = 656 nm and at 2.66 mW cm^{-2} for 10 min before scanning to +0.3 V at 20 mV s^{-1}.

illuminated with supra-bandgap light at λ = 450 nm at 1.1 mW cm^{-2} for 10 min before sweeping the potential out to +0.3 V, two new anodic waves were observed centered at E = 0.0 V and E = -0.125 V. The intensity of these waves depended on the hold time, with longer times eliciting larger oxidation waves. These data indicated that illumination resulted in the generation of additional reduced species at the electrode/electrolyte interface. Integration of the total charge passed above the blank condition corresponded to 1.11 x10^{-5} C cm^{-2}. When a p-GaP photoelectrode that was first soaked in a Fast Green FCF solution for 90s was illuminated with sub-bandgap light at λ = 656 nm at 2.7 mW cm^{-2} for 10 min and then scanned out to 0.3 V, a single anodic peak at E = 0.0 V was observed. The intensity of this wave also depended somewhat on the hold time, but a second peak at more negative potentials was never observed. The sum conclusion from these experiments was that the GaP electrode surface has the capacity to store excess negative charge by the reduction of surface atoms.

Attempts to Sensitize Chemically Passivated p-GaP Photoelectrodes

Although a well-defined, wet chemical passivation method for controlling the surface chemistry of p-GaP(100) does not yet exist, we have previously shown that GaP(111)A surfaces could be effectively stabilized and modified by reaction with alkyl Grignard reagents.[48-49] Accordingly, additional p-GaP photoelectrodes were prepared with single-crystalline wafers with exposed (111)A surface planes. As was observed with freshly etched p-GaP(100) electrodes, freshly etched p-GaP(111)A electrodes that were first immersed in Fast Green FCF solution (*vide supra*) exhibited photoelectrochemical responses suggestive of physisorbed dye (Figure 4.7a). A notable observation is that the sensitization levels with p-GaP(111)A electrodes tended to be consistently lower than that for analogous p-GaP(100), indicating even less dye physisorbed on to this surface plane. In contrast, when p-GaP(111)A electrodes were first reacted with CH_3MgCl and then soaked in dye solution and analyzed for sensitized photocurrent, no sub-bandgap photoresponse was observed. Attempts to soak these CH_3-terminated p-GaP(111)A electrodes in the other triarylmethane dyes consistently showed no evidence of sensitization or persistent physisorption (Figure 4.7b). These data implied that either the low affinity of the anionic Fast Green FCF dye with a CH_3-terminated p-GaP(111)A surface resulted in no sensitized photocurrent or that the storage of injected electrons at the GaP surface was a necessary condition for sensitization. However, when sensitization measurements were repeated with CH_3-terminated

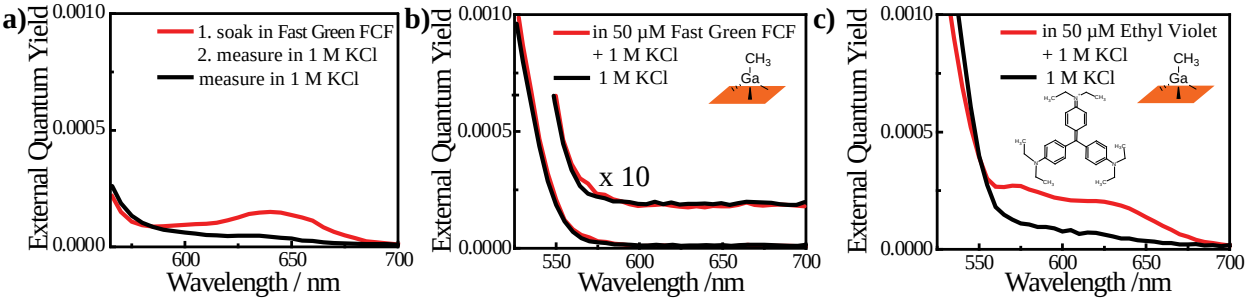

Figure 4.7 Wavelength-dependence of the external quantum yields at E = -0.6V vs E(Ag/AgCl). a) Freshly etched p-GaP(111)A electrode in deaerated 1 M KCl(aq) (black) before and (red) after soaking in Fast Green solution for 90 s. b) A chemically modified p-GaP(111)A electrode reacted first with CH_3MgCl and then immersed in 1M KCl(aq) (black) without and (red) with 50 µM Fast Green. c) A chemically modified p-GaP(111)A electrode reacted with CH_3MgCl and then immersed in 1M KCl(aq) (black) without and (red) with 50 µM Ethyl Violet.

p-GaP(111)A electrodes in electrolytes containing the less hydrophilic triarylmethane dye Ethyl Violet, low but persistent sensitized photocurrents were detected, suggesting that dye affinity for the surface rather than the participation of surface reduction was controlling in these measurements.

4. Discussion

The cumulative data presented here highlight important insights on how to construct sensitized photocathodes with doped p-GaP. First, adsorption of Fast Green FCF and similar triarylmethane dye salts is apparently achieved on native GaP surfaces but the total amount is quite low. Second, the sensitization by hole-injection from adsorbed, photoexcited dye at low light intensities is coupled with chemical attack of the native GaP surface. Third, at high light intensities, the sensitization mechanism transitions to a mode where redox species in solution mediate the regeneration of adsorbed dye. Fourth, chemical passivation of GaP interfaces that inhibits chemical surface degradation but still permits sensitization is possible. These points are detailed below.

Adsorption of Fast Green FCF on Native GaP Interfaces

Since a pristine, oxide-free GaP interface does not present any natural reactive sites for an organic chromophore, the means for persistent adsorption of a dye is not immediately obvious. However, freshly etched GaP surfaces rapidly form a significant density of polar surface groups upon exposure to air and immersion in protic solvents.[50-52] Accordingly, the data are consistent with the premise that resultant surface charges on freshly etched GaP(100) and GaP(111)A supply enough electrostatic attraction to bind Fast Green FCF. To be clear, since no sensitization signal was ever observed with p-GaP that featured a native oxide prior to dye loading, we infer the active sites for charge-injection was not oxide-based. The quantity of adsorbed dye is below the detection limits of X-ray photoelectron spectroscopy and Auger spectroscopy. Nevertheless, the fractional surface coverage of the dye is still enough to elicit appreciable photocurrent external quantum yields at longer, sub-bandgap wavelengths. This necessarily implies that the internal quantum yield for sensitized hole injection is likely high for an individual, adsorbed dye molecule and is in accord with the premise that electrodes operating under depletion conditions are naturally suited for dye-sensitization.[22, 53-54] Although a sufficiently high ionic strength electrolyte and/or extreme pH could facilitate dye desorption, the data shown here indicates that in 1 M ionic strength and neutral

pH, the small amount of physisorbed Fast Green FCF does not desorb appreciably within the timescale of the measurements (i.e. ~10 minutes).

Regeneration of Dye After Sensitized Hole Injection

The sign and wavelength-dependence of the steady-state photocurrent are clear indications that the sub-bandgap photocurrent arises from photoexcitation and regeneration of physisorbed Fast Green FCF. However, the mechanism of regeneration of dye following charge injection appears complex.

At low light intensities, the magnitude of the photocurrent has a zero-order dependence on the concentration (and type) of dissolved redox couples. This finding is unexpected because it is in strong contrast to the typical description of sensitized photocurrents where the dye, following charge injection, is restored to its original state by a redox reaction with a molecular mediator. The findings here make clear that at least one pathway exists for dye regeneration that does not involve charge-transfer with a solution-based redox mediator. One possibility is that after photoexcitation and injection of a hole into the valence band of GaP, dyes are regenerated by charge transfer with adjacent adsorbed, non-photoexcited dye. In principle, this scenario could also produce a saturated sensitized photoresponse above a threshold illumination intensity. However, this possibility would not be expected to induce any net chemical change to the surface, nor would this mechanism expected to be consistent from electrode to electrode. Rather, the data implicate that some charge transfer with the GaP surface itself is what regenerates the dye. As evident from the oxidative waves in the voltammograms in Figure 4.6, electron storage is possible at GaP interfaces. The electroreduction of the surface atoms into (ultimately) Ga and PH_3 is known to occur at potentials within the bandgap.[55] For experiments where GaP itself was photoexcited, accumulation of electrons at the conduction band edge at the surface apparently reduce surface Ga atoms that could then be reoxidized by sweeping the potential out to sufficiently anodic potentials. Steps 5-7 in Figure 4.8 summarize such a process, which is known to occur when there is an absence of efficient acceptors in solution (the native GaP surface is not electrocatalytic for H^+ reduction at neutral pH).[48, 56] For charge compensation, this reduction likely drives insertion of H^+ into the GaP sub-surface.[55, 57] The net result on the GaP surface is the introduction of new (and likely numerous) chemical defects at the surface.

We posit with an adsorbed dye on a native p-GaP interface, a similar process occurs. That is, photoexcitation of the dye not only results in hole injection into the valence band but also electron injection into GaP via a surface state(s) (Steps 1,2, & 4 in Figure 4.8). To be clear, electron injection from the dye does not proceed by injection into the conduction band. In this electrolyte, the conduction band edge of GaP is -1.2 V ± 0.2 vs E(Ag/AgCl),58 far too negative to receive an electron from these photoexcited chromophores. Rather, an electron from the photoexcited dye drives the reduction of surface atoms in GaP. The standard potentials for the first reduction of triarylmethane dyes are < -0.5 V vs E(Ag/AgCl)59 and the re-oxidation of GaP surfaces during anodic sweeps occurs at more positive potentials > -0.1 V vs E(Ag/AgCl) (Figure 4.6) are consistent with this premise. The injection of both electrons and holes into GaP does not translate into appreciable carrier recombination because they remain physically separated. In p-GaP electrodes operating under strong depletion, the internal electric field efficiently sweeps injected holes away from the surface and simultaneously strongly confines injected electrons to the interface. Accordingly, in three-electrode experiments under potentiostatic control and in the absence of a redox mediator in solution, a net photocurrent is possible and was observed.

The effective rate for electron injection from the dye to drive GaP surface redox chemistry must be fast relative to the rate of electron transfer for the reduction of all dissolved redox couples explored here. The data regarding the insensitivity of the photocurrent towards redox couple concentration in solution are clear on this point at low light intensities. Since the photocurrent did not rapidly decay to zero, the regeneration of the adsorbed dye by the reduction of the GaP surface attains a steady-state balance. When sensitized photocurrents were measured at light intensities sufficiently high to afford a sensitivity to the presence of methyl viologen in solution, the rate-limiting aspect was inferred to be charge-transfer between the dye and methyl viologen. This finding indicates that physisorbed Fast Green FCF can in fact be regenerated with a redox couple and the semiconductor/dye pairing can still function in accord with the traditional mechanism of sensitized charge-transfer[60], an important point relating to the prospects of p-GaP photocathodes.

Although it is tempting to analyze how the attributes of different redox couples affect sensitization of native p-GaP electrodes under high light intensity conditions, such data would be inextricably coupled with chemical attack of the GaP surface operating in parallel. No doubt this aspect convolutes the role that redox mediator properties like the standard potential and

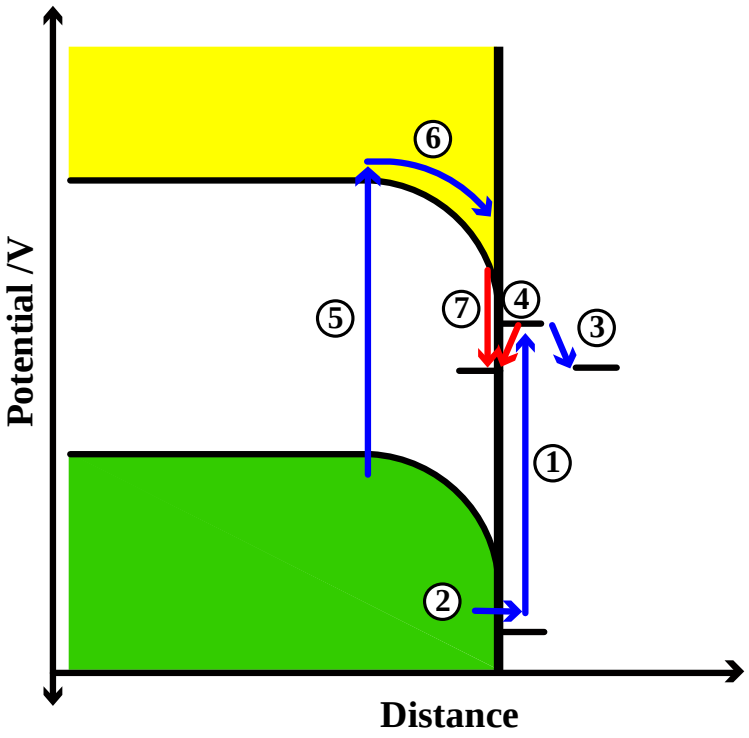

Figure 4.8 Schematic depiction of the flow of electrons for a physisorbed dye on p-GaP under illumination. 1) Sub-bandgap light absorption by physisorbed dye. 2) Electron injection from valence band into the ground state of the photoexcited dye (i.e. hole injection from the ground state of the photoexcited dye into the valence band). 3) Electron capture by a redox mediator from the photoexcited dye. 4) Electron capture by a surface state from the photoexcited dye. 5) Supra-bandgap light absorption by GaP. 6) Field-induced direction of photogenerated electrons to the GaP/electrolyte interface. 7) Electron capture by a surface state from the conduction band edge.

self-exchange rate play. Further, the long-term chemical instability of p-GaP interfaces coated with physisorbed dye in water severely compromises the possibility of such constructs being used in a practical two-electrode sensitized photoelectrochemical cell.

Three possible design motifs are still worth exploring for sensitized p-GaP. First, sensitizers tuned to longer wavelengths could be used if they provide insufficient driving force to reduce surface Ga atoms when photoexcited. Such dyes could then be regenerated with solution-based redox couples in a straight-forward manner. The difficulty then lies in identifying 'red' sensitizers with photoexcited states capable of injecting holes into the valence band of GaP. The rather positive potential of the valence band edge for GaP is mismatched to the standard potentials of the first oxidation of many 'red' dyes previously used in dye-sensitized platforms.[53-54] Moreover, longer wavelength dyes will necessarily require the use of redox mediators with more positive standard potentials, limiting the overall energy conversion efficiencies by capping the attainable photovoltage. Smaller photovoltages are not desirable, limiting the appeal of this approach.

Second, the use of Fast Green FCF and related dyes on native p-GaP interfaces may yet be possible if a redox mediator is identified that possesses a sufficiently fast charge-transfer with the excited state of the dye to outpace the surface reduction pathway. However, the saturated photocurrent density of 7.5 $x10^{-6}$ A cm^{-2} at high light intensities without a redox mediator in solution defines bounds for the necessary rate of charge-transfer. Assuming $3e^-$ reduction process for every Ga atom and an upper limit of 6.6 $x10^{11}$ atoms cm^{-2} for the atomic surface density, the corresponding reaction rate between the dye and the surface is at least 10^2 s^{-1}. This value represents the lower bounds on the charge transfer rate that a redox mediator must attain to match the surface process. To sufficiently outpace the deleterious surface process, a redox mediator should support a rate constant several orders of magnitude greater, as has been described in the context of fast redox mediators outpacing the corrosion of photoelectrodes in conventional regenerative photoelectrosynthetic schemes.[61] Although none of the electrolytes explored here suffice, rate constants for dye regeneration in sensitized photoanodes are known to reach values up to 10^5 s^{-1} through a combination of high concentrations and optimal dye-mediator energetics.[62-63] Accordingly, a more suitable redox mediator that better mitigates cathodic surface degradation of GaP may yet be identified.

A third route that may improve the efficacy of sensitized GaP photocathodes, without limiting the choice of redox mediator, is through chemical modification of the semiconductor surface. Although not fully demonstrated here, the data presented in Figure 4.7 show that the physicochemical properties of CH_3-terminated GaP(111)A are substantially different than native GaP(111)A but still permit sensitization under certain conditions. We have already shown previously that these surfaces are more resistant against both surface oxidation in air[49] and cathodic surface degradation in solution.[48] The latter is possible because the CH_3- groups coordinate the atop Ga atoms and inhibit changes in their redox state. The data are clear here that triarylmethane dyes with less charge and more non-polar groups (i.e. alkyl chains) do have some affinity for CH_3-terminated surfaces, allowing sensitization when dyes like Ethyl Violet are dissolved in solution. Still, in order to represent a path forward, the stabilizing effect of the CH_3- groups must be augmented with a chemical functionality that facilitates persistent dye adsorption. Work along these lines is ongoing in our laboratory.

5. Summary

The cumulative experimental data shown here illustrates the ability of freshly etched p-GaP to function as a photocathode when loaded with triarylmethane dyes. However, several issues were identified with this basic motif. First, dye coverage by simple immersion in dye solutions is low. Second, sensitized hole injection into freshly etched p-GaP surfaces is complicated by redox chemistry of GaP surfaces in water. Electron injection from the photoexcited dye into the interface to drive reductive transformations of the GaP surface is possible and occurs to an appreciable extent relative to electron injection into a species dissolved in solution. The surface redox activity of GaP is insufficient to regenerate dye at illumination intensities commensurate with solar irradiation. A solution to these issues may be realized through modification of p-GaP interfaces with surface groups that inhibit surface redox activity but still permit sensitization. The presented data suggests this is possible. In total, the enumeration of these points in this work represents a necessary step towards the development of sensitized p-GaP photocathodes.

6. References

1. He, J. J.; Lindstrom, H.; Hagfeldt, A.; Lindquist, S. E., *Sol. Energy Mater. Sol. Cells* **2000,** *62* (3), 265-273.
2. Nattestad, A.; Ferguson, M.; Kerr, R.; Cheng, Y. B.; Bach, U., *Nanotechnology* **2008,** *19* (29), 295304-295313.

3. Nattestad, A.; Mozer, A. J.; Fischer, M. K. R.; Cheng, Y. B.; Mishra, A.; Bauerle, P.; Bach, U., *Nat. Mater.* **2010,** *9* (1), 31-35.
4. Nattestad, A.; Perera, I.; Spiccia, L., *J Photoch Photobio C* **2016,** *28*, 44-71.
5. van den Bosch, B.; Rombouts, J. A.; Orru, R. V. A.; Reek, J. N. H.; Detz, R. J., *Chemcatchem* **2016,** *8* (7), 1392-1398.
6. Gibson, E. A., *Chem. Soc. Rev.* **2017,** *46* (20), 6194-6209.
7. Alibabaei, L.; Luo, H. L.; House, R. L.; Hoertz, P. G.; Lopez, R.; Meyer, T. J., *J. Mater. Chem. A* **2013,** *1* (13), 4133-4145.
8. Odobel, F.; Le Pleux, L.; Pellegrin, Y.; Blart, E., *Accounts Chem Res* **2010,** *43* (8), 1063-1071.
9. He, J. J.; Lindstrom, H.; Hagfeldt, A.; Lindquist, S. E., *J. Phys. Chem. B* **1999,** *103* (42), 8940-8943.
10. Borgstrom, M.; Blart, E.; Boschloo, G.; Mukhtar, E.; Hagfeldt, A.; Hammarstrom, L.; Odobel, F., *J. Phys. Chem. B* **2005,** *109* (48), 22928-22934.
11. Hu, Y.; Zheng, Z.; Jia, H. M.; Tang, Y. W.; Zhang, L. Z., *J. Phys. Chem. C* **2008,** *112* (33), 13037-13042.
12. Peng, S. J.; Shi, J. F.; Pei, J.; Liang, Y. L.; Cheng, F. Y.; Liang, J.; Chen, J., *Nano Res.* **2009,** *2* (6), 484-492.
13. Gronet, C. M.; Lewis, N. S., *Nature* **1982,** *300* (5894), 733-735.
14. Kohl, P. A.; Bard, A. J., *J. Am. Chem. Soc.* **1977,** *99* (23), 7531-7539.
15. Bockris, J. O. M.; Uosaki, K., *J. Electrochem. Soc.* **1977,** *124* (9), 1348-1355.
16. Halmann, M., *Nature* **1978,** *275* (5676), 115-116.
17. Ito, K.; Ikeda, S.; Yoshida, M.; Ohta, S.; Iida, T., *Bull. Chem. Soc. Jpn.* **1984,** *57* (2), 583-584.
18. White, T.; Carter, M. A.; Mottram, A.; Peaker, A. R.; Sudlow, P. D., *Nature* **1971,** *232*, 469-470.
19. Memming, R.; Tributsc.H, *J. Phys. Chem.* **1971,** *75* (4), 562-570.
20. Choi, D.; Rowley, J. G.; Parkinson, B. A., *J. Electrochem. Soc.* **2012,** *159* (11), H846-H852.
21. Ilic, S.; Brown, E. S.; Xie, Y.; Maldonado, S.; Glusac, K. D., *J Phys Chem C* **2016,** *120* (6), 3145-3155.
22. Price, M. J.; Maldonado, S., *ECS Trans.* **2011,** *35* (8), 153-163.
23. Wang, Z. J.; Shakya, A.; Gu, J. S.; Lian, S. C.; Madonado, S., *J. Am. Chem. Soc.* **2013,** *135* (25), 9275-9278.
24. Iwamoto, T.; Ogawa, Y.; Sun, L.; White, M. S.; Glowacki, E. D.; Scharber, M. C.; Sariciftci, N. S.; Manseki, K.; Sugiura, T.; Yoshida, T., *J Phys Chem C Nanomater Interfaces* **2014,** *118* (30), 16581-16590.
25. Moser, J.; Gratzel, M., *J. Am. Chem. Soc.* **1984,** *106* (22), 6557-6564.
26. Spitler, M. T.; Calvin, M., *J. Chem. Phys.* **1977,** *66* (10), 4294-4305.
27. Goldberg, Y. A., World Scientific: 2012; pp 104-124.
28. Malmberg, C. G.; Maryott, A. A., *J. Res. Natl. Bur. Stand.* **1956,** *56* (1), 1-8.
29. Ruangchuay, L.; Schwank, J.; Sirivat, A., *Appl. Surf. Sci.* **2002,** *199* (1-4), 128-137.
30. Briggs, D.; Seah, M. P., *Practical surface analysis : by auger and x-ray photoelectron spectroscopy*. Wiley: Chichester ; New York, 1983; p xiv, 533 p.
31. Arning, M. D.; Minteer, S. D., Elsevier: Amsterdam, 2007; pp 813-827.
32. Doine, H.; Whitcombe, T. W.; Swaddle, T. W., *Can. J. Chem.* **1992,** *70* (1), 81-88.
33. Howes, K. R.; Pippin, C. G.; Sullivan, J. C.; Meisel, D.; Espenson, J. H.; Bakac, A., *Inorg. Chem.* **1988,** *27* (17), 2932-2934.
34. Royea, W. J.; Hamann, T. W.; Brunschwig, B. S.; Lewis, N. S., *J. Phys. Chem. B* **2006,** *110* (39), 19433-19442.
35. Yee, E. L.; Hupp, J. T.; Weaver, M. J., *Inorg. Chem.* **1983,** *22* (23), 3465-3470.
36. Gratzel, M., *J Photoch Photobio C* **2003,** *4* (2), 145-153.
37. Gong, J. W.; Liang, J.; Sumathy, K., *Renew. Sust. Energ. Rev.* **2012,** *16* (8), 5848-5860.
38. Tributsch, H., *Coord. Chem. Rev.* **2004,** *248* (13-14), 1511-1530.
39. Lee, J. K.; Yang, M. J., *Mater Sci Eng B-Adv* **2011,** *176* (15), 1142-1160.

40. Wang, Q.; Ito, S.; Gratzel, M.; Fabregat-Santiago, F.; Mora-Sero, I.; Bisquert, J.; Bessho, T.; Imai, H., *J. Phys. Chem. B* **2006,** *110* (50), 25210-25221.
41. Dareedwards, M. P.; Hamnett, A.; Goodenough, J. B., *J. Electroanal. Chem.* **1981,** *119* (1), 109-123.
42. Butler, M. A.; Ginley, D. S., *Appl. Phys. Lett.* **1983,** *42* (7), 582-584.
43. Bansal, A.; Turner, J. A., *J. Phys. Chem. B* **2000,** *104* (28), 6591-6598.
44. Uosaki, K.; Kita, H., *Chem. Lett.* **1984,** (6), 953-956.
45. Li, J.; Peat, R.; Peter, L. M., *J. Electroanal. Chem.* **1984,** *165* (1-2), 41-59.
46. Heller, A.; Vadimsky, R. G., *Phys. Rev. Lett.* **1981,** *46* (17), 1153-1156.
47. Meek, R. L.; Schumake.Ne, *J. Electrochem. Soc.* **1971,** *118* (8), 1148-1152.
48. Brown, E. S.; Peczonczyk, S. L.; Wang, Z. J.; Maldonado, S., *J. Phys. Chem. C* **2014,** *118* (22), 11593-11600.
49. Mukherjee, J.; Peczonczyk, S.; Maldonado, S., *Langmuir* **2010,** *26* (13), 10890-10896.
50. Grundner, M.; Jacob, H., *Appl. Phys. A Mater.* **1986,** *39* (2), 73-82.
51. Morota, H.; Adachi, S., *J. Appl. Phys.* **2006,** *100* (5), 054904-054910.
52. Mukherjee, J.; Erickson, B.; Maldonado, S., *J. Electrochem. Soc.* **2010,** *157* (4), H487-H495.
53. Spitler, M. T.; Parkinson, B. A., *Acc. Chem. Res.* **2009,** *42* (12), 2017-2029.
54. Ushiroda, S.; Ruzycki, N.; Lu, Y.; Spitler, M. T.; Parkinson, B. A., *J. Am. Chem. Soc.* **2005,** *127* (14), 5158-5168.
55. Park, S. M.; Barber, M. E., *J. Electroanal. Chem.* **1979,** *99* (1), 67-75.
56. Butler, M. A.; Ginley, D. S., *Appl. Phys. Lett.* **1980,** *36* (10), 845-847.
57. Yoneyama, H.; Mayumi, S.; Tamura, H., *J. Electrochem. Soc.* **1978,** *125* (1), 68-74.
58. Chitambar, M.; Wang, Z. J.; Liu, Y. M.; Rockett, A.; Maldonado, S., *J. Am. Chem. Soc.* **2012,** *134* (25), 10670-10681.
59. Parkinson, B. A., *Langmuir* **1988,** *4*, 967-976.
60. Gratzel, M., *Nature* **2001,** *414* (6861), 338-344.
61. Wrighton, M. S., *J. Electrochem. Soc.* **1986,** *133* (3), C135-C135.
62. Anderson, A. Y.; Barnes, P. R. F.; Durrant, J. R.; O'Regan, B. C., *J. Phys. Chem. C* **2011,** *115* (5), 2439-2447.
63. Daeneke, T.; Mozer, A. J.; Uemura, Y.; Makuta, S.; Fekete, M.; Tachibana, Y.; Koumura, N.; Bach, U.; Spiccia, L., *J. Am. Chem. Soc.* **2012,** *134* (41), 16925-16928.

CHAPTER 5

Exploring Alkene Grafting on GaP(100) and (111)A

1. Introduction

In a photoelectrochemical energy conversion cell using GaP as a photocathode, two challenges must be solved. The first issue is solving the surface instability of GaP in contact with water. The second challenge is the moderate visible light absorption of GaP at wavelengths longer than 550 nm. Employing surface modification strategies can alleviate these issues. A passivating surface layer can stabilize the GaP surface against chemical degradation in aqueous conditions.[1-2] Grafting, a sensitizer onto that layer could improve photon collection at longer wavelengths of light.[3-8]

A previous chapter focused on the investigation of the sensitization process at bare GaP electrodes containing a physisorbed molecular sensitizer. The cumulative findings indicated that during sensitization, the excited dye molecules were regenerated by injecting charges into surface atoms, rather than being regenerated by a redox couple in solution,.[5] This process results in accumulation of metallic gallium at the interface and accordingly renders the photocathode inactive since the metal acts to trap charge. To combat these issues, GaP(111)A electrodes were functionalized using a two-step process: chlorination followed by a Grignard reaction, to introduce methyl surface groups. Although methyl groups kinetically inhibited electrochemical degradation, these groups also hindered dye loading. Dye sensitization of physisorbed Fast Green on methyl terminated GaP surfaces was not observed and was attributed to the lack of favorable interaction between the nonpolar surface and the charged dye molecules. Therefore, to realize the potential of GaP as a dye sensitized photocathode, surface groups must be introduced on a GaP surface that not only chemically and electrochemically passivate the semiconductor but also facilitate some sort of rational dye attachment. Herein, this chapter develops a strategy of alkene grafting for producing a cationic monolayer on GaP that inhibits chemical degradation but promotes adhesion of anionic sensitizers (Figure 5.1).

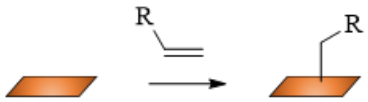

Figure 5.1 Chemical modification route for GaP(100) and GaP(111)A

Three major points are considered for the development of the monolayer species in this chapter. First, the introduction of the monolayer is intended to facilitate dye physisorption through charge affinity with opposite charged dyes. In this way, a range of dye molecules can be investigated, avoiding the constraint of designing unique reaction strategies for a covalent bond for every specific dye. Second, the monolayer must not totally inhibit electronic coupling between the semiconductor and a photoexcited dye. Little to no resistance should be encountered as charge travels from the dye into GaP. Third, the monolayer should consist of densely packed functional groups to inhibit formation of deleterious surface oxides. A high packing density will also allow for greater dye adsorption.

A major disadvantage of using Grignard reagents to design an organic monolayer is their chemical incapability with many desirable functionalities, placing a constraint on the types of monolayers that are possible. With Grignard reagents, there is no straightforward method to graft positively charged functional groups to a surface. Additionally, on GaP, this reaction scheme appears to be limited specifically to the GaP(111)A crystal plane. Accordingly, to achieve the desired objectives, an alternate reaction scheme must be developed. Here we selected alkene grafting, which involves a primary alkene reacting with and binding to the surface through reduction of the C=C bond. Alkene grafting has been reported previously on Si.[9] There is some precedent for this idea on GaP, too,[10] but only using ultraviolet light to initiate the reaction. Although UV irradiation is effective in promoting alkene reactions with GaP, it often leads to surface oxidation.[9, 11] On Si, alkenes can react with surface atoms via hydrosilylation and therefore such reactions can also be initiated thermally.[12] On GaP, it is presently unclear if such a mechanism is possible.

2. Experimental

Chemicals and Materials

Methanol (anhydrous, 99.8%, Aldrich), hexanes (99.9%, Fisher), acetone (HPLC-grade, Fisher), tetrahydrofuran (anhydrous, ≥ 99.9%, Aldrich), 1-octadecene (≥ 95.0%, Aldrich), vinyl ferrocene (97%, Aldrich), (vinylbenzyl)trimethylammonium chloride (99%, Aldrich), Fast Green Dye (≥ 85%), dimethyl sulfoxide (anhydrous, ≥ 99.9%, Aldrich), octadecylmagnesium chloride (0.5M CH_3MgCl solution in THF, Aldrich), phosphorous pentachloride (95%, Aldrich), chlorobenzene (anhydrous, 99.8%, Aldrich), benzyl peroxide (≥ 97%, Aldrich), hydrofluoric acid

(48%, Fisher), methyl viologen dichloride hydrate(98%, Aldrich), potassium chloride (ACS grade, Mallinckrodt), forming gas (5% hydrogen/ 95% nitrogen, Metro Welding), argon gas (Metro Welding), indium (99.99%, Gallium Source), and zinc powder (≥ 99.8%, Baker Analyzed) were used as received. Water with a resistivity of > 18 MΩ cm (Barnsted Nanopure system) was used throughout. n-GaP(100) with S doping level of 4.75 x 10^{17} cm^{-3} and thickness of 302 ± 20 were purchased from El-Cat. Double-side polished (etch pit density = 1.5 x 10^{5} cm^{-2}) p-type GaP(111)A with Zn doping level of 1.4x$10^{18}$$cm^{-3}$ and a thickness of 400 ± 20 μm were obtained from University Wafers.

Chemical Surface Modification

Prior to performing any chemical surface modifications, GaP(100) and GaP(111)A wafers were diced into 0.5 x 0.5 cm squares. The wafers were then degreased in hexanes, acetone, methanol and water for 5 minutes each, etched with oxygen or argon plasma for 5 minutes and etched in concentrated HF for 1 minute, rinsed with water and dried under nitrogen. Immediately after etching, wafers were transferred to a nitrogen-purged glove box. All surface reactions took place in a nitrogen-purged glove box. For reactions with 1-octadecene, wafers were placed in reaction vials containing neat 1-octadecene and reacted at designated temperatures and times. To react vinyl ferrocene with GaP(111)A surfaces, freshly etched surfaces were placed in 0.1 M vinyl ferrocene solution in THF at 90 ºC for 12 h (Figure 5.2). (Vinylbenzyl)trimethylammonium chloride was dissolved in DMSO at a concentration of 0.125M, and the reactions took placed at 90 ºC (Figure 5.3).

To prepare $CH_3(CH_2)_{16}CH_2$-GaP terminated surfaces using a Grignard reaction, freshly etched GaP(111)A surfaces were chlorinated at 90 °C for 50 min using a saturated solution of phosphorous (V) pentachloride in chlorobenzene and a few grains of benzoyl peroxide. Upon completion, samples were washed with THF and transferred to reaction vessels containing octadecylmagnesium chloride. The Grignard reaction was carried out at 100 °C for 12 hours.

Dye adsorption on reacted GaP surfaces

To adsorb Fast Green on bare GaP surfaces or those reacted with (vinylbenzyl)trimethylammonium chloride, wafer sections or electrodes were immersed in

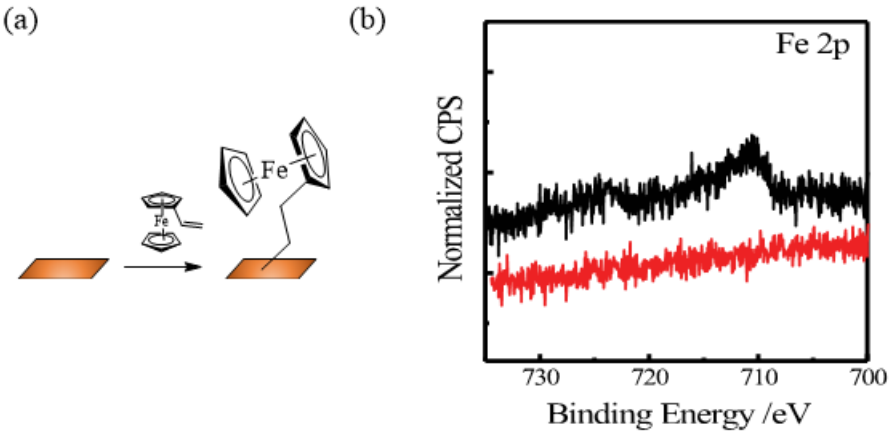

Figure 5.2 (a) Grafting of vinyl ferrocene to GaP(111)A surface. (b) High resolution Fe 2p XP spectra of GaP(111)A samples reacted with vinyl ferrocene for 12 h (black) and after sonication in water for 5 minutes (red).

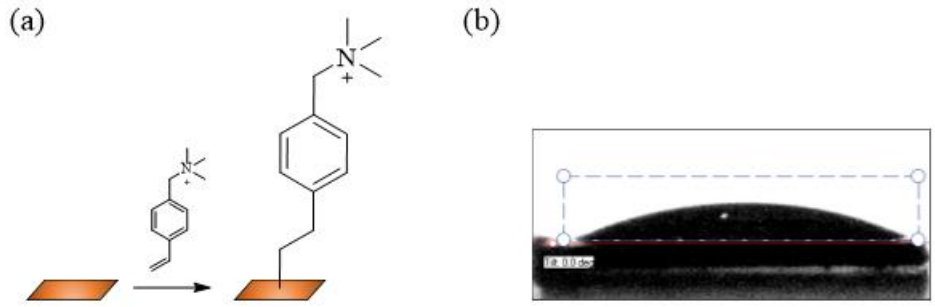

Figure 5.3 (a) Grafting of (vinylbenzyl)trimethylammonium chloride to GaP(111)A. (b) Optical photograph of contact between a H_2O droplet and GaP(111)A wafer reacted with 0.125 M (vinylbenzyl)trimethylammonium chloride in DMSO for 2 h at 90 ºC. CA = 31 ± 5 º.

aqueous solution of dissolved Fast Green dye (6mM). After a designated time, wafer sections or electrodes were rinsed with water 3 times and dried with a dry nitrogen stream.

Electrode Fabrication

P-type GaP(111)A wafers cut into roughly 0.5 cm x 0.5 cm sections, degreased in hexanes, acetone, methanol and water for 5 minutes, oxygen plasma etched for 5 minutes and etched in concentered HF for 1 minute. Ohmic contacts were then prepared by soldering an In-Zn mixture onto the backs of each GaP wafer section, followed by annealing in forming gas for 10 minutes at 400 °C. Prior to chemical modification, excess In-Zn present on the backside was etched off with a drop of concentrated H_2SO_4 for 30 seconds. The front of the wafer sections were then re-etched and transferred to a nitrogen-purge glovebox for reaction with (vinylbenzyl)trimethylammonium chloride. Upon completion of the functionalization step, additional In-Zn was soldered onto the back, but no further annealing was performed. These wafer sections were then mounted on to tinned copper wire using silver print (GC Electronics), which was then threaded through a glass rod. An inert epoxy (Hysol C) was then used to insulate the back and sides, exposing only the front face of the wafer section for use as an electrode.

Static Sessile Contact Angle Measurements

The contact angle formed between a droplet of distilled water and a GaP interface was recorded using a CAM 100 optical contact angle meter (KSV instrument, Helsinki, Finland). KSV software was utilized during data collection and analysis.

X-ray Photoelectron (XP) Spectroscopy

X-ray photoelectron spectra were collected using a PHI 5400 analyzer equipped with Al K α (1486.6 eV, 6 mA current emission and a 12 kV anode high tension) source, without a monochromator. Data collection took place at a pressure of $< 2.5 \times 10^{-9}$ Torr, without charge neutralization. High resolution spectra were collected at pass energy of 23.5 eV. All binding energies were referenced to the expected binding energy for adventitious carbon (284.6 eV). Spectrum analysis was performed with CASA XPS 2.3.13 software.

Photoelectrochemical Measurements

All electrochemical measurements were performed in a three-electrode cell under potentiostatic control (PAR 273) in an airtight Pyrex cell with an optically flat and transparent quartz bottom. All solutions were sparged with N_2(g) and kept under a constant flow of N_2(g). A Pt mesh counter electrode and a Ag/AgCl(sat. KCl) reference electrode were used throughout. All potentials were referenced to *E*(Ag/AgCl(sat. KCl)). Care was taken to ensure the distance between the GaP electrode and electrochemical cell window remained small and constant for all measurements. Oriel 150 W Xe arc lamp (Newport) and a quarter-turn single grating monochromator (Model 74125, Newport) were used to collect wavelength-dependent external quantum yields. Additionally, external quantum yield measurements were conducted under chopped illumination at 15Hz and -0.6V vs *E*(Ag/AgCl). To correct the data for fluctuations in light intensity, a quartz beam splitter directed a portion of the light to a Si photodiode (Model 70316NS, Newport). The output signal from the cell and the reference Si photodiode was passed through a Stanford Instruments SR830 lock-in amplifier and relayed to a computer controlled by custom-written LabVIEW software. Wavelengths were scanned at increments of 5 nm from the longest wavelength to the shortest wavelength.

3. Results

Temperature dependence of 1-octadecene grafting

The temperature dependence of grafting 1-octadecene on GaP was monitored by measurement of contact angles between water and GaP surfaces after performing each reaction. Freshly etched GaP(100) wafers subjected to a reaction with neat 1-octadecene at 23 ºC (room temperature), 90 ºC, and 200 ºC for 24 h. The measured contact angles for GaP(100) reacted for 24 h under various temperatures are summarized in Figure 5.4and Table 5.1. Figure 5.5 shows optical photographs of contacts between a H_2O droplet and GaP wafers after reaction at various temperatures. An independent Student's *t* test was performed to determine whether the data supported the contention that temperature effected a change in the resultant surface layer. Following statistical analyses, a clear difference in the measured contact angles was observed between the data for bare GaP surfaces and surfaces reacted with 1-octadecene. As shown in Figure 5.4, a near two-fold increase in water contact angle was measured. These results are consistent with octadecyl groups chemisorbed onto the surface to render hydrophobic character. On the other

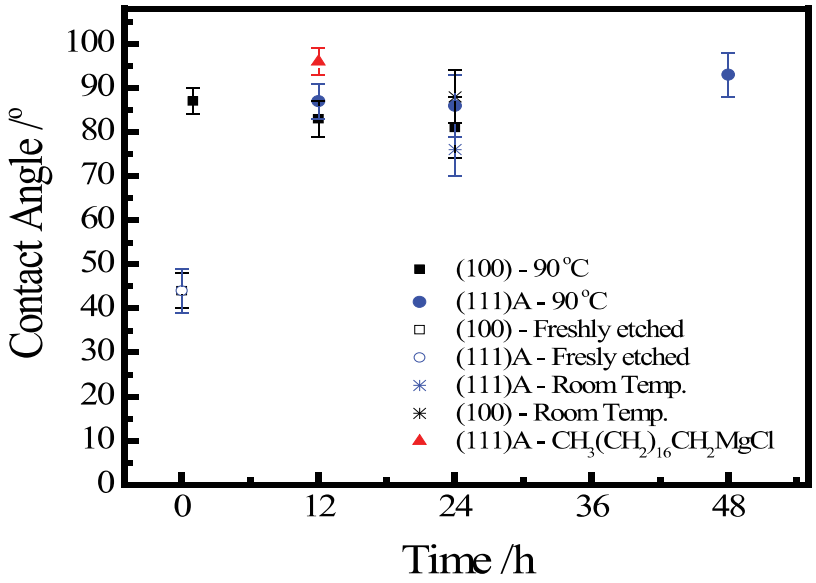

Figure 5.4 Static sessile water contact angle measurements of GaP(100) and (111)A wafers reacted in neat 1-octadecene as a function of reaction time. Grafting occurred at 90 ºC unless noted otherwise. For comparison, water contact angles for freshly etched bare GaP(100) and (111)A are plotted. Additionally, results for GaP(111)A surface reacted with octadecylmagnesium chloride, $CH_3(CH_2)_{16}CH_2MgCl$, are included.

Table 5.1 Contact angle (CA) measurements between water and GaP surfaces reacted with 1-octadecene.

Surface *	**Time / h**	**Temperature / ºC**	**CA / degrees**
(100)	24	RT	88 ± 6 (n = 6)
(100)	24	90	81 ± 7 (n = 6)
(100)	24	200	85 ± 7 (n = 6)
(100)	1	90	87 ± 3 (n = 6)
(100)	12	90	83 ± 4 (n = 6)
(111)A	24	90	86 ± 7 (n = 3)
Argon Plasma - (100)	24	90	93 ± 3 (n = 12)

* All surfaces were degreased, oxygen plasma etched, and HF etched, unless noted otherwise.

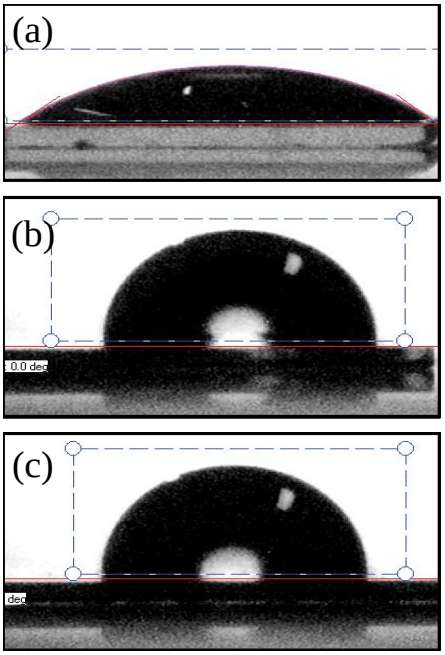

Figure 5.5 Optical photographs of contacts between a H_2O droplet and GaP wafers. (a) freshly etched GaP(100) CA = 44 ± 4 º. GaP(100) after reaction with 1-octadecene (b) at 90 ºC for 24 h CA = 81 ± 7 º, and (c) at room temperature for 24 h CA= 79 ± 5.

hand, we determined that the GaP/water contact angles for reactions performed at 25, 90, and 200 ºC were not statistically different at the 95% confidence interval. This aspect strongly implied that the reaction was not thermally activated in this temperature range.

Time dependence of 1-octadecene grafting

The time dependence for the efficiency of thermal grafting of alkenes on GaP(100) was measured through contact angle measurements between water and GaP surfaces. The assumption in this strategy was that higher contact angles were correlated with higher density of surface coverage. The time dependence was performed at 90 ºC. This temperature was selected since no statistical difference (at a 95 % confidence interval) was seen between samples reacted at 90 ºC and 200 ºC. Results are summarized in Figure 5.4 and Table 2.1, a constant range of water contact angles values was reached, as evidenced by an independent samples *t*-test. Table 5.2 summaries the independent sample t-test results. All measured differences were not statistically significant at the 95% confidence level.

Surface treatment prior to 1-octadecene grafting

To assess whether surface pre-treatments that yield high densities of surface defects/radicals such as plasma etching influenced the reaction with 1-octadecene, additional reactions were performed with GaP sections that were first exposed to either oxygen or argon plasma for 5 minutes. Surface roughness was evaluated using AFM, no significant difference was measured between the two treatments. Contact angle measurements between water and GaP surfaces after grafting were recorded as a function of pre-treatment. Treating GaP(100) surfaces with oxygen or argon plasma prior to a reaction with 1-octadecene resulted in a water contact angle of 81 ± 7 º and 93 ± 3 º, respectively. A Student's *t*-test analysis confirmed that plasma pre-treatment led to statistically significant difference in water contact angles at the 95% confidence level.

Comparison of 1-octadecene grafting and chlorination-Grignard surface functionalization

No significant differences in contact angle values were seen after reacting alkenes on either GaP(100) or GaP(111)A surface. For GaP(111)A surfaces, octadecyl groups grafted through Grignard chemistry showed statistically different contact angle values at the 95% confidence level. Grignard functionalization surfaces led to higher water contact angles, implying higher surface

Table 5.2 Summary of statistical analysis; comparing alkene grafting as a function of (a) reaction time, and (b) temperature.

(a) Grafting of 1-octadecene on GaP (100) as a function of temperature

Reaction Conditions		Temperature	Degrees of Freedom	t-value at 95% confidence	t-value calculated
24hrs in neat 1-octadecene	**RT** (n = 6) M = 88 SD = 6	**90ºC** (n = 6) M = 81 SD = 7	10	2.228	1.720
		200ºC (n = 6) M = 85 SD = 7	10	2.228	0.737
24hrs in neat 1-octadecene	**90ºC** (n = 6) M = 81 SD = 7	**200ºC** (n = 6) M = 85 SD = 7	10	2.228	0.904

(b) Grafting of 1-octadecene on GaP (100) as a function of time

Reaction Conditions		Time	Degrees of Freedom	t-value at 95% confidence	t-value calculated
90ºC, in neat 1-octadecene at	**1hr** (n = 6) M = 87 SD = 3	**12hrs** (n = 6) M = 83 SD = 4	10	2.228	1.832
		24hrs (n = 6) M = 81 SD = 7	8	2.306	1.470
90ºC, in neat 1-octadecene at	**12hrs** (n = 6) M = 83 SD = 4	**24hrs** (n = 6) M = 81 SD = 7	10	2.228	0.533

Table 5.2 continued. Summary of statistical analysis; comparing alkene grafting as a function of (c) crystal orientation, and (d) plasma etching. (e) Comparison between chemical modification strategies on GaP (111)A.

(a) Grafting of 1-octadecene on either GaP (100) or GaP (111) A surfaces

Reaction Conditions		Temperature	Degrees of Freedom	t-value at 95% confidence	t-value calculated
24hrs in neat 1-octadecene at 90ºC	**(100)** (n = 6) M = 81 SD = 7	**(111) A** (n = 3) M = 86 SD = 7	7	2.365	0.891

(b) Grafting of 1-octadecene on GaP (100) after plasma etching

Reaction Conditions		Temperature	Degrees of Freedom	t-value at 95% confidence	t-value calculated
24hrs in neat 1-octadecene at 90ºC	**Oxygen** (n = 6) M = 81 SD = 7	**Argon** (n = 12) M = 93 SD = 3	6	2.447	4.0186

(c) Comparison between chemical modification strategies on GaP (111) A

Reaction Conditions		Temperature	Degrees of Freedom	t-value at 95% confidence	t-value calculated
12hrs in neat 1-octadecene at 90ºC	(n = 5) M = 87 SD = 4	Chlorination- Grignard reaction , 12hrs at 90ºC (n = 6) M = 96 SD = 3	9	2.262	3.957

coverage (i.e. greater packing density). For instance, GaP(111)A reacted with octadecylmagnesium chloride for 12 h at T = 90 ºC lead to a water contact angle of 96 ± 3 º while (111)A and (100) reacted with 1-octadecene lead to a water contact angle of 87 ± 4 º and 83 ± 4 º, respectively (Table 5.1).

Surface passivation of 1-octadecene grafted groups

To probe the ability of the functional monolayer to prevent chemical oxidation under ambient conditions, oxide signal was measured as a function of time using X-ray photoelectron (XP) spectroscopy. Based on the intensity of the oxide signal, oxide thickness was calculated, using the simplified substrate overlayer model[2, 13],

$$d = \lambda_{ov} \sin\varphi \left(\ln\left(1 + \frac{I_{overlayer}}{I_{substrate}} \frac{I^{0}{}_{substrate}}{I^{0}{}_{overlayer}} \right) \right)$$

Equation 2.1 Simplified Substrate Overlayer Equation.

where d is the thickness of the oxide overlayer in nanometer, λ_{ov} is escape depth of emitted electrons through the oxide layer, φ is the takeoff angle (54.6°) between the sample surface and the detector, $I_{substrate}$ is the integrated area for bulk signal, $I_{overlayer}$ is the integrated area of oxide signals, $I^{0}_{substrate}$ is the integrated area of the bulk signal obtained from a freshly etched GaP sample, $I^{0}_{overlayer}$ is the integrated area for a thick (>500 nm) thermal oxide layer on GaP. The escape depths for P 2p electrons was estimated using eq.2

$$\lambda = 0.41 A^{3/2} E^{1/2}$$

Equation 2.2 Electron Escape Depth Calculation.

where A is the mean diameter of one unit in the overlayer (nm) and E is the kinetic energy of the ejected core electron (eV). The mean diameter of one unit (A) can be calculated:

$$A = \sqrt[3]{\frac{MW}{\rho N_A}}$$

Equation 2.3 Mean Diameter Calculation.

where MW is mean atomic weight (g mol^{-1}), ρ is the density (g cm^{-3}), and N_A is Avogadro's number. For comparison, the degree of chemical oxidation was monitored for surfaces reacted with 1-octadecene and for those reacted with octadecylmagnesium chloride. Surfaces reacted with octadecylmagnesium chloride showed superior resistance against oxidation in air than surfaces reacted with 1-octadecene (Figure 5.6).

Grafting of a redox active group

To probe charge transfer across the grafted monolayer, GaP(111)A electrodes were reacted with vinyl ferrocene for 12 h at T = 90 ºC (Figure 5.2a). Fe 2p high resolution XP spectrum were collected before and after reaction. As seen in Figure 5.2b, Fe 2p signal was detected at 710.5 eV and 724 eV corresponding to Fe $2p_{3/2}$ and Fe $2p_{1/2}$, respectively, and confirmed the presence of ferrocenes on the surface. To assess the stability of the linkage between vinyl ferrocene and GaP(111)A, reacted surfaces were sonicated in water for 5 minutes. Afterwards, the Fe 2p signals were lost and no longer detectable by XP spectroscopy (Figure 5.2b). This observation could mean either initially detected vinyl ferrocene was just physisorbed on the GaP surface via non-covalent interactions or the covalent bond was dissociated when placed in water and sonicated. There is no precedent for the latter possibility, but this issue was not resolved and remains an open question. Accordingly, the results precluded further electrochemical experiments to gauge the electronic coupling across the surface bond.

Grafting of cationic surface groups and subsequent dye loading

To study the influence of surface functional groups on the physisorption of an ionic dye, trimethyl ammonium moieties were chosen. Freshly etched GaP(111)A was subjected to a reaction with (vinylbenzyl)trimethylammonium chloride for either 2 or 10 h at 90 ºC in DMSO (Figure 5.3). Contact angle measurements between water and GaP surfaces after reaction showed high surface wettability, 31 ± 5 º (Figure 5.3a). These results were consistent with the presence of polar surface groups that rendered the surface hydrophilic. Subsequently, functionalized GaP surfaces were soaked in a solution of 6 mM Fast Green dye for 90 seconds and then characterized by XP spectroscopy. As shown in Figure 5.7b the peak at 168 eV corresponds to S 2p from the SO_3^- groups of Fast Green.[14] Consistent dye loading was seen in both cases, whether the surface was reacted with (vinylbenzyl)trimethylammonium chloride for 2 or for 10 h. The spectra

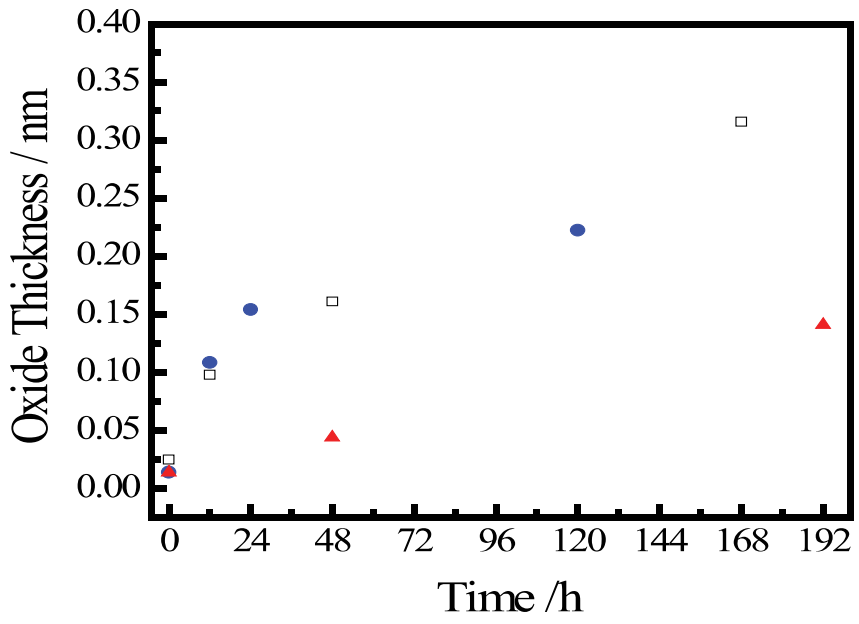

Figure 5.6 Oxide thickness as a function of time in ambient air calculated from high-resolution P 2p XP spectra for bare (□) GaP surfaces, surfaces reacted with (●) 1-octadecene, and surfaces reacted with (▲) octadecylmagnesium chloride.

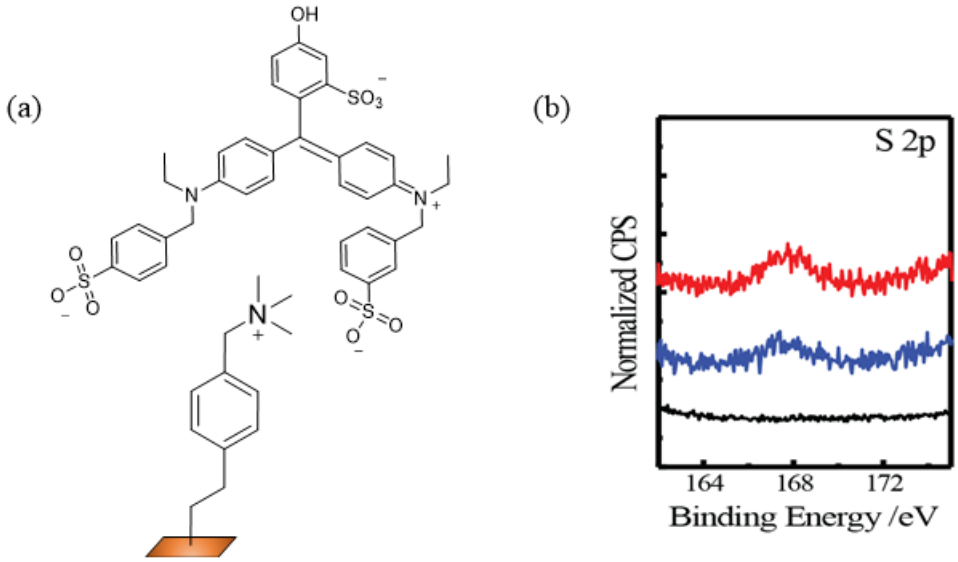

Figure 5.7 (a) Scheme showing a functionalized GaP surface with a cationic functional group and the structure of Fast Green. (b) High resolution S 2p XP spectra of GaP(111)A samples reacted with (vinylbenzyl)trimethylammonium chloride for 2 h (blue) and 10 h (red) followed by soaking in Fast Green solution for 90 sec. For comparison high resolution S 2p XP spectrum of bare GaP(111)A soaked in Fast Green solution for 90 sec is plotted in black.

suggested dye loading was obtained but a reasonable measure of the surface coverage was not obtained. To apply the overlayer model to determine surface coverage, the thickness of the organic monolayer and the packing of the dye on the surface need to be approximated. Since a clear understanding of the structure of the monolayer is not known (i.e how the functional groups are bonded to the surface or their orientation) it is difficult to predict the thickness of the monolayer. Additionally, it is not clear on how the dye is loading on the surface. For instance, a key parameter is the escape depth of electron coming from the sulfur atoms of Fast Green. A simple assumption that the dye is oriented perpendicular to the surface is not valid to calculate escape depth. For comparison, S 2p signal could not be detected on bare GaP surfaces soaked in a Fast Green solution (Figure 5.7b).

Spectral response of p-GaP photocathodes

To investigate whether the positively charged monolayer on GaP afforded persistent dye sensitization, the wavelength dependent the external quantum yields for photocurrent generation were collected. p-GaP(111)A electrodes were reacted with (vinylbenzyl)trimethylammonium chloride for 2 h followed by soaking in a 6 mM Fast Green solution. As shown in Figure 5.8, the spectral response of a GaP electrode after treatment without prior soaking in a dye solution showed no signal at wavelengths longer than 550 nm. When the same electrode was soaked in a solution of Fast Green, an increase in photocurrent at 650 nm was observed. Increasing the soaking time only slightly improved the photocurrent, indicating a limiting condition as obtained. Surprisingly, the response of the functionalized electrode soaked in Fast Green solution (EQY at 650nm = 3.64×10^{-5}) was 2.5 times **lower** than that of bare, freshly etched GaP(111)A (EQY at 650nm = 9.42×10^{-5}).[5]

4. Discussion

The ability to tailor surface properties of GaP for photoelectrochemical applications is highly desirable. The data in this chapter speak to the following three points. First, thermal grafting of alkenes on GaP appears to proceed strictly through surface defects. Two, the mechanism is likely radical based. Three, although limited in attainable functional group density and underlying electronic surface quality, the GaP interfaces produced by this scheme showed measurable sensitization.

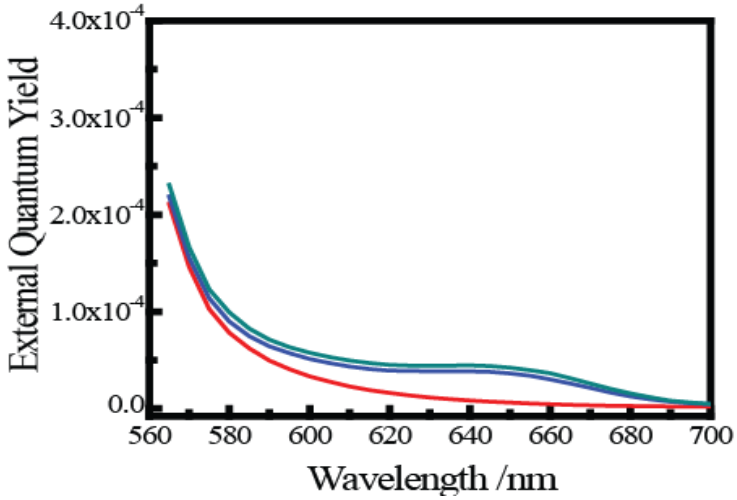

Figure 5.8 Wavelength dependence of the external quantum yields of a p-GaP(111)A electrode reacted with (vinylbenzyl)trimethylammonium chloride for 2 h at 90ºC; (red) before soaking in a 6mm Fast Green solution, (blue) after soaking in a 6mM Fast Green solution for 90 seconds and (green) after soaking in a 6mM Fast Green solution for 25 minutes. In all cases the electrode was poised at E = −0.6 V vs E(Ag/AgCl) and measurements were collected in deaerated electrolyte containing 5mM methyl viologen in 1M KCl.

Consistently, GaP surfaces exhibited a hydrophobic character after reaction with alkenes in comparison to bare GaP surfaces. Regardless of the time and temperature used for reaction, a similar range of contact angles values were attained. In addition, no preferential grafting on either (100) or (111)A surface plane was observed. These observations are quite different than what is observed for the chlorination-Grignard reaction sequence. Successful reaction with Grignard reagents only occurs on chlorinated GaP(111)A surface planes, resulting in Ga-C surface bonds.[2] Here, the data showed that reactions with alkenes and the chlorination-Grignard sequence lead to different densities of monolayers, similar to what was previously reported for Si surfaces where the same organic functional group introduced via two different strategies resulted in different levels of chemical and electrochemical passivation.[15]

No clear dependence was seen on reaction time or temperature. However, a difference was noted if surfaces were pretreated with argon rather than oxygen plasma. The plasma treatment step generally removes adventitious carbons. Oxygen plasma oxidizes organic surface contaminants, leaving oxygenated surface moieties.[16] In contrast, argon plasma generates free radicals on surfaces and leaves a high density of active sites.[16-17] Since surface pre-treatments with argon plasma showed statistically higher contact angles, a reasonable conclusion is that the extent of alkene grafting is limited by the number of surface defects.

The idea of grafting alkenes through surface defects on GaP is contradictory to what is currently known for alkene reactions with Si. This discrepancy is notable, since our lab has previously shown that the chlorination-Grignard sequence works similarly on Si and GaP surfaces. The mechanism of alkene grafting on silicon depends both on surface orientation and method of initiation.[9, 18] Surface radicals can be formed on Si by a homolytic cleavage of surficial Si-H bonds, initiated by UV radiation (< 350 nm).[9] Once a Si radical is formed, it reacts rapidly with an alkene functionality and grafting occurs through radical propagation (Figure 5.9a). Thermal grafting can also create radical at the silicon surface at T > 150 ºC. Hence, at temperatures lower than 150 ºC, the radical pathway is not feasible and instead a concerted mechanism has been discussed (Figure 5.9b).[12] The chemical composition of GaP after wet etching is not well-defined, with a mixture of thin surface oxide and Ga-H have been reported.[19-20] In principle, grafting of alkenes could follow a similar mechanism as on a Si surface. However, the presented findings show that alkene grafting on GaP has no obvious dependence on surface condition, even when Cl-terminated surfaces are

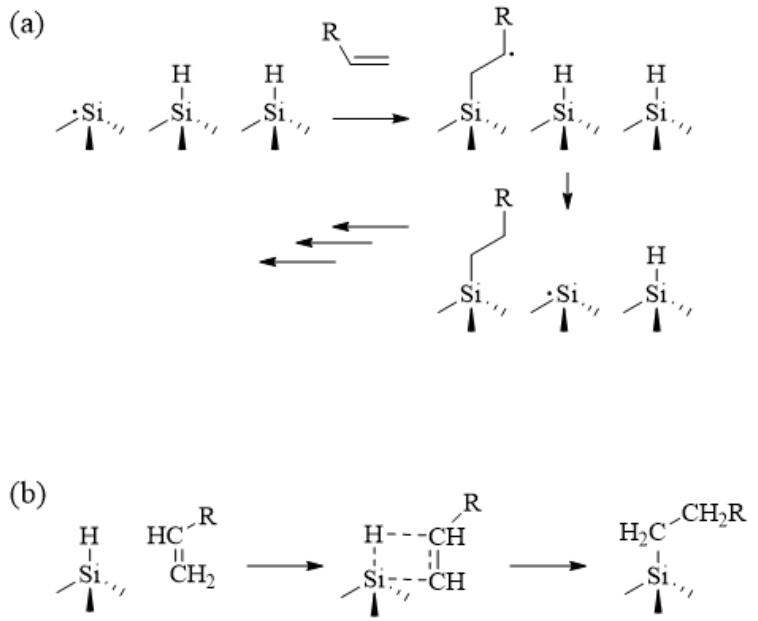

Figure 5.9 (a) Mechanism for radical-based hydrosilylation of a silicon(111) surface. (b) Direct concerted mechanism for thermal hydrosilylation (figure adapted from Colletti *et. al*.[12]).

used for the reaction (data not shown). No statistical difference was seen in grafting 1-octadecene to a freshly etched or a GaP surface treated with PCl_5 first. It is important to note that the Cl 2p signal was still detected on Cl-terminated GaP even after exposure to alkene reagents (Figure 5.10b). Hence, we speculate the mechanism for grafting on GaP is much different and instead specifically involves high energy surface defects. Radicals at dangling bonds could be envisioned to attack alkenes. Further, reactions between alkenes and GaP were not performed in the dark, so photoexcitation of GaP and preferential direction of carriers to defect sites could have occurred to help facilitate reaction. The data thus argue against one potential mechanism that is shown in Figure 5.10a. Additional experiments are necessary to further identify the operative mechanism(s).

To further investigate alkene grafting on GaP, surfaces were reacted with a reagent containing a terminal alkene group and a redox active moiety, ferrocene. Unfortunately, although Fe 2p signal was detected via XP spectroscopy, with further assessment it was found that vinyl ferrocene was not strongly bonded to GaP. Upon sonication in water, vinyl ferrocene fully dissociated from the GaP surface. Two scenarios are speculated. One, the ferrocene groups dissociate from the surface due to instability of bonding at the GaP electrode surface. Two, vinyl ferrocene is merely physisorbed on the surface and when submerged in water, it is simply washed off. It is important to note that previous reports showed grafting of vinyl ferrocene on Si using neat solutions.[21] It is possible reactions attempted here were not successful because diluted vinyl ferrocene in a separate solvent was used instead. That aspect should be investigated more fully.

The previous data has shown that though alkene grafting produces an incomplete monolayer, functional groups can still be added to a GaP surface through this route. Accordingly, the attachment of quaternary amine groups to p-GaP surfaces for dye adsorption was shown. Dye loading was definitely increased on GaP photocathodes reacted first with (vinylbenzyl)trimethylammonium chloride. Still, although an increase in the photocurrent quantum yield at 650 nm was observed, the sensitized signal was lower in magnitude than for a bare GaP(111)A electrode.[5] Still, the shape of the spectral response was different, with a bare surface showing a less defined, broader photocurrent spectrum. Conversely, the profiles for the spectral responses from the chemically modified GaP(111)A electrodes appeared much closer to the absorbance spectrum of the dye in solution. Further, the data only represent the external quantum yield values, as internal quantum yields could not be determined without separate

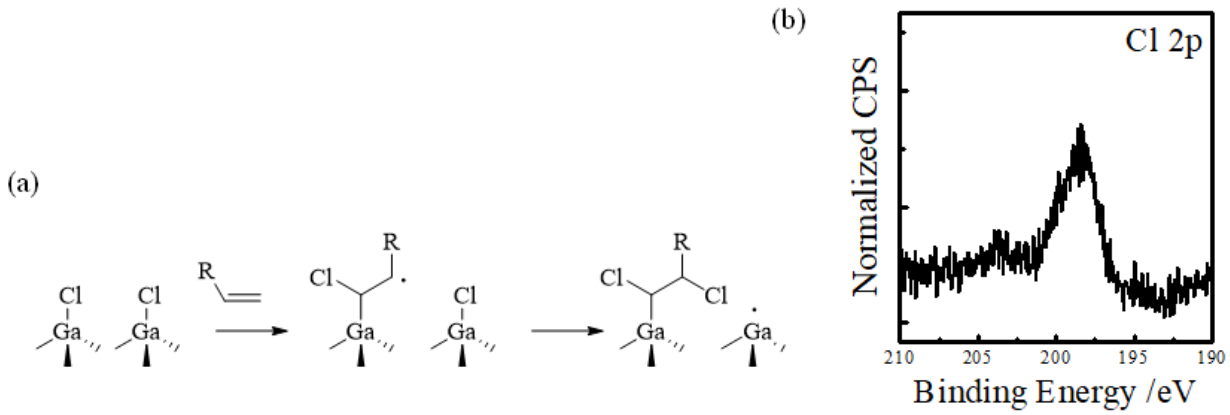

Figure 5.10 (a) Proposed mechanism for alkene grafting on chlorinated GaP(111)A surface. (b) High resolution Cl 2p XP spectra of chlorinated GaP(111)A surface after a reaction with 1-octadecene.

measures of the active dye loading. Cumulatively, the data suggest that a charged monolayer on GaP may lead to an improvement in dye loading.

5. Summary

The cumulative data shown here illustrate the ability to thermally graft alkene groups to GaP surfaces. However, several issues have been identified concerning this functionalization strategy and whether it can ultimately be applied to prepare functioning dye-sensitized p-GaP photocathodes. First, in the specific case of grafting 1-octadecene, the data suggest a short surface reaction independent of reaction time and temperature. Second, changes in grafting were only observed when surfaces were dry etched with either oxygen or argon plasma, suggesting surface defects act as grafting sites and therefore the total density of groups is limited by the quality of the underlying surface. Third, alkyl monolayers grafted via alkenes show worse passivation against surface oxidation than identical alkyl groups grafted onto GaP via Grignard reagents. Fourth, this work briefly introduced a route to affect a cationic monolayer that facilitates dye adsorption. In conclusion, despite being able to introduce organic surface functionalities by alkenes, there is still uncertainty in the type of bonding present at the interface. This lack of understanding limits the further application of this functionalization technique. To introduce a monolayer through alkene grafting that is capable of passivating GaP against chemical and electrochemical degradation, it is imperative that the GaP-organic monolayer interface is further studied. If pristine GaP interfaces are maintained, this functionalization strategy could then be applied to prepare dye sensitized p-GaP photocathodes.

6. References

1. Brown, E. S.; Peczonczyk, S. L.; Wang, Z.; Maldonado, S., *J. Phys. Chem. C* **2014,** *118* (22), 11593-11600.
2. Mukherjee, J.; Peczonczyk, S.; Maldonado, S., *Langmuir* **2010,** *26* (13), 10890-10896.
3. Chitambar, M.; Wang, Z.; Liu, Y.; Rockett, A.; Maldonado, S., *J. Am. Chem. Soc.* **2012,** *134* (25), 10670-10681.
4. Choi, D.; Rowley, J. G.; Parkinson, B. A., *J. Electrochem. Soc.* **2012,** *159* (11), H846-H852.
5. Hlynchuk, S.; MacInnes, M. M.; Maldonado, S., *J. Phys. Chem. C* **2018,** *122* (35), 20073-20082.
6. Ilic, S.; Brown, E. S.; Xie, Y.; Maldonado, S.; Glusac, K. D., *J. Phys. Chem. C* **2016,** *120* (6), 3145-3155.
7. Price, M.; Maldonado, S., *ECS Trans.* **2011,** *35* (8), 153-163.
8. Wang, Z.; Shakya, A.; Gu, J.; Lian, S.; Maldonado, S., *J. Am. Chem. Soc.* **2013,** *135* (25), 9275-9278.
9. Cicero, R. L.; Linford, M. R.; Chidsey, C. E. D., *Langmuir* **2000,** *16* (13), 5688-5695.

10. Beiler, A. M.; Khusnutdinova, D.; Jacob, S. I.; Moore, G. F., *ACS Appl Mater Interfaces* **2016,** *8* (15), 10038-47.
11. Khung, Y. L.; Ngalim, S. H.; Scaccabarozi, A.; Narducci, D., *Sci. Rep.* **2015,** *5*, 11299.
12. Coletti, C.; Marrone, A.; Giorgi, G.; Sgamellotti, A.; Cerofolini, G.; Re, N., *Langmuir* **2006,** *22* (24), 9949-9956.
13. Briggs, D.; Briggs, D.; Briggs, D.; Seah, M. P.; Seah, M. P., *Practical surface analysis*. 2nd ed. ed.; Wiley ;
Salle + Sauerländer: Chichester ; New York : Aarau :, 1990; Vol. Chichester ; New York : Aarau :.
14. Ruangchuay, L.; Schwank, J.; Sirivat, A., *Appl. Surf. Sci.* **2002,** *199* (1-4), 128-137.
15. Webb, L. J.; Lewis, N. S., *J. Phys. Chem. B* **2003,** *107* (23), 5404-5412.
16. Liston, E. M., *J. Adhes.* **1989,** *30* (1-4), 199-218.
17. Franz, G., *J. Vac. Sci. Technol. A* **2001,** *19* (3), 762-772.
18. de Smet, L. C. P. M.; Zuilhof, H.; Sudhölter, E. J. R.; Lie, L. H.; Houlton, A.; Horrocks, B. R., *J. Phys. Chem. B* **2005,** *109* (24), 12020-12031.
19. Mukherjee, J.; Erickson, B.; Maldonado, S., *J. Electrochem. Soc.* **2010,** *157* (4), H487-H495.
20. Flores-Perez, R.; Zemlyanov, D. Y.; Ivanisevic, A., *ChemPhysChem* **2008,** *9* (11), 1528-1530.
21. Lattimer, J. R. C.; Brunschwig, B. S.; Lewis, N. S.; Gray, H. B., *J. Phys. Chem. C* **2013,** *117* (51), 27012-27022.

CHAPTER 6

Conclusions and Future Work

1. Conclusions

This thesis investigates surface functionalization strategies to introduce organic monolayers to Si and GaP surfaces. Doing so allows for the development of highly tailored interfaces that possess properties which are suitable for specific electrical, electrochemical, and photoelectrochemical applications.

This chapter describes several important advancements. In chapter 2 of this thesis, ideas were presented that expand the available surface modification strategies for Si interfaces. This work showed it was possible, even with Grignard-based chemistry, to produce surface coatings that were covalently attached to the underlying Si, that exhibited a low density of electrical defects, and that were hydrophilic due to the presence of alcohol and amine functionalities. In chapter 3, organic monolayers on Si improved adhesive strength of SU8 films on Si(111) wafers. This work showed that it was possible to design deliberate surface chemistry to effect a desirable and long-lasting interfacial property. In chapter 4, sensitization of p-GaP from physiosorbed dyes was demonstrated for the first time. Through the investigated systems, the processes that govern sensitization at bare GaP were identified. The efficacy of sensitization was correlated to reactivity of the GaP interface in water. The cumulative data specifically showed at low light intensities, the reductive degradation of GaP was sufficient to mediate sensitized hole injection. Consequently, this work illustrated the importance of a passivating monolayer on a sensitized GaP photocathode. In chapter 5, a potential method to functionalize GaP photocathodes was investigated. Thermal alkene grafting was shown possible on both GaP(100) and GaP(111)A surfaces. These monolayers were found to be ineffective by themselves at protecting against oxidation but did allow the attachment of functionalities that promoted dye adsorption. Despite the progress represented by this cumulative work, there are still several avenues available for further development.

2. Future Work

Additional Directions for the Work in Chapter 3

Modifying the chemistry of the interface between Si and SU8 unambiguously improved adhesion strength. The exact rationale as to why this happens is still unclear. Moving forward, several potential routes to explore this question are possible. First, regarding nanoindentation measurements, corresponding cross section scanning electron micrographs would be informative. Such images would clarify if the applied force during measurement truly resulted in film delamination as opposed to film fracture. Second, the amount of force needed specifically for delamination ought to be correlated to the dissociation bond energy of attachment to the surface. Knowing the force per unit area, as well as the corresponding density of surface bonds, might provide insight on whether delamination by the application of force scales with the type of surface bond (e.g. Si-O-Si vs Si-C). Third, test reactions involving terminal surface alkenes and epoxy groups should be performed to determine if the mechanism involving photoacids and protonation of the olefin is operative. An ideal reagent would by one with a halogen tag such as Cl or F (i.e. 2-(4-chlorophenyl)oxirane, (Figure 6.1). Following, the reaction should occur in the presence of heat, to resemble the hard bake step used to develop SU8.[1] XP and infrared spectroscopies could then be used to characterize the surface after the reaction, with both the loss of the C=C and the increase of alkyl carbon as expected observables.

Additional Directions for the Work in Chapter 4

To realize p-GaP as a viable dye sensitized photocathode material for water-splitting applications, a broadly applicable surface functionalization strategy that not only passivates the surface against chemical oxidation but also allows for dye loading needs to be developed. To make a direct comparison to work reported in chapter 4, a monolayer that can prevent cathodic degradation and allow dye physisorption needs to be developed. Chapter 5 provides on overview of some relevant factors to consider towards this goal. If a route for covalent attachment is successful, the following experiments should be then performed. First, wavelength-dependent external quantum yield (EQY) measurements should be performed to determine if adsorbed dye molecules are capable of sensitizing GaP. Depending on the method of covalent attachment, dyes such as Fast Green, Rose Bengal and Crystal Violet could be explored since the group has

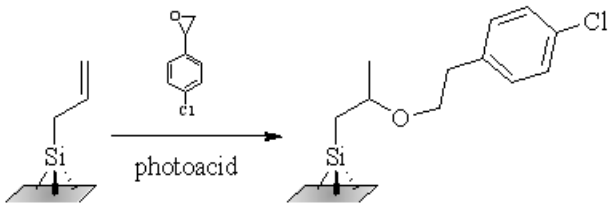

Figure 6.1 Possible test reaction involving an alkene terminated silicon surface and an epoxy group.

accumulated a lot of prior experimental data on sensitization by these specific dyes. One question to investigate is whether the EQY profile is the same for a covalently attached dye as compared to the same dye but just physisorbed. A second question to determine is whether the pathway for mediation of the dye by cathodic surface degradation (see chapter 4) is eliminated. If so, then the sensitization signal should depend on the composition of the electrolyte, where the concentration of a mediator such as methyl viologen in 1M KCl could be assessed. In principle, the sensitization signal should scale linearly with redox mediator concentration until the rate limiting step for sensitization is no longer regeneration of the dye. In addition, the stability of the dye attachment should be assessed. The relative time frame before the dye desorbs from the surface is necessary to deconvolute from other possible effects (e.g. surface oxidation) and to make sure the sensitized electrode systems are stable over a course of a specific experiment. A simple experiment can involve measuring the EQY at a specific wavelength corresponding to the maximum sensitization current as a function of time. For instance, selecting λ = 760 nm for Fast Green is useful. Separately, the spectral response as a function of the identity of the redox mediator should be assessed. In principle, the details underpinning the charge-transfer reaction between mediator and dye will affect dye regeneration. Accordingly, if dye regeneration is rate limiting, a change should be observed between redox mediators like methyl viologen and Eu^{3+}, which have similar standard potentials but very different self-exchange rates. The list provided in chapter 4 should be further consulted. If the response is dependent on the redox identity and its concentration these results would imply that the monolayer can protect the underlying surface and the dye regeneration occurs through a mediator, rather than an undesirable surface mechanism. Moving forward, an ideal combination involving the redox mediator and its concentration should then be determined that leads to maximum sensitization response.

Additionally, the effects of surface concentration of dye on the sensitization current need to be more fully considered. In many cases, high surface loadings are known to result in dye aggregates forming, which has been attributed to internal self-quenching and overall net lower sensitization currents.[2-4] Co-adsorbers such as cholic acid and chenodeoxychlolic acid are often added to suppress aggregation.[5] A possible path to explore is the presence of co-adsorbers on the sensitization response of alkene functionalized GaP photoelectrodes. A possible co-adsorber to use is cholic acid.[6] Functionalized GaP electrodes could be soaked in various concentrations of species like cholic acid. Spectral response measurement could then be collected to examine whether the

sensitization signal (magnitude, stability, wavelength dependence) changes or is invariant to the co-adsorber presence.

2c. ***Additional Directions for the Work in Chapter 5***

Chapter 5 explored one strategy involving alkene grafting. The following avenues are worth exploring. First, quantifying exactly how many surface groups are grafted by this reaction would be informative. Reactions that graft a redox-active functionality should be continued on this front. In this work, attempts were limited by the availability of the vinyl ferrocene reagents, and so experiments with 'neat' reagent were never performed. Grafting vinyl ferrocene onto Si is possible from neat solutions.[7] A neat solution of vinyl ferrocene can be prepared simply by melting the reagent at 100ºC. This reaction should be repeated with GaP. If persistent attachment is successful, then surface coverage can be determined using XP spectroscopy and cyclic voltammetry. Surface coverage values of the redox group using XP spectroscopy and voltammetry should be compared to determine if all the ferrocenes on the surface are redox active. XP spectroscopy approximates the overall surface coverage of the ferrocene groups, not considering if charge transfer is possible. On the other hand, only, redox active species are detected by cyclic voltammetry. The voltammetry experiments will also describe the ability to pass charge to/from the attached ferrocene group. For instance, a set of characteristic peaks is observed at 0.1 V vs *E*(Ag/AgCl) for ferrocene oxidation.[8] The width of these waves (i.e. the peak separations) are indicative of the rate of charge transfer. Fast charge transfer is expected since ferrocene has minimal reorganizational energy penalty. However, if very broad waves are observed, it could indicate the attachment method somehow impedes charge transfer, possibly explaining the results for dye sensitization in Chapter 5.

Second, the alkene reactions should be explored in a presence of radical initiators. Two radical initiators worth exploring are di(dodecanoyl) peroxide and benzoyl peroxide. Grafting in the presence of di(dodecanoyl) peroxide has been previously investigated and is suited for grafting of long alkenes in neat solutions.[9] Due to its aliphatic nature, di(dodecanoyl) peroxide is it able to dissolve in neat solutions of long carbon chain alkenes. If shorter alkenes are of interest a potential candidate is benzoyl peroxide. If these initiators lead to a perceptible difference in surface group coverage, such data could implicate a rate-limiting step in the surface reaction mechanism.

Third, the operative mechanism for alkene grafting should be evaluated. Although there are indications that the mechanism is radical based, there is still no clear description of how this reaction proceeds. A proposed mechanism on chlorinated GaP(111)A was presented in chapter 5 that parallels alkene grafting on H-terminated Si.[10] Preliminary measurements were performed on this front. A chlorinated surface was reacted with 1-octadecene. After completion, a Cl 2p signal was detected by XP spectroscopy. This signal could have arisen from the chlorination of the alkyl chain during surface reaction. Additional experiments should be performed to determine if the Cl 2p signal corresponds to organic Cl. If so, then it is likely that the alkyl chain is chlorinated. If not, then the data could indicate the remaining surficial Cl was simply the original Ga-Cl type and the mechanism for the reaction needs further description.

Fourth, covalent attachment of a dye on functionalized GaP requires development of a protective monolayer that has the capacity for secondary functionalization, as was shown possible for Si in chapter 2. Although such a monolayer on GaP was not fully discussed in the thesis, dye chemisorption on GaP should be possible if such monolayers are realized. I attempted several such experiments. In one attempt, I tried covalently attaching dyes that contained a carboxylic acid group by reacting them with amine-terminated GaP via amide coupling. Amide coupling on an aniline-terminated GaP surface was attempted, (Figure 6.2).As detailed below, the data suggested that these dyes were not covalently attached. One possible reason was the reduced degrees of freedom for motion of the aniline group bonded to the surface. In general, it is preferred that during a surface reaction a nucleophilic species diffuses to the surface leading to a chemical reaction. In this scenario the amine group (the nucleophilic part) was bonded to the surface and this might have impacted the overall success of the reaction. This possibility led me to explore an alternative surface functionality involving a benzyl amine. Two routes were explored to this end, with the goal to prepare a trimethyl silyl (-Si(CH_3)$_3$, TMS) protected benzyl amine containing a halogen at a para position of the benzene ring. If successful, the protected benzyl amine would be converted to a Grignard reagent and reacted with a surface. The first route involved protecting benzyl amine using trimethyl silyl chloride (TMS-Cl) reagent. The primary amine needs to react with TMS-Cl two times to become fully protected. The first reaction is quick, while the second is sluggish as the bulkiness of the TMS groups slows down the rate. Full conversion could not be obtained. Attempts were made to purify the product using column chromatography, but the product ended up decomposing on the column. A potential alternative could have been using reverse phase, but this

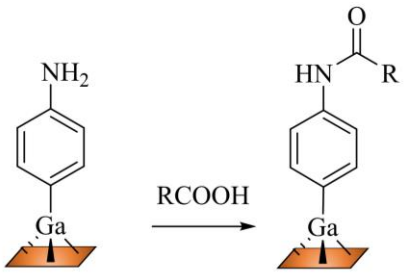

Figure 6.2 Propose amide coupling on a GaP surface containing amine groups.

was not attempted. These results ultimately prevented me from using this TMS-Cl to protect the benzyl amine TMS-Cl as the product could not be purified, which was essential to being able to convert it to a Grignard reagent.

To prepare an aniline terminated GaP surface, I adopted a procedure from Brown *et. al*.[11] Chlorinated GaP(111)A surfaces were reacted with 4-[bis[trimethylsilyl)amino]phenylmagnesium bromide. The amine was deprotected in the presence of trifluoracetic acid and reacted with various reagents containing a COOH functionality. For instance, test reactions were performed using 4-bromobutyric acid and ferrocene carboxylic acid. Reaction conditions were adapted from Sam *et. al.*[12] Briefly, equal concentrations (4mM) of 1-ethyl-3-(3-dimethylaminopropyl)carbodiimide (EDC) and N-hydroxysuccinimide (NHS) were dissolved in water. 1.3 equivalences of acid were then added and the mixture was stirred for 90 minutes. Following, aniline-functionalized GaP surfaces were added. Figure 6.3 shows the overall attempted reaction scheme using EDC/NHS to facilitate amide coupling. As seen in the obtained XP data, a Br 2p signal was not detected after the reaction. I took this observation to mean that amide coupling did not take place. Attempts were also made to couple ferrocene carboxylic acid to a GaP(111)A surface. After the reaction, surfaces were again characterized by XP spectroscopy. As seen in Figure 6.4c, no Fe 2p signals were detected above the baseline. Amide coupling between aniline terminated surface and acyl chlorides was also attempted. Acyl chlorides are derivatives of carboxyl acids and they are more prone to amide coupling. 4-Chlorobenzoyl chloride was reacted with GaP surface (Figure 6.5) in this vein. In a sealed, 3-neck round bottom flask, a 1:1 equivalent of acid to diisopropylamine was dissolved in dichloromethane (2mL). Following, aniline-terminated GaP(111)A was added to the solution. The solution was purged with N_2, and placed on heat (45^{o}C) for 12 h. Although Cl 2p XP spectrum shows a possible peak at 200 eV corresponding to Cl 2p, upon further evaluation this was attributed to signal coming from GaP substrate.

To prepare a benzyl amine terminated GaP surface, two strategies were explored. One idea was to protect 4-bromobenzylamine with TMS-Cl followed by conversion of the protected amine to a Grignard reagent (Figure 6.6). 0.1g of benzyl amine and 1.1 equivalences of trimethyl amine were dissolved in a 3-neck round bottom containing 1.6 mL of dichloromethane. Mixture was purged with N_2(g) for 5 minutes and kept under constant nitrogen flow. Following, 150 µL of TMS-Cl was slowly added to the mixture. Reaction proceeded with stirring for 2.5 h at room

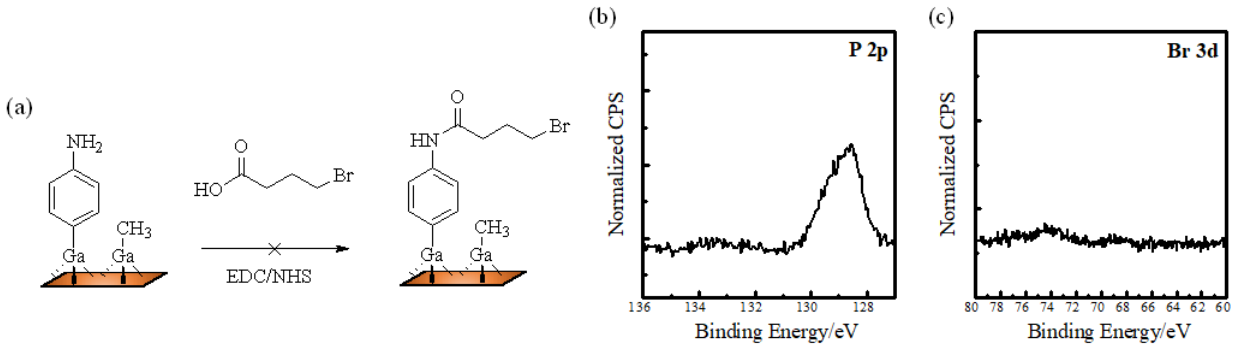

Figure 6.3 (a) Proposed amide coupling on amine terminated surface. (b) High resolution P 2p XP spectra after 12 h reaction. (c) High resolution Fe 2p XP spectra after 12 h reaction.

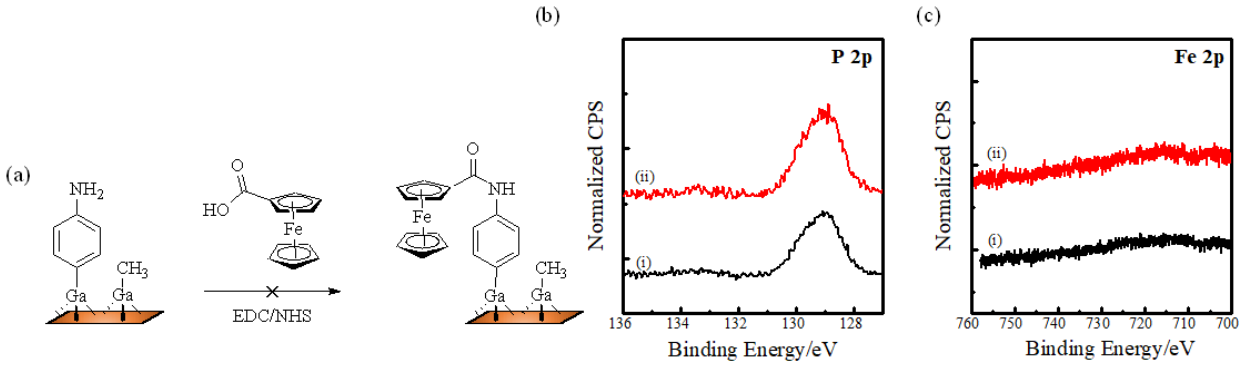

Figure 6.4 (a) Proposed amide coupling on amine terminated surface. (b) High resolution P 2p XP spectra after reaction, (i) reaction time 2h, (ii) reaction time 12 h. (c) High resolution Fe 2p XP spectra after reaction, (i) reaction time 2 h, (ii) reaction time 12 h.

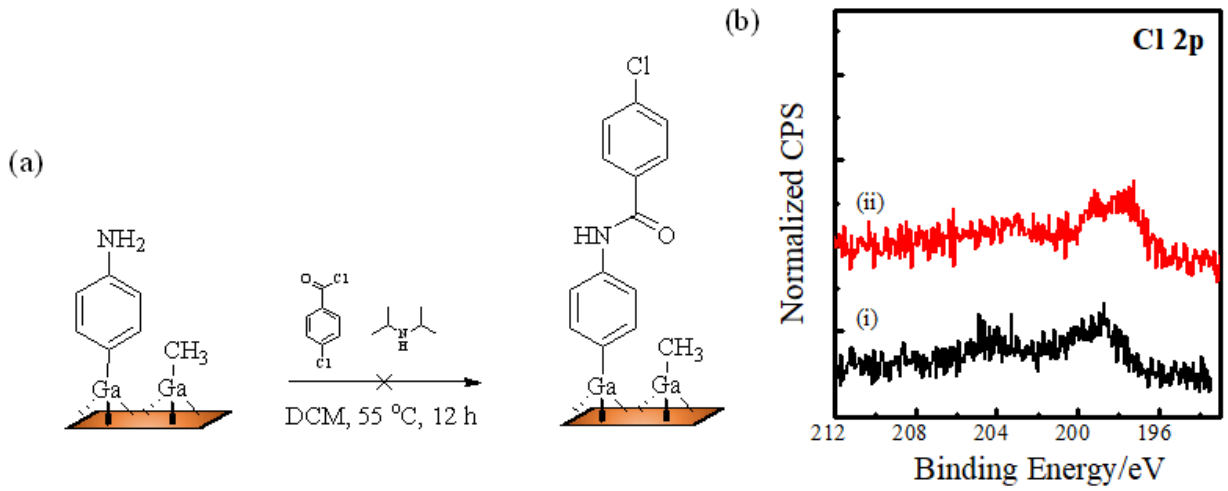

Figure 6.5 (a) Proposed amide coupling on amine terminated surface. (b) High resolution Cl 2p XP spectra; (i) high resolution Cl 2p XP spectrum for a bare GaP(111)A, (ii) after amide coupling reaction.

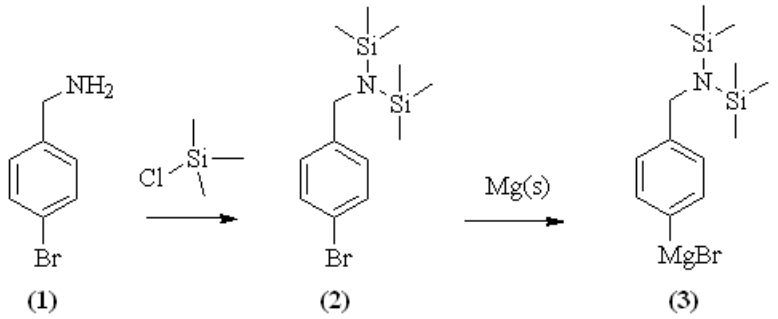

Figure 6.6 Proposed route for preparing a protected benzyl amine Grignard.

temperature. Afterwards, the mixture was quenched with ammonium chloride, the organic phase was separated, and then the solute was dried with Na_2SO_4. However, a complete reaction of TMS-Cl with 4-bromobenzylamine was not observed. Instead, several products were seen, as shown by mass spectrometry (Figure 6.7). To purify the product, column chromatography was employed. The solvent system consisted of a mixture of ethyl acetate in hexanes. The products could not be purified as the mixture underwent decomposition quite rapidly and was highly retained on the silica column. Further experiments on this idea were not attempted. However, the following could be explored. First, a reverse phase column could be tried to purify the product. Second, one of the hypothesis of why the reaction does not proceed to completion is the inability of the mono-substituted amine to further react with TMS-Cl. A possible solution could be performing the reaction in two sequential steps. The first addition of the $Si(CH_3)_3$ group is quick, leading to the mono substituted product. If it is confirmed by ^{1}H-NMR or mass spec that the starting material is consumed and only the mono-substituted product is present, then a strong base such as sodium hydride can be added to allow the di-substituted product to form.

A second strategy involved 4-bromobenzyl bromide and KHMDS (Figure 6.8). KHMDS reacts with 4-bromobenzyl bromide by an SN_2 mechanism effectively placing a protected amine on the benzyl position.[13] The appeal of this route is that it allowed for a near quantitative conversion of 4-bromobenzyl bromide to a protected benzyl amine. This product was characterized by ^{1}H-NMR, confirming conversion. Unfortunately, the protected benzyl amine was not successfully converted into a Grignard regent. The following attempts at Grignard synthesis were made. A reaction was carried out in a presence of magnesium (Mg) turnings and protected amine (1.25: 1 equivalence). In a dried 3 neck round bottom flask Mg(s) was added to tetrahydrofuran and the solution was purged with $N(_2)$ for 10 minutes. Then a few crystals of I_2(s) were added to activate Mg(s). Reaction was stirred at RT for 2 hr. Following, protected amine was added, and mixture was heat to 100^{o}C. Visually looking at the mixture it was determined that the Grignard reagent was not synthesized. Mg turnings should be consumed during the processes, but this did not occur. Additional route to prepare a Grignard reagent involved using isopropylmagnesium chloride lithium chloride complex. Unfortunately, no success was seen. ^{1}H-NMR results could not collaborate that a protected benzyl amine Grignard was formed. The inability to form a Grignard reagent using this route lead me to believe the product was not pure. This is not surprising for two reasons (1) a clear purification route could not be developed and (2) the data suggests that N-Si

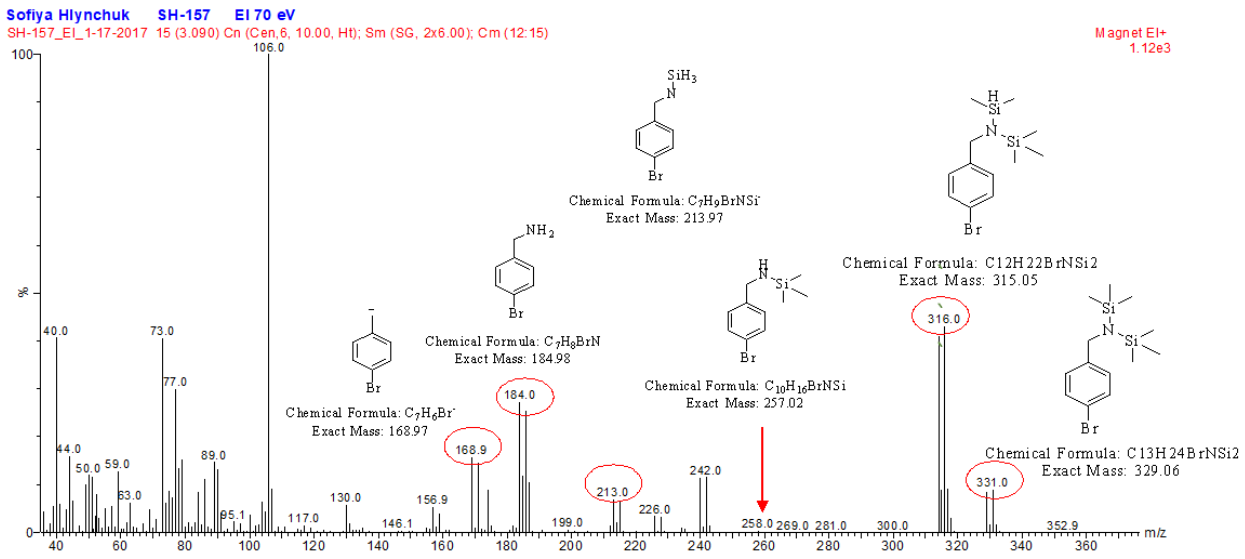

Figure 6.7 Mass spectrum results of compound 2.

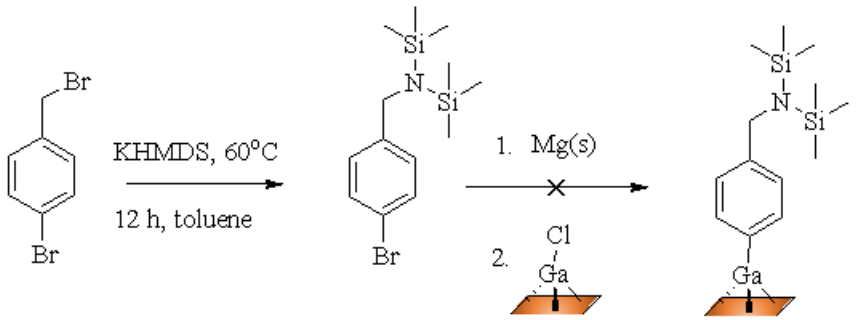

Figure 6.8 Preparation of protected benzyl amine followed by conversion reaction to a Grignard and subsequent reaction with chlorinated GaP(111)A surface.

bonds are cleaved readily, reforming the R-NH_2 group. Grignard are highly reactive, and any presence of protons will quench the Grignard. Moving forward, if amide coupling is of interest, new protecting groups need to be considered that can protect a primary amine during a Grignard reaction. Unfortunately, it is very difficult to find a protecting group for an amine against a nucleophilic species such as a Grignard reagent. I highly suggest alternative groups are explored other than amines to perform covalent attachment. For instance, introducing an azide at a surface could allow for click coupling.

My conclusion from my cumulative observations is that alternative protecting groups are needed to make primary amines that survive the Grignard reaction. I suspect that N-Si bonds were cleaved either during purification of the reagent prior to surface reaction or during exposure to moisture before reacting with the dyes. Data illustrating this point to be a fact, and why it happens on GaP but not on Si, would be interesting. However, for the purpose of making a purposeful, functionalized GaP surface, identifying an altogether different strategy is more important.

3. References

1. Fahrenkrug, E.; Biehl, J.; Maldonado, S., *Chem. Mater.* **2015,** *27* (9), 3389-3396.
2. Anikin, M.; Tkachenko, N. V.; Lemmetyinen, H., *Langmuir* **1997,** *13* (11), 3002-3008.
3. Imahori, H.; Norieda, H.; Nishimura, Y.; Yamazaki, I.; Higuchi, K.; Kato, N.; Motohiro, T.; Yamada, H.; Tamaki, K.; Arimura, M.; Sakata, Y., *J. Phys. Chem. B* **2000,** *104* (6), 1253-1260.
4. Sayama, K.; Tsukagoshi, S.; Mori, T.; Hara, K.; Ohga, Y.; Shinpou, A.; Abe, Y.; Suga, S.; Arakawa, H., *Sol. Energy Mater. Sol. Cells* **2003,** *80* (1), 47-71.
5. Han, L.; Islam, A.; Chen, H.; Malapaka, C.; Chiranjeevi, B.; Zhang, S.; Yang, X.; Yanagida, M., *Energy & Environmental Science* **2012,** *5* (3), 6057-6060.
6. Zhang, L.; Cole, J. M., *J. Mater. Chem. A* **2017,** *5* (37), 19541-19559.
7. Lattimer, J. R. C.; Brunschwig, B. S.; Lewis, N. S.; Gray, H. B., *J. Phys. Chem. C* **2013,** *117* (51), 27012-27022.
8. Booth, M. A.; Kannappan, K.; Hosseini, A.; Partridge, A., *Langmuir* **2015,** *31* (29), 8033-8041.
9. Linford, M. R.; Fenter, P.; Eisenberger, P. M.; Chidsey, C. E. D., *J. Am. Chem. Soc.* **1995,** *117* (11), 3145-3155.
10. Coletti, C.; Marrone, A.; Giorgi, G.; Sgamellotti, A.; Cerofolini, G.; Re, N., *Langmuir* **2006,** *22* (24), 9949-9956.
11. Brown, E. S.; Hlynchuk, S.; Maldonado, S., *Surf Sci.* **2016,** *645*, 49-55.
12. Sam, S.; Touahir, L.; Salvador Andresa, J.; Allongue, P.; Chazalviel, J. N.; Gouget-Laemmel, A. C.; Henry de Villeneuve, C.; Moraillon, A.; Ozanam, F.; Gabouze, N.; Djebbar, S., *Langmuir* **2010,** *26* (2), 809-814.
13. Bonar-Law, R. P.; Davis, A. P., *Tetrahedron* **1993,** *49* (43), 9829-9844.